OVERTONE PRE-EXCITATION - INFRARED MULTIPLE PHOTON DISSOCIATION UNDER COLLISIONAL CONDITIONS: NEW POTENTIAL FOR LASER ISOTOPE SEPARATION

THÈSE N^{O} 3084 (2004)

PRÉSENTÉE À LA FACULTÉ SCIENCES DE BASE

Institut des sciences et ingénierie chimiques

SECTION DE CHIMIE ET GÉNIE CHIMIQUE

ÉCOLE POLYTECHNIQUE FÉDÉRALE DE LAUSANNE

POUR L'OBTENTION DU GRADE DE DOCTEUR ÈS SCIENCES

PAR

Mikhail Nikolaevich POLIANSKI

Master of physics, Saint-Petersburg State University, Russie
et de nationalité russe

acceptée sur proposition du jury:

Prof. Th. Rizzo, directeur de thèse
Prof. M. Chergui, rapporteur
Prof. A. Makarov, rapporteur
Dr G. Seyfang, rapporteur

Lausanne, EPFL
2004

Тигрёнку

Contents

Abstract

With a view towards developing a method for molecular laser isotope separation (MLIS) of carbon, silicon and nitrogen, this work investigated the overtone pre-excitation - infrared multiple photon dissociation (OP-IRMPD) of CF_3H, $SiHCl_3$ and NH_3. The study of isotopically selective OP-IRMPD of CF_3H resulted in a qualitative understanding of the dynamics of the OP-IRMPD process under collisional conditions. This understanding prompted us to make some crucial improvements which made the OP-IRMPD based approach to laser separation of carbon isotopes economically feasible. The typical value of isotopic selectivity reached in our experiments is 2000-3000 at the highest yield and can be further increased up to at least 7000-8000 with a simultaneous drop in productivity. We have also performed an estimation of the required parameters for an industrial-scale separation and of the energy consumption by a single separation act.

The experimental study of OP-IRMPD of the $SiHCl_3$ molecule has shown a limited applicability of this approach on this molecule for highly selective silicon isotope separation due to the low discrimination in the dissociation of pre-excited *vs.* ground state molecules under the conditions of moderate dissociation yield.

Overtone pre-excitation of the ammonia molecule makes its multiphoton dissociation considerably easier and allows a high level of discrimination in dissociation of pre-excited *vs.* ground state molecules. However the high fluence of the dissociation laser required for effective multiphoton excitation of NH_3 makes the OP-IRMPD approach on this molecule impractical for MLIS. We have shown that the probability of the dissociation of a pre-excited ammonia molecule depends on the pre-excitation level and on the wavelength of the dissociation laser.

Version abrégée

Afin de développer une méthode de séparation moléculaire des isotopes par laser (MLIS[1]) du carbone, du silicone et de l'azote, nous avons étudié le processus de la pré-excitation overtone – dissociation multiphotonique infrarouge (OP-IRMPD[2]) des molécules CF_3H, $SiHCl_3$ et NH_3. Les investigations sur le processus sélectif par isotopes OP-IRMPD de la molécule CF_3H ont amené à la compréhension qualitative de la dynamique du processus OP-IRMPD sous des conditions de collision. Cette compréhension nous a permis de faire quelques améliorations importantes donnant des perspectives intéressantes à une application sur une échelle industrielle du processus OP-IRMPD pour la séparation des isotopes par laser. La valeur typique de la sélectivité isotopique dans nos expériences est de 2000-3000 dans des conditions de productivité maximale. Cette valeur peut même être augmentée à 7000-8000. On observe alors une diminution simultanée de la productivité. Nous avons également estimé les paramètres nécessaires à l'installation industrielle et à la dépense d'énergie pour un acte de séparation.

Les études expérimentales du processus OP-IRMPD de la molécule $SiHCl_3$ ont montré la possibilité d'application limitée de l'approche pour cette molécule pour la séparation à haute sélectivité des isotopes du silicone. C'est la conséquence de la discrimination faible entre la dissociation des molécules pré-excitées et celle des molécules à l'état fondamental.

La pré-excitation overtone de la molécule d'ammoniaque facilite considérablement sa dissociation multiphotonique et permet d'atteindre un haut niveau de discrimination entre la dissociation des molécules pré-excitées et celle des molécules à l'état fondamental. Cependant, le haut flux d'énergie du laser de dissociation, nécessaire à une excitation multiphotonique effecace de la molécule NH_3, rend l'approche OP-IRMPD inefficace sur cette molécule. Nous avons montré que la probabilité de la dissociation d'une molécule pré-excitée d'ammoniaque dépend du niveau de la pré-excitation ainsi que de la longueur d'onde du laser de dissociation.

[1] **M**olecular **L**aser **I**sotope **S**eparation (*angl.*)
[2] **O**vertone **P**re-excitation – **I**nfra**R**ed **M**ultiple **P**hoton **D**issociation (*angl.*)

Автореферат

В целях разработки методики молекулярного лазерного разделения изотопов (MLIS[3]) углерода, кремния и азота, исследован процесс обертонного предвозбуждения - инфракрасной многофотонной диссоциации (OP-IRMPD[4]) молекул CF_3H, $SiHCl_3$ и NH_3. Изучение изотопически селективного процесса OP-IRMPD на молекуле CF_3H привело к качественному пониманию динамики процесса OP-IRMPD в столкновительных условиях. Достигнутое таким образом понимание позволило внести ряд усовершенствований, делающих OP-IRMPD подход к лазерному разделению изотопов углерода перспективным для практического применения. Типичное значение изотопической селективности, достигаемое в наших экспериментах составляет 2000-3000 при максимальном выходе процесса. При более низких значениях продуктивности, селективность может быть увеличена по крайней мере до 7000-8000. Были также произведены оценки требуемых параметров промышленной разделительной установки и энергозатрат на единичный акт разделения.

Экспериментальное исследование OP-IRMPD молекулы $SiHCl_3$ показало ограниченную применимость данного подхода на этой молекуле для высоко селективного разделения изотопов кремния вследствие невозможности достижения высокой дискриминации между диссоциацией предвозбужденных молекул и молекул в основном состоянии при условии достаточно высокого выхода диссоциации.

Обертонное предвозбуждение молекулы аммиака существенно облегчает его многофотонную диссоциацию, что дает возможность достижения высокой дискриминации между диссоциацией предвозбужденных молекул и молекул в основном состоянии. Однако, высокий поток энергии диссоциирующего лазера, требующийся для эффективного многофотонного возбуждения NH_3, делает практическое использование OP-IRMPD подхода для MLIS с использованием данной молекулы неэффективным. Показано, что вероятность диссоциации предвозбужденной молекулы аммиака зависит как от уровня возбуждения, так и от длины волны диссоциирующего лазера.

[3] **M**olecular **L**aser **I**sotope **S**eparation (*англ.*)

[4] **O**vertone **P**re-excitation – **I**nfra**R**ed **M**ultiple **P**hoton **D**issociation (*англ.*)

Chapter 1

Introduction and motivation

The history of studying the isotopes of chemical elements began almost a century ago when Frederick Soddy introduced the term "isotopes" for elements occupying the same place in the periodic table but possessing different atomic masses [1–3]. Development of electro-magnetic mass spectrography by Joseph John Thomson [4] and Francis W. Aston [5] lead to the discovery by the beginning of 1930's of isotopes of most of the elements known by that time [5,6]. In 1932 Gustav Hertz demonstrated the possibility of isotope separation by gaseous diffusion [7]. By the end of the 1950's most of the currently used methods of isotope separation have been developed: gaseous diffusion, gas centrifuge, chemical exchange, rectification (low temperature distillation) and electro-magnetic separation. A complete overview of the achievements in understanding the nature of isotopes and in the field of isotope separation during that period is done by F. W. Aston [8]. Initially, such a fast progress has been driven mostly by the demand by the weapon industry for uranium-235. Later, however, the materials with isotopically changed composition have found a wide application in various spheres of human life. Currently, both radioisotopes (nonstable isotopes) and enriched stable isotopes are used in practical applications as well as for fundamental research. A rather complete overview of isotopes applications and separation methods is given in Reference [9]. According to [9], the most frequent application of radioactive isotopes is as a source of α-, β-, γ- and neutron radiation and of both radioactive and stable isotopes as "labelled" atoms for study of distribution and dynamics of substances in different systems.

One of the promising fields of application of isotopes is medicine, where they are used in the diagnosis and treatment of illness [10]. One example is the carbon-13 Diagnostic Breath Test (DBT), which is used for diagnostics of the human digestive system. The idea of the DBT is rather simple. A carbon-13 labelled substrate is ingested by the patient. After certain metabolic processes occur, the enriched isotope appears in the patient's breath as $^{13}CO_2$. Analysis of the concentration of $^{13}CO_2$ as a function of time allows one to make certain conclusions about the

condition of the organs in the digestive system.

One of the main factors limiting the spread of methods assuming a high consumption of isotopes is the high price of the isotopes which is conditioned by high energy consumption of conventional separation methods. One approach to achieving efficient isotope separation is to use the spectroscopic differences between different isotopic species (either atoms or molecules) in combination with specific properties of laser radiation [11]. The use of lasers for isotope separation is based on three fundamental principles:

1. The difference in the absorption spectra of isotopically different atoms and molecules;

2. The ability of lasers to produce very narrow bandwidth radiation, allowing selective excitation of the desired isotopic species by making use of this spectral difference;

3. The possibility to distinguish between excited and unexcited molecules, for instance, using difference in their reactivity.

Despite the apparent natural suitability of lasers for optical isotope separation, the tremendous progress in laser technology and the huge body of research dedicated to laser isotope separation (see, for example [9, 11–13]), only recently has a laser based approach been implemented for commercial production of carbon-13 [14] (Gas-Oil JSC [15]). This approach, called molecular laser isotope separation (MLIS), is based on the phenomena of isotopically selective infrared multiphoton dissociation (IRMPD) of polyatomic molecules by the radiation of a pulsed TEA CO_2 laser [16, 17]. The IRMPD based isotope separation approach is competitive with conventional methods when required carbon-13 enrichment is on the order of 35-50%. The production of high purity (>99% of carbon-13) isotopic materials demanded by the market of medical components requires, however, a multi-cycle realization of the IRMPD based separation process making it considerably more expensive. Thus, the bulk of carbon-13 is still produced by low temperature distillation by companies such as ISOTEC (a division of Sigma-Aldrich [18]) and Cambridge Isotope Laboratories [19].

A new highly selective approach to molecular laser isotope separation, overtone pre-excitation - infrared multiphoton dissociation (OP-IRMPD), has been developed recently in the Laboratory of Molecular Physical Chemistry of Swiss Federal Institute of Technology [20, 21]. The OP-IRMPD process consists of two major steps (Figure 1.1). In the first step, a near-infrared laser pulse pre-excites molecules containing the desired isotope *via* a low vibrational overtone transition of a high frequency vibrational mode. In the second step, a CO_2 laser pulse selectively dissociates the pre-excited molecules. Finally, the dissociation products enriched in the desired isotope are chemically converted to a stable molecule that is different from the parent molecule and physically separated from the latter, for instance, by distillation.

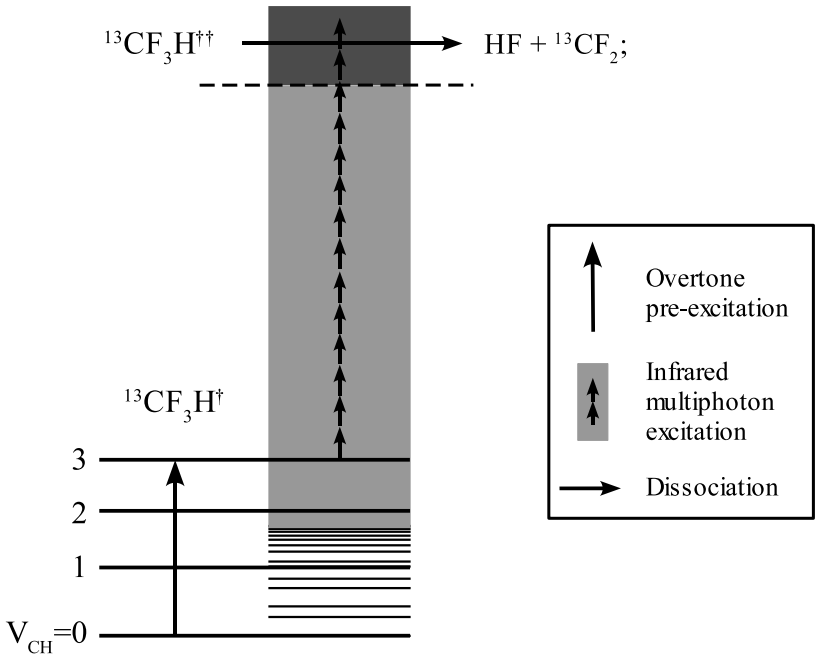

Figure 1.1: OP-IRMPD approach to molecular laser isotope separation.

Previous research on the OP-IRMPD process has demonstrated that an isotopic selectivity as high as 9000 can be reached in application to carbon-13 isotope separation, which corresponds to an increase of carbon-13 concentration from 1.07% natural abundance to 99% in the resulting product. While this high selectivity is largely determined by the selective pre-excitation step, it has been found that collisional vibrational deactivation subsequent to the pre-excitation pulse can increase this selectivity more than by an order of magnitude, contrary to normal expectations [20, 21]. This allows running the process at moderate pressure of 7-25 mbar and, therefore, makes it potentially attractive for practical implementation. However, an estimate of the process productivity suggests that it is still low for the process to be economically competitive. Further increase of productivity requires understanding details of the process and in particular, overtone pre-excitation and IRMPD under collisional conditions.

The main objective of this work is a comprehensive investigation of the OP-IRMPD process in view of its potential development as an industrial technique for carbon-13 isotope separation. We also study the possibility of using the OP-IRMPD approach to separation of silicon and nitrogen isotopes.

In Chapter 2 we summarize the basic principles underlying the basis of the OP-IRMPD approach to laser isotope separation.

Chapters 3, 4 and 5 describe our research of the possibility of using the OP-IRMPD approach

for separation of carbon, silicon and nitrogen isotopes respectively with CF_3H, $SiHCl_3$ and NH_3 as the parent molecules.

Chapter 6 briefly summarizes the major conclusions from this work and the perspectives for the future.

Bibliography

[1] F. Soddy, *Chemical News*, 1913, **107**, 97–99.

[2] F. Soddy, *Nature*, 1913, **92**, 399–400.

[3] F. Soddy, *The origins of the conceptions of isotopes*, Nobel Lecture, December 12, 1922.

[4] J. J. Thomson, *Proceedings of the Royal Society*, 1913, **A89**, 1–20.

[5] F. W. Aston, *Mass spectra and isotopes*, Nobel Lecture, December 12, 1922.

[6] H. C. Urey, *Some thermodynamic properties of hydrogen and deuterium*, Nobel Lecture, February 14, 1935.

[7] G. Hertz, *Die Naturwissenschaften*, 1933, **21**, 884–885 (in German).

[8] F. W. Aston, *Mass spectra and isotopes*, London Edward Arnold & Co, 1942.

[9] ed. V. Y. Baranov, *Isotopes: properties, production, applications*, IzdAT, Moscow, 2000 (in Russian).

[10] S. J. Adelstein and F. J. Manning, *Isotopes for medicine and the life sciences*, National Academy Press, Washington, 1995.

[11] V. S. Letokhov, *Science*, 1973, **180**, 451–458.

[12] V. S. Letokhov, *Nature*, 1979, **277**, 605–610.

[13] V. S. Letokhov, *Sov. Phys. Uspekhi*, 1986, **29**, 70–81.

[14] V. S. Letokhov, *Laser und Optoelektronik*, 1998, **30**, 29–33.

[15] Gas-Oil JSC, http://www.c13.ru.

[16] R. V. Ambartsumyan, V. S. Letokhov, E. A. Ryabov, and N. V. Chekalin, *JETP Lett.*, 1974, **20**, 273–274.

[17] J. L. Lyman, R. J. Jensen, J. Rink, C. P. Robinson, and S. D. Rockwood, *Appl. Phys. Lett.*, 1975, **27**, 87–89.

[18] Sigma-Aldrich Co., http://www.sigmaaldrich.com.

[19] Cambridge Isotope Laboratories, INC, http://www.isotope.com.

[20] M. Kowalzcyk *Highly Selective Molecular Laser Isotope Separation of Carbon-13* PhD thesis, Ecole Polytechnique Fédérale de Lausanne, Switzerland, 2000.

[21] O. V. Boyarkin, M. Kowalzcyk, and T. R. Rizzo, *J. Chem. Phys.*, 2003, **118**, 93–103.

Chapter 2

Physical basis of the overtone pre-excitation - infrared multiphoton dissociation technique

The following sections describe the basic concepts underlying the overtone pre-excitation - infrared multiphoton dissociation technique and the main processes resulting in isotopic selectivity of the OP-IRMPD. Understanding these principles is essential to achieving the goal of optimizing this technique to be an economically competitive method for the enrichment of stable isotopes.

2.1 Infrared multiphoton dissociation (IRMPD)

Since the theoretical predictions and first experimental observations of Infrared Multiphoton Dissociation (IRMPD), this phenomenon has been studied in a number of works (see, for example, review of early works in [1]). We will concentrate here on the descriptions of the IRMPD process suggested by Letokhov [1] and by Quack [2, 3]. Comprehensive reviews of advances in infrared laser photochemistry, and, in particular, in understanding the infrared multiphoton excitation (IRMPE) process, are given, for example, in [1, 4–7].

2.1.1 General theoretical description of IRMPD

The most rigorous description of the IRMPD process uses the solution of time dependent Schrödinger equation in the presence of intensive laser radiation described as a classical electromagnetic wave. Obviously, a sufficiently accurate solution of such a problem may be possible only for some particular cases where density of vibrational states under consideration is relatively low. As it is mentioned in Reference [7], this description is applicable:

1. for small molecules (diatomic and some triatomic),

2. for very short times, when only a small subsystem of the entire molecule interacts with laser field, and

3. for modest radiation intensities, when only a few atomic or molecular levels are effectively coupled through the radiation field.

However, for typical parameters of IRMPD experiments (five or more atoms in a molecule, few to hundreds nanoseconds excitation times, MW to GW cm^{-2} laser intensities) the number of states which has to be taken in account is enormous (more than 10^{10} even for relatively small polyatomic molecules such as CF_3I or SF_6 [7]).

Thus, it has been proposed to use a statistical mechanical theory approach to the description of IRMPE process [2]. The fundamental idea of this theory is to derive simplified equations of motion for more coarse grained quantities than the complete molecular wavefunctions, quantum state populations, or density matrix elements. In the case of the IRMPD process, this coarse graining applies to level populations, which are sums over many individual quantum state populations.

$$p_K = \sum_{k=1}^{N_K} p_{k(K)}, \tag{2.1}$$

where K designates the 'grained' levels (bins) and k the individual, nondegenerate quantum states.

The definition of bins in the case of stepwise multiphoton excitation arises from the number of quanta absorbed from the radiation field. The population dynamics of the bins described by the master equations, written in matrix notation:

$$\frac{d\mathbf{p}}{dt} = \mathbf{K}\mathbf{p}, \tag{2.2}$$

where $\mathbf{K}$ is a real matrix combined from the rate coefficients of transitions between particular pairs of bins.

The solutions of the master equations for the case when $\mathbf{K}$ does not depend on time are:

$$\mathbf{p}(t) = \mathbf{p}(t_0) exp[\mathbf{K}(t - t_0)]. \tag{2.3}$$

The transition rate coefficients have been derived for the most important statistical mechanical cases of multiphoton excitation:

Case A: Excitation from the single state into a dense set of final states. This situation can be applied for a very large polyatomic molecule generated in the ground state as the initial state by supersonic jet cooling;

Case B: Transitions between dense sets of states at each level. This case applies when initially in some level I a dense set of states with average frequency spacing $\delta_I << \omega$ is populated, either thermally or by optical pre-excitation (where w is the spacing between I and J levels corresponding approximately to the energy of the photon used for IRMPE). Radiative coupling occurs resonantly to the neighboring level J with an average frequency spacing δ_J;

Case C: Transitions between groups of specific, nearly pairwise coupled states. This case can arise through selection rules or because of modest coupling at low intensity and low densities of states;

Case D: Transitions between groups of states with a strong global interaction.

Figure 2.1 shows the IRMPD process for typical molecule as described by statistical mechanical theory.

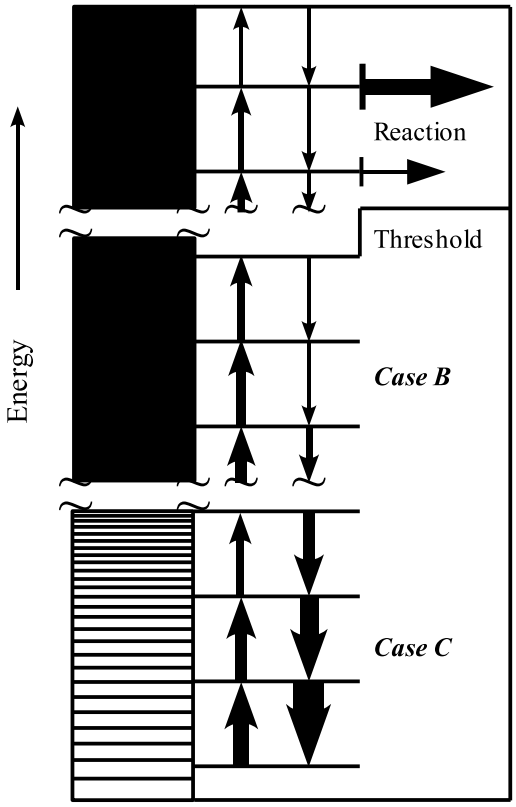

Figure 2.1: Level scheme for the statistical mechanical treatment of multiphoton excitation in typical molecule allowing for general mechanisms of ***case C*** at low energies and ***case B*** at high energies, including chemical reactions at higher energies [3].

As it can be seen from the Figure 2.1, such a process may be described by taking into consideration only the cases ***B*** and ***C***.

The statistical mechanical theory description of the multiphoton excitation provides a realistic model of the IRMPD process that can be used for reasonably accurate calculations of the multiphoton excitation dynamics under the condition that one has sufficiently complete information about the spectroscopy of the molecule. In the absence of such information, which is often the case, one can use a semi-empirical model. These models do not give a complete "physical" description of the process, but provide a simplified, intuitive approach to obtaining a qualitative understanding of the phenomenon, which in certain limits may be quantitative. Apart from that, a semi-empirical approach can be used for a simplified numerical modelling of IRMPD process, which does not require long computing time. One such approach, which is the one adopted in this work is described below.

2.1.2 Semi-empirical description of IRMPD

Figure 2.2 represents a model of the IRMPD process proposed in Reference [1].

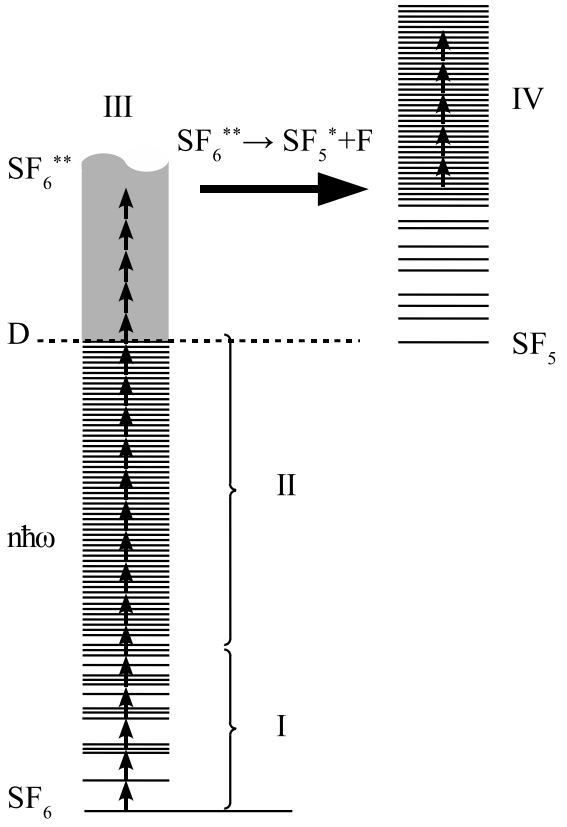

Figure 2.2: Model for the dissociation process of a polyatomic molecule in a strong IR laser field, showing the four major steps of IRMPD [1].

This model describes the process of IRMPD of a polyatomic molecule in an intense IR laser

field as a series of consequent steps of excitation through different zones of energy.

Zone I: Lower vibration levels. The excitation of the molecule through this energy region is a resonant process, because in a region of low density of states, only a few vibrational transitions are possible from a given vibrational-rotational state. Vibrational anharmonicity leads to a rapid detuning of successive vibrational levels from the fixed laser frequency. This detuning can be partially compensated by changes in the molecule's rotational energy, by anharmonic splitting of excited vibrational state or by power broadening of transitions by the intense laser field. Moreover, two- or three-photon vibration transitions can be involved in the case of an intense laser field. However, the average absorption cross-section of the molecules in Zone ***I*** is generally low, and hence the excitation through this energy region is the main factor limiting the dissociation yield of the entire process.

Zone II: Highly excited states or vibrational quasi-continuum. This region is characterized by a high density of mutually interacting vibrational energy levels, so that for a fixed frequency of infrared laser radiation always exist a possible vibrational transition. If a molecule has reached the quasi-continuum, it can accumulate an amount of energy comparable to the dissociation energy, provided that the laser fluence is high enough and relaxation of absorbed energy is slow compared to excitation rate.

Zone III: Dissociation of the molecule excited above the dissociation limit. Dissociation process has a statistical character conditioned by energy flow between vibrations. Thus, even if the molecule is excited by a short laser pulse above the dissociation limit known from thermochemical data, the dissociation will occur only after a certain delay which is shorter for larger excess of energy. Under collisional conditions the dissociation of the molecule is in competition with collisional relaxation, so for effective IRMPD the dissociation has to occur faster than the relaxation below the dissociation limit, which requires for high pressures a considerable over-excitation of the molecule above the dissociation limit.

Zone IV: Multiphoton excitation of a dissociation fragment. This is possible when one of the dissociation fragments is a polyatomic molecule and there is a resonance between the IR radiation and one of the vibrational modes, or if the polyatomic fragment obtains the excess vibrational energy from the super-excited parent molecule and is itself in the vibrational quasicontinuum.

One can notice a certain similarity between the models of the IRMPD process shown in the Figures 2.1 and 2.2. Namely, Cases ***C*** and ***B*** of the statistical mechanical description approximately corresponds to zones ***I*** and ***II*** of the simplified model. The main difference between these two descriptions is that the simplified model does not consider the down-pumping process. This simplification is excused if we assume that the up-pumping rate in this model represents the difference between up- and down-pumping rates in the more general theory.

Indeed, due to the rapid increase of the density of states with energy, the probability of an upward transition is considerably higher than the probability of downward one. In the absence of downward transitions and constant up-pumping rate, the distribution of vibrational energy in excited molecules would be described by a Poisson distribution:

$$N(n) = \frac{\lambda^n e^{-\lambda}}{n!}, \tag{2.4}$$

where n is the number of absorbed photons and λ the average number of photons absorbed by one molecule. Although this simplification makes it impossible to use fundamental molecular constants (energy levels couplings) for calculations of multiphoton excitation dynamics, it provides a simple semi-empirical description of IRMPD applicable, for example, for a simplified numerical modelling of multiphoton excitation process.

The next simplification could be, for example, to decrease the number of up-pumping steps required by the molecule to reach the dissociation limit. In this case, absorption of several photons is considered as one up-pumping step with a certain average rate. The mathematical description of such a model would be quite simple, but its use would at best be limited to very particular cases. However, as it will be shown later in this work, in some cases a properly selected simplified model can provide a not only qualitative, but also quite consistent quantitative description of a process.

2.1.3 Isotopic selectivity of IRMPD

Early experiments on IRMPD of polyatomic molecules in an intense CO_2 laser field demonstrated that the efficiency of the process (dissociation yield) is different for molecules with different isotopic composition [1, 8–10]. Although the isotopic selectivity of IRMPD was expected based on the differences in absorption spectra of molecules containing different isotopes, only after the first experimental realizations of multiphoton dissociation did the significance of the isotopic effects become clear. Initial qualitative explanations of isotope selectivity of IRMPD suggested that only a few initial resonant steps of multiphoton excitation are selective. Once the molecule reaches the region of the vibrational quasicontinuum, its absorption spectrum considerably broadens due to the high density of energy levels and mutual couplings between vibrational modes. This results in a non-resonant character of excitation through this region and hence excludes the isotopically selective effects. Recent experiments on IRMPD of molecules pre-excited to the vibrational quasicontinuum region (see section 2.2.3) have shown, however, that in spite of broadening of the absorption spectrum in the quasicontinuum, the isotopic shift still plays an important role due to the large number of absorption steps required for a molecule to reach the dissociation limit.

2.1.4 Role of collisions in the IRMPD process

The role of collisions between molecules in multiphoton excitation has not been discussed in previews sections. In cases were IRMPD is performed in the static gases at sample pressures above 0.5-1 Torr, where the average time delay between collisions is shorter or comparable with the typical CO_2 laser pulse duration, the influence of this phenomenon cannot be neglected. Moreover, the application of the IRMPD process for industrial scale isotope separation must use high sample pressures to achieve reasonable levels of productivity, and this requires the collisional IRMPD processes to be understood. There are a number of collisional processes that will influence the IRMPD. Lyman *et al.* [11] have given an extensive compilation of collision effects in multiphoton excitation. The following principal effects were discussed:

1. Rotational hole filling. In the case when multiphoton excitation of a molecule through a certain energy region is possible only by one or very few resonant transitions starting at some particular rovibrational states, depletion of these states ("rotational hole burning") creates a bottleneck for the process. This effect is particulary important for the molecules with a relatively high onset of the vibrational quasicontinuum. Collisions between molecules lead to redistribution of rotational energy and, hence, re-population of the depleted levels, or "hole filling", which increases the efficiency of IRMPE.

2. Collisional line broadening. This effect can facilitate the excitation through the zone of lower vibrational levels (***Zone I*** in Figure 2.2), since it helps counteract the detuning caused by vibrational anharmonicity. However, under typical experimental conditions, its role is negligible in comparison with power broadening and rotational compensation of anharmonic shift of vibrational levels.

3. V-T and V-R relaxation. Quenching of the vibrational energy into translation or rotation leads to decrease of multiphoton dissociation probability and to increased possibility of thermally induced effects.

4. Collisional V-V energy transfer. Collisions between molecules leads to redistribution of vibrational energy between excited and non-excited molecules and creation of a Boltzmann energy distribution. If this process is fast enough in comparison with multiphoton excitation, this results in lowering the dissociation yield and a loss in the selectivity of the IRMPD process. On the other hand, collisions between excited molecules may lead to transfer of a portion of vibrational energy from one of the colliding molecules to another (energy pooling). This may help the acceptor molecule to "jump" over the energy region where stepwise multiphoton excitation is low-probable.

5. Collisionally induced intramolecular energy transfer (IVR). Due to this effect the vibrational energy randomizes between different vibrational modes within a single molecule. If collisionless IVR process is rapid and complete, this type of collisional process will have no effect.

A few studies have observed that under certain conditions, collisions seem to enhance isotopic selectivity of IRMPD [12, 13]. In these IRMPD studies of CF_2HCl for carbon-13 enrichment increasing selectivity with increasing pressure of the working gas has been demonstrated. This effect has been attributed to different rates of V-V exchange of "hot" ensembles of carbon-12 and carbon-13 containing molecules with the ensemble of "cold" unexcited molecules of the main isotope (carbon-12) [13].

2.2 Overtone pre-excitation - IRMPD

As has been discussed in previous sections, the energy region of lower vibrational levels (***Case C*** of statistical mechanical model (Figure 2.1) and ***Zone I*** of the simplified model (Figure 2.2)) represents a natural obstacle for the multiphoton excitation process. Pumping through this region is the main factor limiting the final yield of IRMPD, and hence its utility for industrial-scale applications. However, IRMPE can be rather efficient once the molecule possesses sufficient energy to be in the vibrational quasicontinuum. Thus, preparing molecules directly in the quasicontinuum should considerably increase the overall efficiency of the IRMPD process. This idea has been realized for polyatomic molecules possessing a high-frequency vibration, for example CH or SiH stretch bands [14–16]. The overtones of these high-frequency modes can be used for excitation of molecules by radiation of visible or near-IR laser field. As the energy of excitation quickly distributes over all the molecular vibrational coordinates due to IVR [1, 17–19], in the time-scale of the IRMPD process (nanoseconds to tens of nanoseconds) the state of the molecules excited to quasicontinuum does not depend on the method of excitation - stepwise IRMPE or one-step excitation of a high-frequency vibration. The two-step dissociation process which consists of pre-excitation of an overtone of a high frequency vibration and consequent multiphoton dissociation of pre-excited molecules is called overtone pre-excitation - infrared multiphoton dissociation (OP-IRMPD).

2.2.1 Vibrational overtone excitation

In the harmonic oscillator approximation, the selection rule for transitions between vibrational states is $\Delta v = \pm 1$, where v is the vibrational quantum number. Thus, overtone transitions, which involve a change in the vibrational quantum number by more than 1, are forbidden in this approximation. In real molecules, this rule is slightly relaxed due to the effect of anharmonicity

of the oscillator wave function and/or non-linearity of dipole moment function. Nevertheless, absorption cross-sections of overtone transitions are weak and sharply decrease with increasing change in vibrational quantum number. As an example, absorption cross sections for transitions corresponding to the fundamental CH stretch vibration of the CF_3H molecule and some of its overtones are presented in Table 2.1[1].

Transition	G, pm^2
$1 \leftarrow 0$	0.132
$2 \leftarrow 0$	$(2 \pm 0.4) \times 10^{-4}$
$3 \leftarrow 0$	$(3 \pm 1) \times 10^{-5}$
$4 \leftarrow 0$	$(2.4 \pm 1) \times 10^{-6}$

Table 2.1: Integral absorption cross sections of CH stretch fundamental vibration and some its overtones for CF_3H molecule [20].

Here G is the integral absorption cross section of a band defined as:

$$G = \int_{band} \sigma(\tilde{\nu}) \left(\frac{d\tilde{\nu}}{\tilde{\nu}} \right), \tag{2.5}$$

where $\sigma(\tilde{\nu})$ is the absorption cross section as a function of frequency.

As one can see, the efficiency of first overtone excitation is almost three orders of magnitude smaller than for excitation of the fundamental vibration. The efficiency of excitation of higher overtones drops off approximately by an order of magnitude for each additional quantum of vibrational excitation. However, as it will be demonstrated later in this work, even such a small absorption cross section of the vibrational overtone transitions can be sufficient for application of the overtone pre-excitation approach for a highly efficient isotope separation process.

2.2.2 Infrared laser assisted photofragment spectroscopy

The OP-IRMPD approach was first developed for high-resolution spectroscopy of highly vibrationally excited states of jet-cooled polyatomic molecules [14, 21]. The spectroscopic technique developed on the basis of this approach has been named infrared laser assisted photofragment spectroscopy (IRLAPS). Figure 2.3 describes the idea of this technique using the CF_3H molecule as an example.

[1] Due to a strong Fermi resonance between the CH stretch (ν_1) and the HCF bend (ν_4) vibrations in CF_3H molecule its CH stretch overtone transitions are split into $(N + 1)$ components, where N is the number of quanta in the zeroth-order CH stretch state [20]. These split levels form so-called polyads. Table 2.1 shows the integral absorption cross sections of the strongest lines of polyads corresponding to different CH stretch overtone transitions.

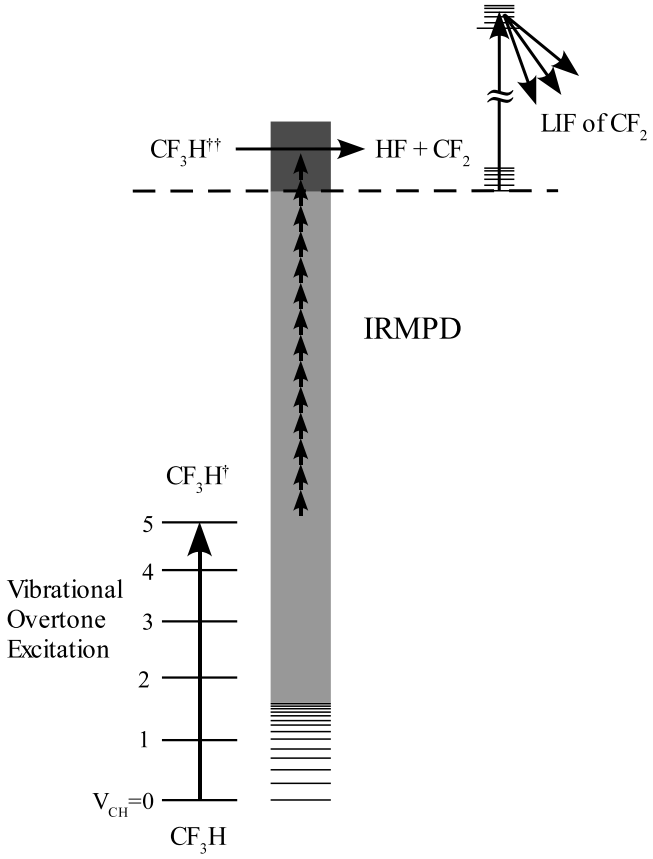

Figure 2.3: Energy level schematic for infrared laser assisted photofragment spectroscopy (IRLAPS) of vibrational overtones of CF_3H [21].

In the first step of this process a tunable dye laser pre-excites the molecule to a vibrational overtone level - it is measurement of the spectrum resulting from this transition that is the goal of the experiment. The amount of the pre-excited molecules is a function of the frequency of the pre-excitation laser, and in the absence of saturation it is simply proportional to the absorption cross section $\sigma(\tilde{\nu})$. To detect this absorption, the pre-excited molecules are dissociated by IRMPD and the resulting fragments are detected spectroscopically by laser induced fluorescence (LIF). Scanning the excitation laser while monitoring the LIF intensity produces the excitation spectrum that mirrors the vibrational overtone absorption spectrum. Because the overtone transitions are weak, one wants to dissociate selectively only the pre-excited molecules and not a large excess of ground state molecules, since the products resulting from the dissociation of the latter would mask any change due to the overtone excitation. To avoid dissociation of ground state molecules the three following properties of the IRMPD process can be used.

1. The laser intensity dependence. Multiphoton excitation through the region of lower vibrational levels is facilitated by power broadening which occurs at high laser intensity

(energy unit per unit area per second). On the other hand, excitation of the molecules pre-excited to the region of vibrational quasicontinuum depends mostly on the integral fluence of the dissociation laser pulse (energy per unit area) [9, 22]. Thus, using moderate laser intensities may prevent dissociation of the ground-state molecules, whereas pre-excited molecules still may be efficiently dissociated provided the fluence of the dissociation laser is sufficient.

2. Anharmonic red-shift of the absorption spectrum of excited molecules [8, 14]. Because of this red-shift, applying a dissociation laser wavelength detuned to the red side from the maximum of the absorption spectrum of ground-state molecules will result in preferential multiphoton excitation of pre-excited molecules.

3. Fluence dependence. The initial energy level of the multiphoton excitation process for pre-excited molecules lies higher than the one for ground state molecules. It means that pre-excited molecules need to collect less infrared photons from the dissociation laser to reach its dissociation threshold. Thus, the laser fluence required for dissociation of pre-excited molecules is lower [8, 23]. The correct choice of the dissociation laser fluence may further increase the discrimination between the ground-state and pre-excited molecules.

The advantage of the IRLAPS method as a spectroscopic technique is its high sensitivity which allows the detection of extremely weak vibrational overtone transitions under molecular jet expansion conditions. Since its development in the beginning of 1990's, the IRLAPS method has been applied for obtaining high resolution overtone spectra of a number of molecules, contributing to understanding the dynamics of intramolecular vibrational energy redistribution (IVR) process [14, 15, 21, 24–28].

2.2.3 Isotopic selectivity of OP-IRMPD

The total isotopic selectivity of the two-step overtone pre-excitation - infrared multiphoton dissociation process is the product of the selectivities of the individual steps:

$$S = S_{op} S_d, \tag{2.6}$$

where S_{op} is the selectivity of overtone pre-excitation and S_d the selectivity of the IRMPD step.

Under the usual conditions when overtone pre-excitation is a linear process (no multiphoton absorption and saturation effects), the selectivity of this step is simply determined by the overlap of absorption spectra of different isotopes at the wavelength of pre-excitation laser. The question about isotopic selectivity of the IRMPD step is more complex. On the one hand it is known that the multiphoton dissociation of the ground state molecules is isotopically selective (see section 2.1.3 on page 22). On the other hand, as has been emphasized in section

2.1.3, the earlier explanations of the isotopic selectivity of IRMPD suggested that only the initial, resonant steps of multiphoton excitation of ground state molecules are isotopically selective, whereas the excitation through the vibrational quasicontinuum is non-selective. In the OP-IRMPD approach, the starting level of the multiphoton excitation process lies already in quasicontinuum, so if this were true, one should not expect any additional selectivity in the second step ($S_d = 1$). However, one of the results of the IRLAPS experiments on the CF_3H molecule [24] shows that IRMPD of vibrationally pre-excited molecules still can be isotopically selective. Figure 2.4 reproduces the IRLAPS spectra of the second CH stretch overtone of jet-cooled CF_3H molecules. The 3_1 and 3_2 bands are two components of the $3\nu_1$ level which is

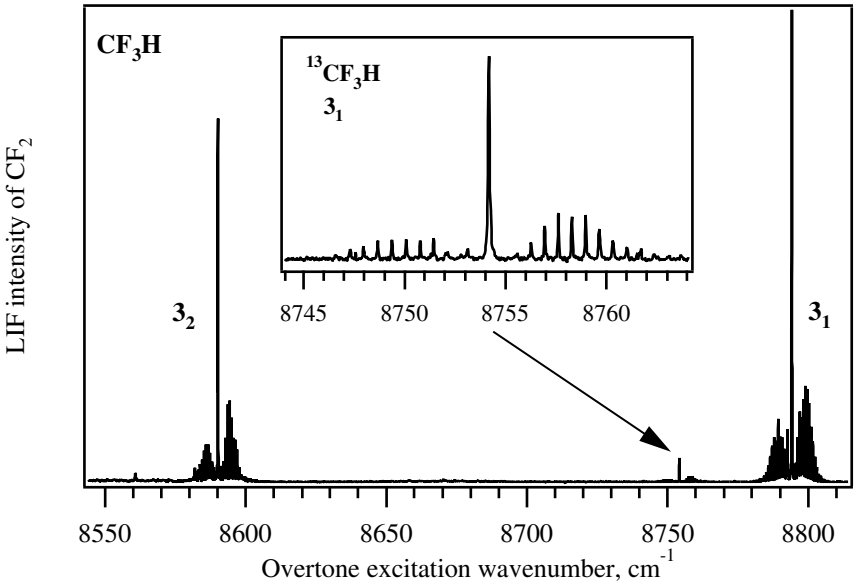

Figure 2.4: IRLAPS spectra of the jet cooled CF_3H molecule in the region of the second CH stretch overtone [24].

split due to Fermi resonance (see footnote on page 25). The small feature centered at 8752.9 cm^{-1} has been assigned to the 3_1 band of $^{13}CF_3H$. The integral intensity of this weak band is 2.9% of the 3_1 band of $^{12}CF_3H$, which is 2.5 times greater than expected from the natural abundance of carbon-13 (1.07% [29]). Since the overtone excitation under the experimental conditions of this experiment was linear, this discrepancy can be explained only by additional selectivity of the IRMPD step. Further experiments [30, 31] in which the mass spectrometric detection of the dissociation products was applied, has confirmed this suggestion.

2.2.4 Role of collisions in the OP-IRMPD process

As stated in Section 2.1.4 on page 23, several collisional processes can play an important role in the IRMPD of ground state molecules:

1. Rotational hole filling;
2. Collisional line broadening;
3. V-T and V-R relaxation;
4. Collisional V-V energy transfer;
5. Collisionally induced IVR.

The most important processes in the case of IRMPD of ground state molecules are collisional line broadening and collisional V-V energy redistribution. Unlike the situation of IRMPD of ground state molecules, rotational hole filling is not so important for multiphoton excitation of molecules pre-excited to the vibrational quasicontinuum region. However, if the molecules are pre-excited to an energy below the lower limit of the quasicontinuum, this phenomenon may still influence the IRMPD process, but its effect is not so considerable as for ground state molecules. The role of collisional V-V energy transfer, however, may in some sense be more important in the OP-IRMPD process. This is explained by lower intensities of the dissociation laser needed for dissociation of pre-excited molecules in comparison with those needed for IRMPD of ground state molecules. Using lower intensities will make the rate of the multiphoton excitation through the quasicontinuum lower in the case of the OP-IRMPD, and, hence, the competition between multiphoton excitation and collisional relaxation processes may be more influenced by collisional relaxation.

The isotopic selectivity of dissociation also depends on the collisions between excited molecules. As it has been demonstrated in [30, 31], an increase of the sample pressure or the time-delay between pre-excitation and dissociation laser pulses results in an increase of selectivity and a drop in the dissociation yield. This phenomenon has been explained by selectivity of the collisional deactivation of pre-excited molecules (see for example [32–34]). The deactivation rate for the $^{12}CF_3H$ molecules could be higher than for $^{13}CF_3H$ due to the resonant character of collisional vibrational energy transfer between excited molecules and the bulk of ground state molecules, which are mostly $^{12}CF_3H$, due to the natural abundance of carbon-12 isotope over carbon-13. Another suggested explanation of collisionally enhanced selectivity in the IRMPD of pre-excited molecules is that due to the loss of the energy in the collisions absorption of more photons are required for the molecule to reach the dissociation threshold. If we assume that the absorption of each photon is an elementary isotopically selective step, then an increase of

the number of photons will lead to an increase of total selectivity of the multiphoton process. Latest experiments on the OP-IRMPD of isotopically inverted CF_3H shows that both suggested mechanisms have a considerable influence on the phenomenon of collisionally enhanced isotopic selectivity of the OP-IRMPD process [35].

2.3 Molecules of interest

Due to the nature of overtone excitation and infrared multiphoton dissociation processes, only the molecules having certain specific properties are suitable for studying by the IRLAPS technique or for use as parent molecules in OP-IRMPD laser isotope separation approach. Below we list the major requirements which a molecule has to fulfill to be considered as a suitable candidate for the MLIS by OP-IRMPD.

1. Possibility of (isotopically selective) excitation to the vibrational quasicontinuum *via* overtone excitation
   (a) Existence of high-frequency vibration coordinate (OH, CH, SiH, SH, ... stretch vibrations);
   (b) Overtone absorption cross-section sufficient for excitation of considerable fraction of molecules;
   (c) Good spectral discrimination between molecules containing different isotopes at the wavelength corresponding to the excited overtone;
   (d) Relatively low lower limit for the onset of the vibrational quasicontinuum.
2. Possibility of selective dissociation the pre-excited molecules *via* multiphoton excitation:
   (a) Existence of a vibrational coordinate suitable for multiphoton excitation by existing high-power pulsed laser sources (for example CO_2 laser or NH_3 laser having tuning regions between 9.7 and 10.8 μm and between 10.8 and 12.8 μm respectively);
   (b) Good spectral discrimination between pre-excited and ground state molecules at the wavelength of the dissociation laser.
3. Low dissociation energy.
4. Existence of a method of a chemical stabilization of photofragments.

Requirements for the molecules to be suitable for the IRLAPS technique are slightly less stringent in the sense that the productivity of the process is not critical in this case. So,

absorption cross sections can be relatively low and the dissociation threshold relatively high in comparison with the requirements of the OP-IRMPD based MLIS approach.

In this work, the process of OP-IRMPD under collisional conditions has been studied for several molecules fulfilling the above requirements. Table 2.2 represents the important spectroscopic properties of the molecules which have been selected for studying in this work.

CF_3H

CH stretch (ν_1)

v	$^{13}CF_3H$	$^{12}CF_3H$
1_1	3024.6[a]	3035.5[b]
2_1	5936.6[a]	5959.4[b]
3_1	8753.0[a]	8792.7[b]

CF sym. stretch (ν_2)

$^{13}CF_3H$	$^{12}CF_3H$
1115.9[c]	1141.5[d]

$SiHCl_3$

SiH stretch (ν_1)

v	$^{30}SiHCl_3$	$^{28}SiHCl_3$
1_1	2257.8[f]	2260.3[e,f]
2_1		4450.4[e]
3_1		6570.8[e]

SiH bend (ν_4)

$^{30}SiHCl_3$	$^{28}SiHCl_3$
	807.9[f]

NH_3

NH sym. stretch (ν_1) / umbrella NH bend (ν_2)

ν_1	ν_2	$^{15}NH_3$	$^{14}NH_3$
1	0^+		3336.02[g]
1	0^-		3337.08[g]
0	1^+	928.46[h]	932.43[i]
0	1^-	962.89[h]	968.12[i]
0	2^+	1591.2[j]	1597.47[k]
0	2^-	1870.9[j]	1882.18[k]
0	3^+	2369.3[j]	2384.15[l]
0	3^-	2876.1[j]	2895.52[l]

[a] Reference [36]; [b] Reference [20]; [c] Reference [37]; [d] Reference [38];
[e] Reference [39]; [f] Reference [40]; [g] Reference [41]; [h] Reference [42];
[i] Reference [43]; [j] Reference [44]; [k] Reference [45]; [l] Reference [46].

Table 2.2: Important spectroscopic properties of the studied molecules.

Table 2.3 represents the fastest dissociation channels, activation energies for unimolecular decomposition and possible photofragments stabilization reactions for the studied molecules.

Molecule	Fastest dissociation channel	Activation energy for unimolecular decomposition (cm^{-1})	Photofragments stabilization reaction
CF_3H	$CF_3H \longrightarrow CF_2 + HF$ [47]	25650 [48]	$CF_2 + CF_2 + M \longrightarrow C_2F_4 + M$ [49,50] or $CF_2 + NO_2 \longrightarrow COF_2 + NO$ [51]
$SiHCl_3$	$SiCl_2 \longrightarrow CF_2 + HCl$ [52]	25205 [53]	$n{\cdot}SiCl_2 \longrightarrow (SiCl_2)_n$ [53,54]
NH_3	$NH_3 \longrightarrow NH_2 + H$ [55,56]	37352 [57]	

Table 2.3: Dissociation channels, activation energies for unimolecular decomposition and product stabilization reactions for the studied molecules.

Most of research presented in this work has been done on the CF_3H molecule in view of carbon isotope separation. This research results in a better understanding of the process of OP-IRMPD under collisional conditions. The optimization of process parameters based on this understanding led us to considerably enhance the performance of the isotope separation process. The research on carbon isotope separation and CF_3H OP-IRMPD under collisional conditions is represented in Chapter 3.

Chapter 4 presents a study of the possibility of using the OP-IRMPD approach for silicon isotope separation with $SiHCl_3$ as the parent molecule.

Chapter 5 describes the investigation of the OP-IRMPD process as applied to the NH_3 molecule under collisional conditions. The levels splitting in this molecule make it an interesting candidate for such a study in that the spacing of higher vibrational levels of the umbrella mode are very different than the lower ones. This should provide an extremely high degree of discrimination between IRMPD of pre-excited molecules and those in the ground vibrational state. Results of NH_3 IRMPD experiments [55, 56, 58–62] show that multiphoton dissociation of ground state molecules is indeed very difficult, occurring only under irradiation by a very intense laser field or at pressure where there are substantial numbers of collisions. Overtone pre-excitation should decrease the threshold fluence of IRMPD process considerably.

Bibliography

[1] V. S. Letokhov, *Nonlinear Laser Chemistry*, Springer-Verlag, Berlin, Heidelberg, New York, 1983.

[2] M. Quack, *J. Chem. Phys.*, 1978, **69**, 1282–1307.

[3] M. Quack, *Adv. Chem. Phys.*, 1982, **50**, 395–473.

[4] V. S. Letokhov, *Progress in optics*, 1978, **16**.

[5] M. Quack, *Infrared Phys.*, 1989, **29**, 441–466.

[6] M. Quack, *Infrared Phys.Technol.*, 1995, **36**, 365–380.

[7] M. Quack in *Encyclopedia of Computational Chemistry*, Vol. 3; John Wiley & Sons, Chichester, UK, 1998; pp. 1775–1791.

[8] V. N. Bagratashvili, V. S. Letokhov, A. A. Makarov, and E. A. Ryabov, *Multiple Photon Infrared Laser Photophysics and Photochemistry*, Harwood, Amsterdam, 1985.

[9] T. B. Simpson, J. G. Black, I. Burak, E. Yablonovitch, and N. Bloembergen, *J. Chem. Phys.*, 1985, **83**, 628–640.

[10] V. S. Letokhov, *Laser Spectroscopy of Highly Vibrationally Excited Molecules*, Adam Hilger, Bristol, New York, 1989.

[11] J. L. Lyman, G. P. Quigley, and O. P. Judd in *Multiple-photon excitation and dissociation of polyatomic molecules*, Vol. 3; Springer-Verlag, Berlin, Heidelberg, New York, London, Paris, Tokyo, 1986; pp. 9–94.

[12] M. Gauthier, C. G. Cureton, P. A. Hackett, and C. Willis, *Appl. Phys. B*, 1982, **28**, 43–50.

[13] A. V. Evseev, V. S. Letokhov, and A. A. Puretzky, *Appl. Phys. B*, 1985, **36**, 93–103.

[14] R. D. F. Settle and T. R. Rizzo, *J. Chem. Phys.*, 1992, **97**, 2823–2825.

[15] O. V. Boyarkin and T. R. Rizzo, *J. Chem. Phys*, 1995, **103**, 1985–1988.

[16] J. Makowe, O. V. Boyarkin, and T. R. Rizzo, *J. Phys. Chem. A*, 2000, **104**, 11505–11511.

[17] M. Quack, *Annu. Rev. Phys. Chem.*, 1990, **41**, 839–874.

[18] K. K. Lehmann, G. Scoles, and B. H. Pate, *Annu. Rev. Phys. Chem.*, 1994, **45**, 241–274.

[19] D. J. Nesbitt and R. W. Field, *J. Phys. Chem.*, 1996, **100**, 12735–12756.

[20] H.-R. Dübal and M. Quack, *J. Chem. Phys.*, 1984, **81**, 3779–3791.

[21] O. V. Boyarkin, R. D. F. Settle, and T. R. Rizzo, *Ber. Bunsen Ges. Phys. Chem.*, 1995, **99**, 504–513.

[22] O. V. Boyarkin, T. R. Rizzo, D. Rueda, M. Quack, and G. Seyfang, *J. Chem. Phys.*, 2002, **117**, 9793–9805.

[23] M. C. Gower and T. K. Gustafson, *Optics Commun.*, 1977, **23**, 69–72.

[24] O. V. Boyarkin and T. R. Rizzo, *J. Chem. Phys*, 1996, **105**, 6285–6292.

[25] O. V. Boyarkin, L. Lubich, R. D. F. Settle, D. S. Perry, and T. R. Rizzo, *J. Chem. Phys.*, 1997, **107**, 8409–8422.

[26] O. V. Boyarkin, T. R. Rizzo, and D. S. Perry, *J. Chem. Phys.*, 1999, **110**, 11346–11358.

[27] O. V. Boyarkin, T. R. Rizzo, and D. S. Perry, *J. Chem. Phys.*, 1999, **110**, 11359–11367.

[28] A. Chirokolava, D. S. Perry, O. V. Boyarkin, M. Schmid, and T. R. Rizzo, *J. Chem. Phys.*, 2000, **113**, 10068–10072.

[29] Commission on Atomic Weights and Isotopic Abundances report for the International Union of Pure and Applied Chemistry, *Pure and Applied Chemistry*, 1998, **70**, 217–235.

[30] M. Kowalzcyk *Highly Selective Molecular Laser Isotope Separation of Carbon-13* PhD thesis, Ecole Polytechnique Fédérale de Lausanne, Switzerland, 2000.

[31] O. V. Boyarkin, M. Kowalzcyk, and T. R. Rizzo, *J. Chem. Phys.*, 2003, **118**, 93–103.

[32] J. C. Stephenson, R. E. Wood, and C. B. Moore, *J. Chem. Phys.*, 1968, **48**, 4790–4791.

[33] C. Coletti and G. D. Billing, *J. Chem. Phys.*, 2000, **113**, 4869–4875.

[34] C. Coletti and G. D. Billing, *Chem. Phys. Lett.*, 2002, **356**, 14–22.

[35] R. Bossart PhD thesis, Ecole Polytechnique Fédérale de Lausanne, Switzerland, to be published.

[36] H. Hollenstein, M. Lewerenz, and M. Quack, *Chem. Phys. Lett.*, 1990, **165**, 175–183.

[37] H. F. Chambers, R. W. Kirk, J. K. Thompson, M. J. Warner, and P. M. Wilt, *J. Mol. Spec.*, 1975, **58**, 76–86.

[38] J. P. Champion and G. Graner, *Mol. Phys.*, 1986, **58**, 475–484.

[39] Y. Ding, S.-G. He, J.-J. Zheng, S.-M. Hu, X.-H. Wang, and Q.-S. Zhu, *Mol. Phys.*, 2001, **99**, 1669–1678.

[40] W. Fuß and S. Weizbauer, *Ber. Busenges. Phys. Chem.*, 1995, **99**, 289–295.

[41] V. Špirko, *J. Mol. Spectr.*, 1983, **101**, 30–47.

[42] Š. Urban, D. Papoušek, S. P. Belov, A. F. Krupnov, M. Y. Tret'yakov, K. Yamada, and G. Winnewisser, *J. Mol. Spectr.*, 1983, **101**, 16–29.

[43] Š. Urban, V. Špirko, D. Papoušek, J. Kauppinen, S. P. Belov, L. I. Gershstein, and A. F. Krupnov, *J. Mol. Spectr.*, 1981, **88**, 274–292.

[44] G. DiLonardo, L. Fusina, A. Trombetti, and I. M. Mills, *J. Mol. Spectr.*, 1982, **92**, 298–325.

[45] Š. Urban, V. Špirko, D. Papoušek, R. S. McDowell, N. G. Nereson, S. P. Belov, L. I. Gershstein, A. V. Maslovskij, A. F. Krupnov, J. Curtis, and K. N. Rao, *J. Mol. Spectr.*, 1980, **79**, 455–495.

[46] I. Kleiner, G. Tarrago, and L. R. Brown, *J. Mol. Spectr.*, 1995, **173**, 120–145.

[47] K. P. Schug, H. G. Wagner, and F. Zabel, *Ber. Bunsenges. Phys. Chem.*, 1979, **83**, 167–175.

[48] Y. Okamoto and M. Tomonari, *J. Phys. Chem. A*, 2000, **104**, 2729–2733.

[49] F. W. Dalby, *J. Chem. Phys.*, 1964, **41**, 2297–3203.

[50] F. Battin-Leclerc, A. P. Smith, G. D. Hayman, and T. P. Murrells, *J. Chem. Soc., Faraday Trans.*, 1996, **92**, 3305–3313.

[51] M. M. Ivanenko, H. Handreck, J. Göthel, W. Fuß, K.-L. Kompa, and P. Heiring, *Appl. Phys. B*, 1997, **65**, 577–582.

[52] B. B. Lavrushenko, A. V. Baklanov, and V. P. Strunin, *Spechtrochim. Acta*, 1990, **46A**, 479–481.

[53] M.-D. Su and H. B. Schlegel, *J. Phys. Chem.*, 1993, **97**, 9981–9985.

[54] G. H. Kruppa, S. K. Shin, and J. L. Beauchamp, *J. Phys. Chem.*, 1990, **94**, 327–331.

[55] J. D. Campbell, G. Hancock, J. B. Halpern, and K. H. Welge, *Opt. Commun.*, 1976, **17**, 38–42.

[56] J. D. Campbell, G. Hancock, J. B. Halpern, and K. H. Welge, *Chem. Phys. Lett.*, 1976, **44**, 404–410.

[57] S. T. Gibson, J. P. Greene, and J. Berkowitz, *J. Chem. Phys*, 1985, **83**, 4319–4328.

[58] R. V. Ambartsumyan, V. S. Letokhov, G. N. Makarov, A. G. Platova, A. A. Puretski, and O. A. Tumanov, *Sov. Phys. JETP*, 1973, **37**, 392–398.

[59] V. S. Letokhov, E. A. Ryabov, and O. A. Tumanov, *Sov. Phys. JETP*, 1973, **36**, 1069–1073.

[60] A. Hartford Jr., *Chem. Phys. Lett*, 1978, **57**, 352–356.

[61] P. Avouris, M. M. T. Loy, and I. Y. Chan, *Chem. Phys. Lett.*, 1979, **63**, 624–629.

[62] I. Hanazaki, K. Kasatani, and K. Kuwata, *Chem. Phys. Lett.*, 1980, **75**, 123–127.

Chapter 3

Molecular laser isotope separation of carbon-13

3.1 Introduction

3.1.1 State of research in the field of carbon-13 laser isotope separation

The bulk of the carbon-13 currently on the market is produced by multi cycle low temperature distillation of carbon monoxide. Natural CO (containing 1.07% carbon-13 [1]) is cryogenically liquefied and then distilled in liquid nitrogen cooled columns which measure kilometers in length and which need several months to reach the separation equilibrium. The end product of the process is carbon monoxide with greater than 99% carbon-13, although this particular method simultaneously enriches the oxygen-18 isotope. The relatively high market price of carbon-13 provides motivation for developing more economical separation technologies. One of the directions of the search for effective isotope separation methods is to use the spectroscopic differences between different isotopic species (either atoms or molecules) in combination with specific properties of laser radiation (in particular, the ability of lasers to produce very narrow bandwidth radiation) [2–6].

Recently a laser based approach has been implemented for commercial production of carbon-13 [7, 8]. This approach, called molecular laser isotope separation (MLIS), is based on the phenomena of isotopically selective infrared multiphoton dissociation (IRMPD) of polyatomic molecules by the radiation of a pulsed TEA CO_2 laser [9, 10]. Selectivity arises from the fact that the vibrational frequencies of different isotopic species are slightly shifted. Tuning the frequency of the dissociating laser to an absorption feature of the desired isotopomer allows preferential multiphoton dissociation of these molecules, resulting in isotopic enrichment of the dissociation products. Among the many compounds tested for the molecular laser isotope

separation of carbon, the most interesting results have been achieved on molecules of the type CF_3X, where X=Br, Cl, I [11–13], and on CF_2HCl [2, 3, 14–21]. In all these molecules, the frequency of the ^{13}CF stretch vibration is within the tuning range of TEA CO_2 laser, and the isotopic shift from the carbon-12 species is appreciable.

A few parameters are conventionally used to characterize the IRMPD process, and we introduce them here to compare the merits of different approaches. The first is the selectivity factor S, defined as a ratio of dissociation probabilities of two different isotopic species. For practical use it can be expressed as

$$S = \frac{^{13}e_f}{^{13}e_0}, \tag{3.1}$$

where $^{13}e_f$ is the $^{13}C/^{12}C$ ratio in the final product and $^{13}e_0$=0.011 is the $^{13}C/^{12}C$ ratio in natural abundance. Table 3.1 illustrates the correspondence between the selectivity calculated using Equation (3.1) and the carbon-13 concentration in final product (enrichment). A second

Enrichment	S
10%	10
50%	90
80%	360
90%	810
95%	1710
97%	2900
98%	4400
99%	8900

Table 3.1: Carbon-13 enrichment and the corresponding selectivity.

factor for characterizing the IRMPD process is the dissociation yield, β, which provides a measure of the productivity. It is defined as the ratio of the number of dissociated molecules per laser pulse to the total number of molecules of this isotopic species within irradiated volume.

Presently, the only commercial approach for MLIS of carbon-13 is based on IRMPD of CF_2HCl by a pulsed CO_2 laser [7]. This method relies on the 27 cm^{-1} isotopic shift [22] in the IR absorption spectrum of the carbon-13 molecules relative to those with carbon-12 to achieve selective IRMPD of CF_2HCl, which occurs through the lowest energy reaction channel

$$CF_2HCl \xrightarrow{n h\nu} CF_2 + HCl.$$

The CF_2 dissociation fragments recombine *via* 3-body collisions with a rate constant of 2.2×10^{10} cm^3/mol.sec [23], resulting in stable C_2F_4 molecules that are separated from the parent molecules by cryogenic distillation. One of the most comprehensive studies of this process, which

summarizes most of the earlier observations, has been reported by Gauthier and coworkers [14]. In this work, a CO_2 laser with well-defined 80 ns pulses is employed for isotopically selective IRMPD of chlorodifluoromethane. The selectivity, dissociation yield and laser energy expenditure per $^{13}CF_2$ fragment have been measured for various frequencies and energy fluence (energy per unit area) of the laser over a wide range of sample pressures. Their results can be summarized as follows:

1. Selectivity up to 1000 has been reached for CO_2 laser lines, which are well shifted to the low frequency side of the ν_3 band of ground state $^{13}CF_2HCl$. This corresponds to an enrichment of carbon-13 to 91.7% and can be achieved at sample pressure up to 100 mbar.

2. The dissociation yield is 0.1-0.2% for this selectivity. Both the selectivity and yield are achieved at an optimal laser fluence of about 3 J/cm^2.

3. Under these conditions, the energy expenditure is near 2000 CO_2 laser photons per dissociated molecule. This value is very high, since only 18 CO_2 laser photons are required for an isolated CF_2HCl molecule to reach its dissociation threshold.

4. Relatively high dissociation yield (4%) and fairly low laser energy expenditure (130 photons) could be achieved at 100 mbar sample pressure but at reduced selectivity (S <100).

To be able to understand the fundamental limitations of this or any MLIS approach, one must consider the mechanism of IRMPD. The IRMPD process can be conceptually divided into two stages. In the first stage, a laser field promotes a vibrationally ground state molecule through a region where the density of vibrational states is low. For small polyatomic molecules like CF_2HCl, the lack of exact resonances for the absorption of each photon creates a bottleneck to the up-pumping process. Pumping through this region is facilitated by increased intensity (i.e., energy per unit area per unit time) of the laser field, as power broadening of the energy levels partially compensates the sparcity of resonances [24]. At some level of excitation, the molecule reaches an energy region called the vibrational quasicontinuum where the state density is high enough such that there is essentially a vibrational level within the laser bandwidth at every excitation energy. In this region, which is characterized by a substantially higher absorption cross-section, the molecule must simply collect enough laser photons to reach the dissociation threshold, and pumping through this region is governed primarily by the laser fluence (energy per unit area) rather than intensity [25].

It is clear that isotopic selectivity in the single-frequency IRMPD work of Gauthier *et al.* comes primarily from exploiting the isotopic spectral shift and is achieved mostly in the first stage of the process. Consequently, overlap of the absorption bands of different CF_2HCl isotopic species produces an intrinsic limit to the selectivity.

The next major advance in highly selective carbon-13 MLIS using CF_2HCl was achieved by performing IRMPD using multiple CO_2 lasers of different frequencies [15,17]. In this approach, the frequency and fluence of one laser can be optimized for high selectivity in pumping through the low energy region of discrete vibrational levels, while the frequency and fluence of the second or subsequent lasers can be optimized for efficient pumping through the quasicontinuum to dissociation. One of the most comprehensive studies of this general approach has been reported by the group of Letokhov [15], in which they use up to four different CO_2 laser frequencies simultaneously to achieve IRMPD of CF_2HCl. They investigate the isotopic selectivity and dissociation yield of the process as a function of the number of different lasers, their frequencies, the time-delay between the laser pulses, the fluence of each laser, and the sample temperature and pressure. The main results of this multi-parameter study can be summarized as follows:

1. In two-frequency IRMPD experiments, selectivity up to 1000 at 1.7% dissociation yield was achieved for 5 mbar of CF_2HCl at room temperature. The required laser fluence was on the order of 1.5-2 J/cm^2. Three and four frequency dissociation further improves the output characteristics of the process, but not as dramatically as changing from single-frequency to two-frequency IRMPD.

2. Selectivity as high as S=6000 at appreciable dissociation yield ($^{13}\beta$=1.2%) was achieved using a 2.5 mbar sample cooled to t=-64 °C.

Although the multi-frequency IRMPD approach greatly improves both the selectivity and the dissociation yield of the process, the highest selectivity is achieved only at relatively low sample pressure (2.5 mbar) and only with the parent molecules cooled. Moreover, the measured dissociation yield of 1.2% is still relatively low. Taken together, these factors diminish the practicality of the multi-frequency IRMPD approach for producing high purity carbon-13.

Commercial implementation of single-laser MLIS process by IRMPD of CF_2HCl in Kaliningrad is based on an elegant engineering solution that places a dissociation gas reactor into the TEA CO_2 laser cavity [7]. The high fluence of laser radiation inside the cavity allows an increased dissociation yield that makes this process economically profitable. However, the level of isotopic enrichment in the final C_2F_4 product is typically only 35-50%. While there are some applications of moderately enriched carbon-13, the vast majority of enriched carbon-13 is currently used for medical applications in so-called breath tests [26], which require 99% isotopic purity. Because of this, the C_2F_4 pre-enriched in Kaliningrad undergoes further enrichment to 99% using gas centrifuge facilities. This significantly increases the production cost of the isotopes and makes the single-laser technology difficult to compete with conventional low temperature distillation.

To summarize the cited studies of carbon laser isotope separation, one can conclude that

IRMPD is only competitive with conventional techniques for moderate (below 50%) carbon-13 enrichment. To achieve 99% enrichment required for medical applications, the process has to be repeated several times, and each time the enriched product has to be chemically converted to a molecule suitable for the next MLIS cycle. Alternatively, the process could be combined with a traditional technology to reach the final highly enriched product. Either approach complicates the overall process and significantly increases cost of the product. An efficient, highly-selective single-stage process would therefore be highly desirable.

3.1.2 OP-IRMPD approach to carbon-13 isotope separation

A further step forward in the MLIS technique has been recently carried out in the Laboratory of Molecular Physical Chemistry at the Swiss Federal Institute of Technology. In this approach, vibrational overtone pre-excitation of the parent molecules is used to overcome the bottleneck that occurs when pumping them through the zone of low lying vibrational levels with a CO_2 laser. The applicability of the new approach has been demonstrated for carbon [27, 28] and silicon [29, 30] isotope separation using CF_3H and SiH_4 respectively. A schematic diagram representing the OP-IRMPD based approach to laser carbon isotope separation with CF_3H as a parent molecule is represented in the Figure 3.1.

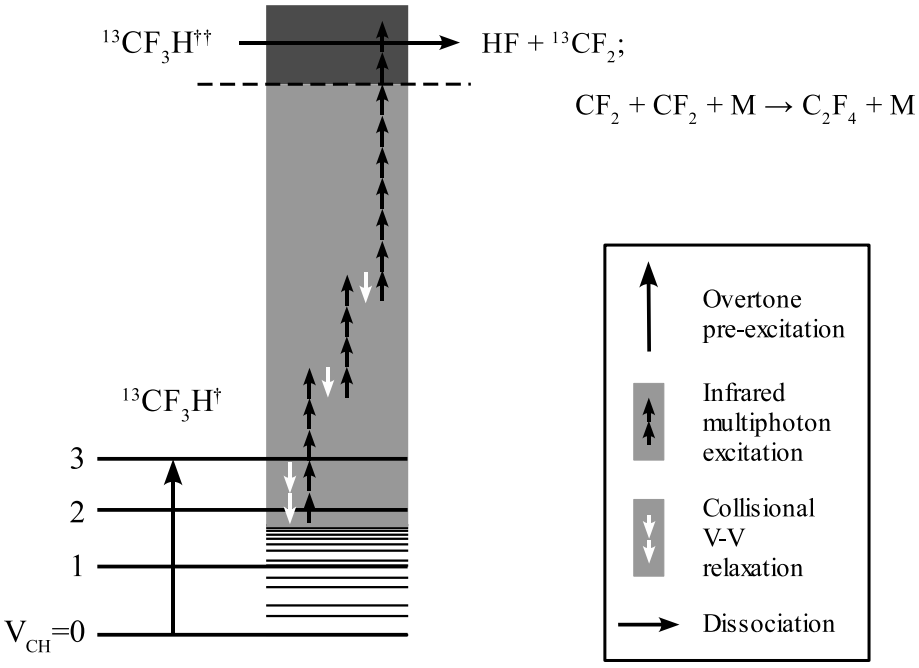

Figure 3.1: Schematic energy diagram of the overtone pre-excitation-IRMPD approach as it is applied for highly selective isotope separation of carbon-13 using CF_3H as the starting material.

The OP-IRMPD MLIS process consists of two major steps. In the first step, a near-infrared

laser pulse pre-excites molecules containing the desired isotope *via* a low vibrational overtone transition of a high frequency vibration mode (CH stretch-bend vibration). In the second step, a CO_2 laser pulse selectively dissociates the pre-excited molecules by multiphoton absorption *via* the CF stretch vibration. Isotopic selectivity is gained at each of these two steps. The selectivity of the first step is highest and it is determined by the ratio of absorption cross-sections of $^{13}CF_3H$ and $^{12}CF_3H$ at the wavelength of pre-excitation laser. For instance, pre-excitation of CF_3H to the second CH stretch-bend overtone results in an isotopic selectivity of up to 620 for this step, meaning that up to 87% of the pre-excited molecules are $^{13}CF_3H$. The isotopic selectivity of the IRMPD step is significantly less, especially in the absence of significant collisional vibrational deactivation (low pressure and/or short delay between the two laser pulses). Boyarkin *et al.* have found, however, that an increase in selectivity by up to a factor of 16 can be achieved in the IRMPD step if the process occurs under collisional conditions (high pressure and/or long delay between the two pulses) [28]. This has allowed up to 99 % of carbon-13 enrichment of the final product in a single stage process. As described below, this phenomenon of collisionally-induced selectivity has been attributed to isotopic effects in vibrational energy deactivation.

As Figure 3.1 attempts to illustrate, the processes of collisional vibrational relaxation occurs during the time delay between the pre-excitation and dissociation pulses as well as during the multiphoton dissociation process. It has been demonstrated that partial collisional deactivation of pre-excited molecules during the time delay between the laser pulses leads to enhancement in the selectivity of the process [27, 28]. A major drawback of this approach, however is that simultaneous with the increase of selectivity, there is a steep drop in the dissociation yield (productivity) of the process. A semi-empirical model of this phenomenon has been suggested [28] that assumes different relaxation rates for vibrationally excited parent molecules containing different isotopes of carbon. Indeed, as it has been demonstrated both experimentally and theoretically for some diatomic and small polyatomic molecules (see, for example, [31–33]), rate constants for collisional energy transfer depends steeply on the vibrational energy mismatch between collision partners, with a smaller energy mismatch resulting in higher transfer rates. In the case of CF_3H excited using the OP-IRMPD technique, the bulk of the ground state molecules consists almost exclusively of $^{12}CF_3H$, so, a vibrationally excited molecule of either isotope undergoes most of its collisions with the unexcited molecules containing carbon-12. Analysis of the energy mismatch in the collisions $^{12}CF_3H^{\dagger}+^{12}CF_3H$ and $^{13}CF_3H^{\dagger}+^{12}CF_3H$ and the corresponding experimental data [34] suggest that the probability of vibrational energy transfer during the collision between excited and ground state carbon-12 containing molecules is higher than deactivation of excited $^{13}CF_3H$ in collisions with ground state $^{12}CF_3H$. Another possible explanation for collisional enhancement of isotopic selectivity suggested in the work of Boyarkin *et al.* [28] is that the dissociation yield depends on the energy from which the partially

relaxed CF_3H molecules are dissociated in a manner that is different for the two isotopes, due to the isotopic shift of their respective absorption spectra. In other words, the two suggested explanations of the collisionally enhanced selectivity are based on

1. isotopic selectivity of collisional V-V relaxation and
2. isotopic selectivity of the IRMPD process.

The current state of research in this direction speaks in favor of simultaneous action of both mechanisms with a slight domination of the second one (different rates of multiphoton excitation process for molecules containing different isotopes of carbon) [34].

3.1.3 Motivation for this work

Along with high isotopic selectivity, the overall productivity has to be high enough for any isotope separation process to be practically relevant. The productivity of the OP-IRMPD based process is determined by the overall dissociation yield (fraction of irradiated $^{13}CF_3H$ converted to C_2F_4 final product for a given fluence of lasers), the concentration of working molecules and dissociation volume. Evaluated in Reference [28], the overall yield of the process per pair of laser shots is around 0.1% per 1 J/cm^2 fluence of pre-excitation laser and with 3-9 J/cm^2 of dissociation fluence at an optimal CF_3H pressure of 20 mbar. It is mainly determined by the absorption intensity of the 3_1 band and by the considerable fraction of pre-excited $^{13}CF_3H$ species that are deactivated in collisions between the time of pre-excitation and dissociation. To some extent this relatively low yield can be compensated by the use of a higher working pressure with the simultaneous shortening of the delay between the laser pulses, such that the collision number, which is proportional to the product of the pressure and the delay, is maintained, since this is necessary for high isotopic selectivity. However in the implementation of this technique by Boyarkin *et al.*, the width of pre-excitation pulse and rise-up time of the dissociation pulse posed a limit to the minimum delay. If this delay is comparable or less than these characteristic times, different molecules will experience substantially different numbers of collisions before being dissociated, resulting from the uncertainty in the moment of pre-excitation and the beginning of IRMPE. Consequently, their contribution to isotopic selectivity will differ as well. Some pre-excited molecules will be deactivated in collisions to a level from which they cannot be dissociated, while the others may be dissociated rapidly before having experienced a collision, significantly decreasing the isotopic selectivity. The need for a certain (long) delay to create high isotopic selectivity by collisions contradicts to the desire of increasing productivity by working at high pressures (and short delays). The infrared multiphoton excitation (IRMPE) process under collisional conditions is one of the major subjects of the investigation in the present work. In the experiments reported here we

find an elegant way to increase both dissociation yield and working pressure while conserving high isotopic selectivity.

As in most of the IRMPD-based approaches, the dissociation volume used by Boyarkin and coworkers [27, 28] is relatively small, limited by the small size of the focussed CO_2 laser beam near the focal point where the dissociation fluence is high. This volume can be greatly increased if the fluence that saturates IRMPD is below the typical damage threshold of IR materials, so that collimated (instead of focused) laser beams can be used. The results of Boyarkin and coworkers [27, 28] suggest that a proper shaping of a dissociating CO_2 laser pulse should lower this threshold to a few J/cm^2. One of the objectives of the present work is to study IRMPD of the pre-excited $^{13}CF_3H$ with temporary modified CO_2 laser pulses in view of using unfocussed laser beams for isotope separation. Shaping CO_2 laser pulses is technically not simple, however. We therefore begin with a long pulse characteristic of a conventional TEA CO_2 laser, "cut" it by measuring the dissociation yield at a certain moment after the beginning of the pulse. This is done by *in situ* LIF detection of CF_2 fragments created by the part of the CO_2 laser pulse from the beginning until the moment of the LIF detection. Having gained a basic understanding of the optimal pulse shape from these experiments, we then construct such a pulse and study some quantitative aspects of isotope separation with mass-spectrometric detection of the products.

Another problem that is important for molecular isotope separation is the collection of dissociation products. Usually the photofragments are chemically reactive, so a suitable process of chemical stabilization must be developed. Depending on the dissociation product, either the photofragments may react with each other in 3-body collisions forming a new stable molecule or thy must be scavenged by the addition of another molecule. The first situation is realized in the case of carbon-13 isotope separation using the OP-IRMPD approach on CF_3H. Unstable CF_2 fragments form a stable C_2F_4 in the reaction (3.2) [35, 36]

$$CF_2{+}CF_2 + M \longrightarrow C_2F_4 + M, \tag{3.2}$$

where M is a particle required for the removing of excess of energy.

Alternatively, CF_2 can stick to the reactor walls [2], reducing the yield of the C_2F_4 final product. In our study we will quantitatively evaluate these losses as a function of our experimental conditions.

Below we first describe details of the experimental approach and the apparatus we use in this work (Section 3.3.1). We then present the results of our LIF measurements of the IRMPD yield of the pre-excited $^{13}CF_3H$ as a function of effective duration of the CO_2 laser pulse and as a function of delay between the pre-excitation and the dissociation lasers (Section 3.3.2). The results of these measurements prompted us to make some modifications to our hardware, primarily to the dissociating CO_2 laser. Following the description of these modifications, we

present the results of mass-spectrometric measurements of the overall process yield and selectivity with a short dissociation pulse in nearly collimated laser beams (Section 3.3.3). We then analyze these data in the frame of our improved semi-empirical model.

Having obtained a basic understanding of the mechanism of the isotopically selective collisional IRMPD step of the OP-IRMPD process, we directed our efforts towards the investigation of this effect for different levels of pre-excitation in the parent CF_3H molecule (Section 3.4). Reducing the pre-excitation level to the first overtone of CH stretch vibration allowed us to increase by several times the overall productivity of our isotope separation process while conserving its high isotopic selectivity. We also investigated the OP-IRMPD process using different shapes of the dissociation laser pulse.

In the Section 3.5 we evaluate practical relevance of the OP-IRMPD approach to carbon-13 isotope separation.

Finally, a short remarks about evaluation experiments of applicability of pre-excitation of fundamental CH stretch vibration of CF_3H are given in Section 3.6.

3.2 Vibrational modes in CF_3H

CF_3H (trifluoromethane) is a symmetric top molecule of C_{3v} symmetry. It has six normal modes (three totally symmetric and three degenerate), the frequencies of which are reported for $^{12}CF_3H$ and $^{13}CF_3H$ in Table 3.2. CH stretch (ν_1) and HCF bend (ν_4) fundamentals and overtone frequencies are shown separately in the bottom part of the Table 3.2 for the following reason. This molecule exhibits a classic example of a 2:1 stretch-bend resonance [38] as the frequency of the ν_1 is nearly twice that of the ν_4. Strong anharmonic coupling mixes the $N\nu_1$ and $2N\nu_4$ states (where N is integer or half-integer), resulting in splitting of each CH stretch and HCF bend overtone band into a polyad of $(N + 1)$ or $(N + 1/2)$ well separated sub-bands for integer and half-integer N respectively. The individual sub-bands are labeled by N together with a subscript enumerating them from high to low energy [38]. An example of a polyad ($N = 3$) is shown in Figure 3.2 representing a part of high resolution FTIR spectrum of $^{13}CF_3H$ reported by Hollenstein *et al.* [37].

In this work we study isotopically selective OP-IRMPD of CF_3H pre-excited to different CH stretch - HCF bend overtone bands. Symmetrical CF stretch vibration mode ν_2, whose frequency lies in the tuning range of CO_2 laser is used for multiphoton excitation of pre-excited molecules.

	Vibration	ν_{vacuum}, cm^{-1}	
		$^{13}CF_3H$	$^{12}CF_3H$
ν_2	CF symm. stretch (A_1)	1115.9[c]	1141.5[d]
ν_3	CF_3 umbrella bend (A_1)	695.3[c]	700.1[e]
ν_5	CF a.s. stretch (E)	1132.4[c]	1158.3[d]
ν_6	CF_3 deformation (E)	506.7[c]	507.8[e]
$\begin{cases}\nu_1\\ \nu_4\end{cases}$	$\begin{cases}\text{CH stretch } (A_1)\\ \text{HCF bend } (E)\end{cases}$		
$(1/2)_1$		1368.9[c]	1377.85[f]
1_1		3024.6[a]	3035.5[b]
1_2		2695.1[a]	2710.2[b]
$(3/2)_1$		...	4400[b]
$(3/2)_2$		...	4044[b]
2_1		5936.6[a]	5959.4[b]
2_2		5680.9[a]	5710.4[b]
2_3		5311.2[a]	5337[b]
$(5/2)_1$		...	7322[b]
$(5/2)_2$		...	7018[b]
$(5/2)_3$		...	...
3_1		8753.0[a]	8792.7[b]
3_2		8548.9[a]	8589.3[b]
3_3		8244.0[a]	8286.0[b]
3_4		7855.3[a]	7890[b]

[a] Reference [37]; [b] Reference [38]; [c] Reference [39];
[d] Reference [40]; [e] Reference [41]; [f] Reference [42, 43].

Table 3.2: CF_3H vibrational fundamentals and overtones of combinational (CH stretch + HCF bend) vibrations

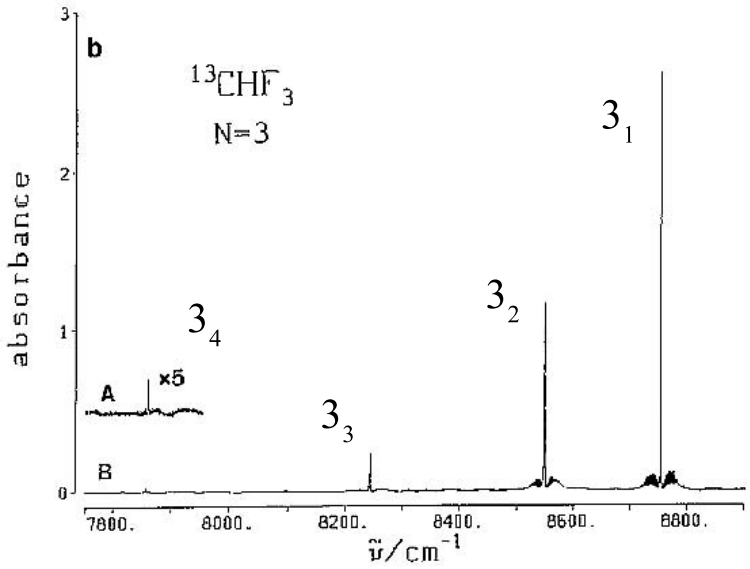

Figure 3.2: Polyad structure of the second overtone of CH stretch vibration in $^{13}CF_3H$ (from Reference [37])

3.3 Overtone pre-excitation of 3_1 band

3.3.1 Experimental setup

Figure 3.3 depicts the main features of the optical layout in our experimental setup. First, a 40-50 ns laser pulse (FWHM) at 1.14 μm pre-excites room temperature CF_3H molecules through the Q-branch transition of the 3_1 vibrational band [38]. Following this, a pulse from a tunable TEA CO_2 laser promotes some fraction of the vibrationally excited molecules to energies above the dissociation limit by infrared multiphoton excitation (IRMPE). The CF_2 fragments can be monitored by a third laser pulse *via* LIF. Alternatively, in some experiments we monitor the isotopic composition of the C_2F_4 final product by mass-spectrometry.

The 40-50 ns pre-excitation pulse of up to 200 mJ is generated by stimulated Raman scattering the 410 mJ output of a 0.1 cm^{-1} bandwidth tunable alexandrite laser in a one meter long cell filled with 50 bar of H_2 (Light Age Inc.). The high, ($\sim$74%) quantum efficiency of this scattering process is facilitated by an internal gas circulator that displaces the pumped H_2 between subsequent laser pulses.

The tunable CO_2 laser (Lumonics, TEA-840) that we use in our experiment with LIF product detection generates pulses that consist of an intense 150 ns (FWHM) spike followed by a 4-5 μs tail of much lower intensity. The laser can be forced to run on the TEM_{00} mode by inserting a 10 mm iris in the laser cavity. The total pulse energy is up to 3 J without and 250 mJ with the intracavity iris when operating on the 9P(20) line at 1046.85 cm^{-1}, which we employ for most experiments. For mass-spectrometric product detection, this laser was

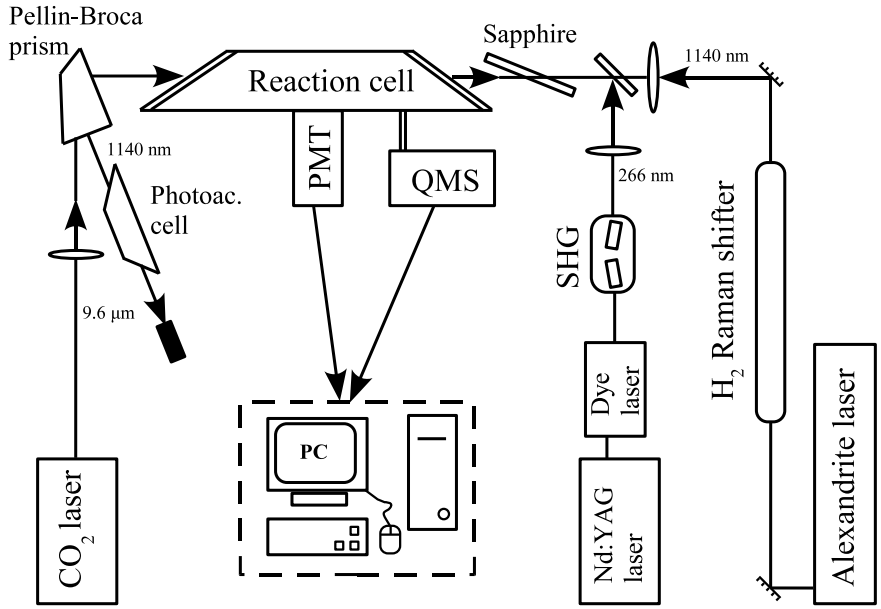

Figure 3.3: Experimental set-up.

replaced by a CO_2 laser (PIC, model SP-7000 [44]) capable of generating 50-60 ns (FWHM) pulses in which the long tail is almost entirely suppressed. This laser delivers up to 600 mJ per pulse (80% within the first 100 ns) in a near TEM_{00} beam. The beam is focused to the center of the reaction cell by a f=100 cm AR coated ZnSe lens.

For LIF detection of CF_2, we use the 5-10 mJ output of a Nd:YAG pumped dye laser, operating with Coumarin-500 dye and frequency doubled in a BBO crystal. This laser is tuned to the $A(0,1,0)^1B_1 \leftarrow X(0,1,0)^1A_1$ electronic transition in CF_2 at *ca.* 269.9 nm [45]. The total, undispersed, LIF signal is collected and imaged onto a UV sensitive photomultiplier tube (PMT) by a 1:1 condensor lens through a 2 X 5 mm slit. This slit limits the LIF detection of CF_2 to a 5 mm long region near the focal point of the CO_2 laser, where the dissociation fluence along the CO_2 laser beam is almost constant.

The counter-propagating 1.14 μm pre-excitation and the 9.6 μm dissociation beams enter the reaction cell from opposite sides through BaF_2 windows. Care has been taken to avoid damage of laser optics by these two counter-propagating beams. After it exits the cell, the pre-excitation beam is decoupled from the incoming CO_2 laser beam by a Pellin-Broca prism. The CO_2 beam is itself absorbed by a Sapphire Brewster plate after exiting the cell (Figure 3.3). In experiments with LIF detection of CF_2, the UV beam is combined with the pre-excitation beam on a dichroic mirror prior to entering the cell. Two different reaction cells have been used in our experiments. For measurements with LIF detection we use a 50 cm long stainless steel cell equipped with a condensor lens and a photomultiplier tube to collect and to measure total

fluorescence of CF_2. For mass-spectrometric measurements we use a Pyrex cell of 2 cm length and 16 mm internal diameter. Such a short cell allows one to maintain nearly constant laser fluences over the length of the cell. The cells are pumped down to 8×10^{-3} mbar by a forepump through a LN_2 trap.

The relative timing of laser pulses is continuously monitored by a photodiode for pre-excitation and LIF pulses and by a fast Ge photon-drag detector (occasionally) for the dissociation pulse. The frequency and linewidth of the pre-excitation and LIF probe lasers are continuously monitored by a pulsed wavemeter (Burleigh). After passing through the reaction cell, the pre-excitation beam is sent into a photoacoustic cell filled with CF_3H. The frequency of the alexandrite laser is first tuned to the desired value using the wavemeter reading and fine-tuned to the Q-branch of $^{13}CF_3H$ by maximizing the photoacoustic signal. This signal is continuously recorded along with the LIF signal of CF_2. Since at our conditions the pre-excitation step is a linear process, we use the photoacoustic signal to correct the recorded LIF signal for any change of power or spectral shift of the pre-excitation radiation during an experiment. We also continuously monitor the relative power of the UV probe laser maintaining it at a constant level by changing the power of the pumping Nd:YAG laser when necessary.

We determine the isotopic composition of the final C_2F_4 product by by sampling the gas mixture in the cell and measuring signals at masses 82 and 83 ($^{12,13}C_2F_3$, $^{13,13}C_2F_3$) in a quadrupole mass-spectrometer (Balzers, QMS-422). The signal at mass 81 ($^{12,12}C_2F_3$) has not been taken into account, because at the typically high levels of isotopic selectivity in our experiments it is 3 to 4 orders of magnitude smaller than the signal at mass 83. We do, however, strictly account for the contribution of $^{12,12}C_2F_3$ to isotopic selectivity using the following statistical expressions (assuming an equal recombination rate for different isotopic species):

$$\begin{aligned} S(81) &\propto [^{12,12}C_2F_4] \propto [^{12}CF_2]^2, \\ S(82) &\propto [^{12,13}C_2F_4] \propto 2\cdot[^{12}CF_2][^{13}CF_2], \\ S(83) &\propto [^{13,13}C_2F_4] \propto [^{13}CF_2]^2, \end{aligned} \tag{3.3}$$

where $S(81)$, $S(82)$ and $S(83)$ are mass-signals at masses 81, 82 and 83 respectively[1].

Using (3.3) one can derive the following expression for carbon-13 to carbon-12 concentrations ratio in dissociation product:

$$\frac{[^{13}C]}{[^{12}C]} = \frac{[^{13}CF_2]}{[^{12}CF_2]} = 2\cdot\frac{S(83)}{S(82)}, \tag{3.4}$$

where $[^{13}C]$ and $[^{12}C]$ are concentrations of the respective isotopes in CF_2 and, hence, in C_2F_4.

[1]Equations (3.3) can be derived also using the dynamic description of the reaction process as it is described in Appendix A.

We typically irradiate the gas mixture in the reaction cell for 5 min at 10 Hz repetition rate of the CO_2 laser and then sample it through a leak valve into the mass-spectrometer. We record a mass-spectrum by taking an average of 10-20 mass-scans. Several additional measurements are made to allow us to determine the absolute yield of the process. A known mixture of C_2F_4 in CF_3H was prepared in the reaction cell and leaked into the QMS to reach the same pressure as is used when we sample the irradiated mixture. This allowed us to calibrate the QMS mass-spectrometer in units of $[C_2F_4]$ to $[CF_3H]$ ratio. The total volume of the cell and of all the connecting tubes V_{total} was determined by measuring a change of pressure when a filled cell was connected to a calibrated volume. The active volume V_{active} in the reaction cell is determined by the overlap of pre-excitation and dissociation beams. In our mass-spectrometric experiments the pre-excitation beam diameter normally exceeds the diameter of CO_2 laser beam ($\sim$2 mm), so, the active volume is determined by the product of the CO_2 laser beam diameter and the length of the reaction cell. The absolute C_2F_4 productivity P in units of molecules per unit active volume per laser pulse can be calculated as:

$$P = \frac{[C_2F_4]}{[CF_3H]}[CF_3H]_0 V_{total} / \left(V_{active} N_{pulses}\right), \tag{3.5}$$

where $[CF_3H]_0$ is the initial CF_3H concentration and N_{pulses} the number of laser pulses.

The final C_2F_4 concentration in an isotope separation measurement depends on the sticking of the CF_2 dissociation fragments to the reaction cell walls (see Appendix D). This sticking efficiency depends in its turn on the reaction cell material, geometry, and on the initial concentration of CF_2. In order to exclude the influence of these configuration specific factors on our measurements, we have also employ an alternative method to determine the absolute yield of the process. This method consists of measuring the isotopic composition of the parent CF_3H molecules before and after irradiation. The decrease in the $[^{13}C]/[^{12}C]$ ratio determines the fraction of $^{13}CF_3H$ molecules dissociated as a result of the irradiation:

$$\frac{[^{13}CF_3H]_{diss}}{[^{13}CF_3H]_0} = 1 - \frac{[^{13}C]/[^{12}C]}{([^{13}C]/[^{12}C])_0}. \tag{3.6}$$

If the initial amount of $^{13}CF_3H$ in the cell N_0 is known, one can calculate the absolute amount of dissociated molecules N_{diss}:

$$N_{diss} = \left(1 - \frac{[^{13}C]/[^{12}C]}{([^{13}C]/[^{12}C])_0}\right) N_0. \tag{3.7}$$

We can also make a correction for the fact that some $^{13}CF_3H$ is used up during the experiment. To do this one has to consider the dynamic equation describing the $^{13}CF_3H$ consumption:

$$\frac{dN_{diss}}{dt} = R\left(N_0 - N_{diss}\right) \quad \Rightarrow \quad N_{diss} = N_0\left(1 - e^{-Rt}\right), \tag{3.8}$$

where R is a constant. If the $^{13}CF_3H$ consumption during the experiment is negligible, the Equation (3.8) can be re-written as:

$$\frac{dN'_{diss}}{dt} = RN_0 \quad \Rightarrow \quad N'_{diss} = N_0 Rt. \tag{3.9}$$

In this case N'_{diss} stands for the amount of $^{13}CF_3H$ that would be dissociated if its concentration did not change during the experiment (for example, if a larger passive volume would be used). Comparing equations (3.8) and (3.9) one can write for N'_{diss}:

$$N'_{diss} = -ln\left(1 - \frac{N_{diss}}{N_0}\right) N_0 = -ln\left(\frac{[^{13}C]/[^{12}C]}{([^{13}C]/[^{12}C])_0}\right) N_0. \tag{3.10}$$

Direct measurement of C_2F_4 concentration using the calibrated mass-spectrometer has been applied in the first series of experiments (with second CH stretch vibration overtone pre-excitation). The second method was used in the experiments with pre-excitation of the first overtone and fundamental frequency.

3.3.2 Study of CF_3H dissociation dynamics by LIF detection of dissociation products

In a first set of experiments, we examine the dynamics of the IRMPD step of the overall process by fixing the delay between the pre-excitation laser and CO_2 dissociation laser and varying the delay between the CO_2 laser and the LIF probe laser. These experiments should reveal what part(s) of the CO_2 laser pulse contribute most significantly to the dissociation. Figure 3.4 shows the LIF signal from the CF_2 dissociation fragments for CF_3H molecules pre-excited to the 3_1 overtone level (*via* the Q-branch in the carbon-13 species at 8753 cm^{-1}) as a function of delay between the beginning of the CO_2 laser pulse and the leading edge of the LIF probe laser pulse. The measured LIF signal is proportional to the dissociation yield in the volume near the focal point of the CO_2 laser. The delay between the end of the overtone excitation pulse and the beginning of the CO_2 laser pulse is fixed to zero (see lower panel in Figure 3.4). As shown in the figure, measurements were made for three different CF_3H pressures, and they have been arbitrary scaled for convenient graphical presentation. The total fluence of the CO_2 laser at its beam waist is 12 J/cm^2. The part of the CO_2 laser pulse that occurs between the overtone excitation pulse and the LIF probe pulse gives an effective fluence that the pre-excited molecules experience before the dissociation yield is measured by LIF detection of CF_2. This effective fluence, along with the overtone excitation and the CO_2 laser pulses, is plotted as a solid line in the lower panel of the Figure 3.4. This curve allows a conversion of the time-delay scale into an effective fluence scale.

The dissociation yield measured at a pressure of 0.7 mbar, where collisional relaxation of pre-excited molecules during the multiphoton excitation is negligible exhibits (Figure 3.4) a rapid

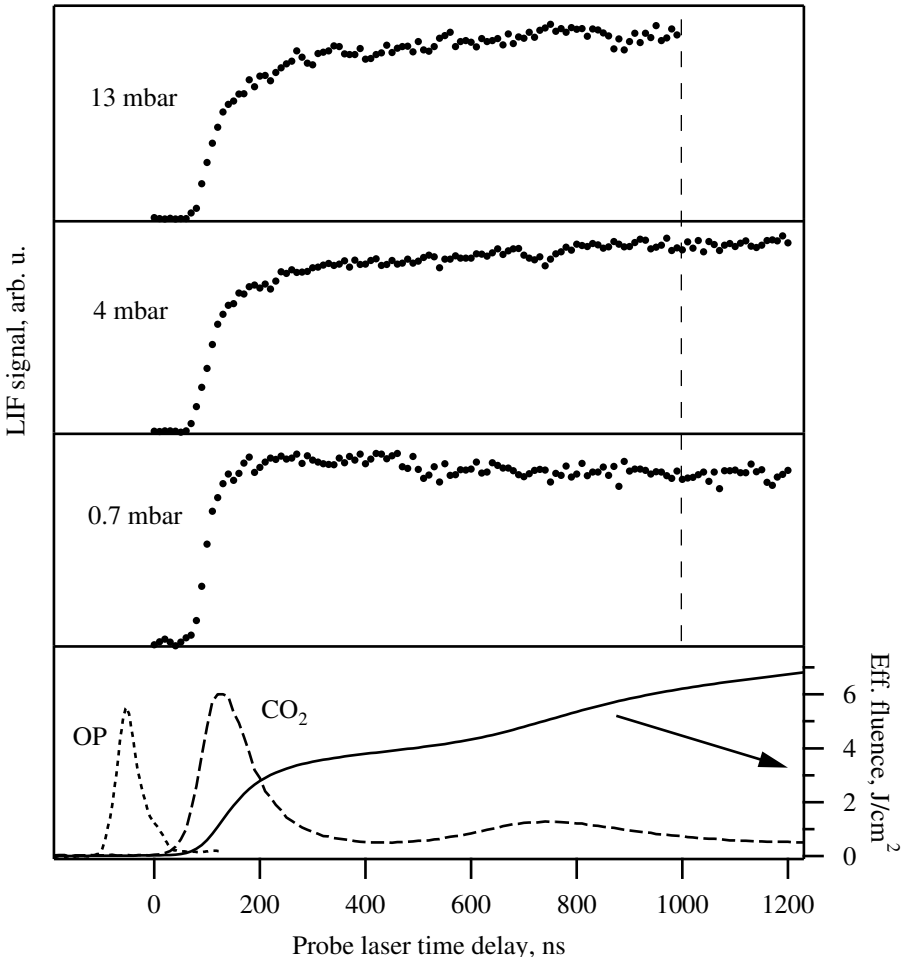

Figure 3.4: LIF signal (CF_2 dissociation yield) as a function of delay between the dissociation and the probe laser pulses for different pressures of CF_3H (upper panel). The lower panel shows positions and profiles of the overtone pre-excitation (OP) pulse and the CO_2 laser dissociation pulse together with effective fluence (time-integrated intensity) of the latter in the time between its start and the arrival of the LIF probe laser pulse.

growth that starts at 70 ns delay and reaches its maximum already at 180 ns. This corresponds to an increase of the effective fluence from 0.2-0.3 J/cm^2 at the dissociation threshold to 2.7 J/cm^2 at saturation. Both the threshold and the saturation fluences for IRMPD of the pre-excited CF_3H are very low compared with 30-40 J/cm^2 needed to dissociate the ground state species [46]. One can clearly see that the fluence needed to saturate the dissociation is much lower than the total fluence of our CO_2 laser pulse, since the part of the pulse after 180 ns from the beginning, which carries up to 80% of the total pulse energy does not participate in the dissociation. After reaching its maximum, the LIF signal stays nearly constant, with a slow, monotonic decay. We attribute the slight drop of the LIF signal to the flight of the CF_2 fragments out of the probed volume. The estimated mean free-path of these fragments at 0.7

mbar pressure is 0.5 mm, and during the 1.2 μs delay between beginning of the CO_2 laser pulse and the probe pulse, room-temperature CF_2 fragments can fly approximately 0.3 mm out of the 1.5 mm diameter probe beam without collisions. Moreover, because the dissociation fragments will have a slightly elevated translational temperature, the expected loss of signal due to fly-out may be even higher. The loss of CF_2 from the probed volume is therefore not negligible and is the likely source of the observed drop in signal at longer delay time.

In the case of 4 and 13 mbar of CF_3H the CF_2 flight-out is negligible and, therefore, the LIF signal is proportional to the dissociation yield. The dissociation curves obtained with 4 and 13 mbar exhibit similar qualitative behavior, although they differ in some important details from the 0.7 mbar curve. The initial growth of the dissociation yield becomes less steep with increase of pressure resulting in late reaching the near constant region (250 ns for 4 mbar and 370 ns for 13 mbar). Apart from that the dissociation yield continues to slowly increase for at least 1.2 μs after the beginning of the dissociation laser pulse. This increase, however, is much slower than the corresponding increase of the effective CO_2 laser fluence (see Figure 3.4, low panel), implying higher efficiency of the dissociation process at higher dissociation laser intensities. Continuously increasing dissociation yield implies that under conditions, where collisional vibrational relaxation occurs during the IRMPE process, we do not dissociate all the pre-excited molecules during the early part of the CO_2 laser pulse as is the case at low pressure, although most of the dissociation still occurs within the initial 200-300 ns. The rest of the pulse that still carries significant fraction of its energy does not contribute significantly to dissociation and, hence, is useless for the process. Most of the molecules which are not dissociated by the initial part of the CO_2 laser pulse undergo collisional vibrational deactivation and never reach the dissociation threshold. This implies that the fraction dissociated can be increased using a dissociation pulse with higher intensity during the first few hundred nanoseconds. This conclusion is a guide in selecting a CO_2 laser with an optimal pulse.

Boiarkin *et al.* have shown in their work that collisional vibrational deactivation of pre-excited CF_3H during the delay between the pre-excitation and dissociation pulses dramatically increases the isotopic selectivity of the separation process, although with simultaneous drop of the dissociation yield [27, 28]. While one can increase the number of collisions either by increasing this delay or by increasing the pressure at a fixed delay, the latter approach has the advantage that a larger number of molecules participate in the process. To achieve the maximum productivity of the overall process while maintaining the desired high selectivity, this delay should be as short as possible and the pressure increased to achieve the necessary collision number. The possibility to decrease the time delay between pre-excitation and dissociation laser pulses is limited, however, by the time profiles of the laser pulses. Relatively long ($\sim$ 100 ns) rise-up time of the CO_2 laser pulse and the length of the the pre-excitation pulse (40-50 ns

(FWHM) for Alexandrite laser) poses the limit to the minimum time delay between the pulses (see also Section 3.1.3 on page 43). In this work we study the possibility to use collisions occurring during the multiphoton excitation process for increasing the isotopic selectivity of the OP-IRMPD process instead of collisions between pre-excitation and dissociation pules used in the work of Boiarkin and coworkers. In this case we can conceive overlapping the pre-excitation and dissociation laser pulses, which correspond to zero time delay between pre-excitation and IRMPD step of the OP-IRMPD process, whereas the number of collisions a pre-excited molecules undergoes before been dissociated is determined by the time required to the molecule to reach the dissociation limit. This could allow us to use higher working pressures, and, respectively, to reach higher absolute productivity of the OP-IRMPD isotope separation process.

Figure 3.5 presents the dissociation yield near the focal point (measured by LIF detection of CF_2) as a function of relative position of pre-excitation and dissociation laser pulses. In these experiments, the LIF detection pulse is always delayed from the pre-excitation pulse by 1120 ns as we scan the latter across the CO_2 laser pulse. The time delay between the pre-excitation and the LIF detection pulses is chosen to be substantially longer than the time required for dissociation yield to reach the value where it almost does not depend on the probe laser pulse position (see Figure 3.4, where the vertical dashed line shows the position of the LIF probe laser corresponding to the 1120 ns delay from the beginning of the pre-excitation laser pulse). The vertical dashed line in the Figure 3.5 corresponds, in it's turn, to the time delay between the pre-excitation and dissociation laser pulses used in the previous set of experiments (Figure 3.4). Thus, data points lying on the dashed lines in the Figures 3.4 and 3.5 correspond to the same relative positions of the three laser pulses.

At low CF_3H pressure (1.3 mbar) dissociation yield is in its maximum already in the initial position of laser pulses (low panel in Figure 3.5) and stays constant until the OP and probe pulses shifts 2μs from the initial position, when only the part of the CO_2 laser pulse after $\sim$ 1800 ns from the beginning participates in the dissociation process. This speaks in favor of the unity dissociation probability for pre-excited molecules under collisionless conditions even at low effective dissociation fluences (tail of the CO_2 laser pulse in the experiments represented in Figure 3.5 and short initial part of the pulse in the Figure 3.4).

At higher pressures, where collisions before and during the IRMPD step are not negligible, the curve representing the dissociation yield becomes less flat and with increasing pressure its shape approaches the temporal profile of the CO_2 laser pulse confirming our suggestion that the dissociation process is governed primarily by the dissociation laser pulse intensity rather than by fluence. The maximum concentration of CF_2 fragments occurs at a delay, where the pre-excitation pulse is overlapped with the most intense spike of the CO_2 laser pulse. At this

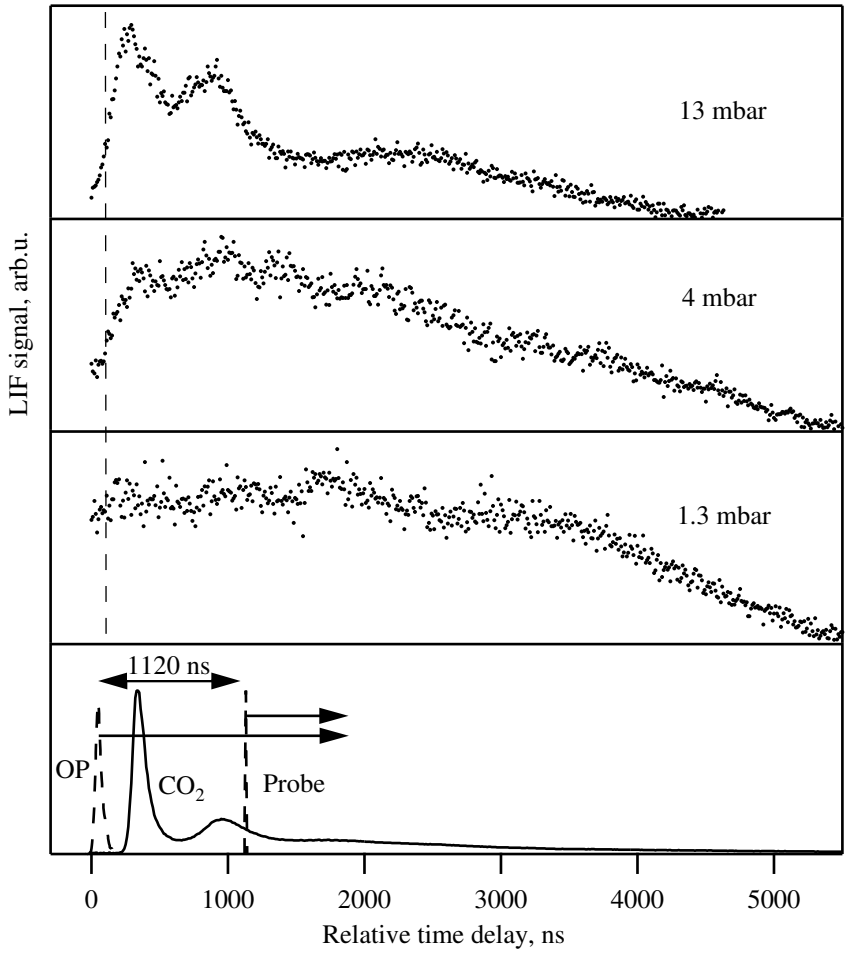

Figure 3.5: LIF signal (CF_2 dissociation yield) as a function of relative position of pre-excitation and dissociation laser pulses for different CF_3H pressures. The probe laser pulse is kept delayed from the pre-excitation pulse by 1120 ns. The initial positions of the pulses are depicted. The total fluence of the CO_2 laser pulse is 12 J/cm^2 .

time delay the CF_2 concentration is about 2.5 times for 4 mbar and 4 times for 13 mbar higher than at the delay corresponding to the closest position of the non-overlapped pulses (dashed vertical line in the Figure 3.5). We assume, that the maxima of the curves represented in the Figure 3.5 correspond to the saturation of IRMPD, *i.e.* to the dissociation of almost all the pre-excited molecules. This suggestion is supported by the observation that at 13 mbar ratio of the two dissociation yield peaks corresponding to the two peaks of the CO_2 laser pulse is about 5:4, whereas ratio of the corresponding peaks of the CO_2 laser pulse is about 5:1 implying the saturation effect. Thus, we can estimate the relative IRMPD yields[2] for the non-overlapped OP and CO_2 lasers as 40% of pre-excited molecules for 4 mbar and 25% for 13 mbar, whereas in

[2] *Relative IRMPD yield* (dissociation probability of pre-excited molecules) is the ratio of the numbers of dissociated and pre-excited $^{13}CF_3H$.

the overlapped pulses configuration one can acheve almost unity dissociation probability even at relatively high 13 mbar pressure.

Figure 3.6 shows the optimal relative position of the pre-excitation and dissociation laser pulses which corresponds to maximum dissociation yield together with the probe laser pulse position as it is used in the experiments described earlier. Fixing this relative position of the

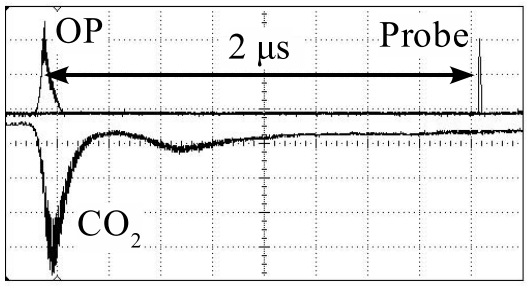

Figure 3.6: Relative positions and shapes of overtone pre-excitation (OP), dissociation (CO_2) and LIF probe laser pulses.

laser pulses ("timing") we measured the CF_2 LIF signal as a function of CF_3H pressure in view of finding the pressure corresponding to the maximum overall yield of the OP-IRMPD process. Figure 3.7 represents the results of this experiment. The focal fluence of the CO_2 laser is about

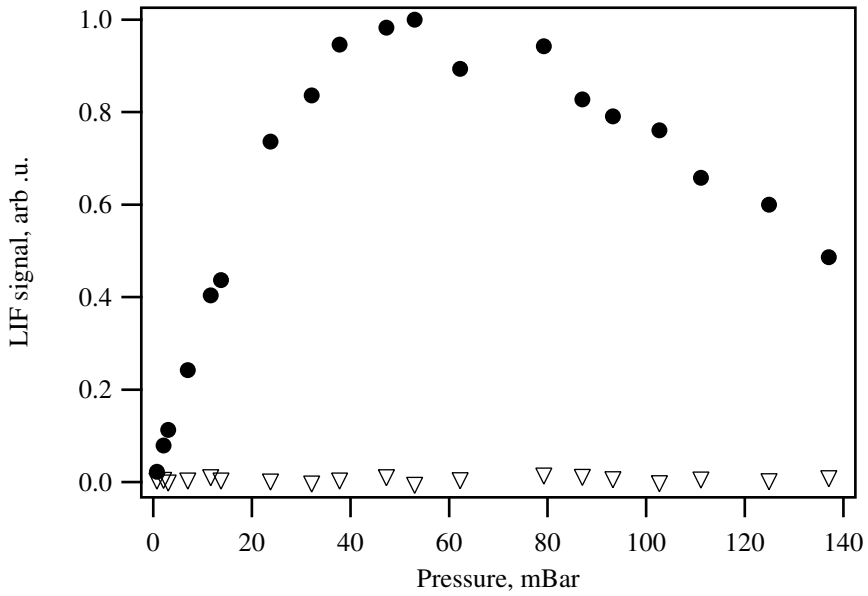

Figure 3.7: CF_2 LIF signal as a function of CF_3H pressure for ground state (triangles) and pre-excited (dots) molecules. The overtone pre-excitation and the dissociation laser pulses are overlapped. The total fluence of the dissociation laser pulse is 12 J/cm^2.

12 J/cm^2, and the maximum of the LIF signal is reached at about 50-60 mbar. The efficiency of LIF detection itself drops with increasing pressure due to collisional quenching of electronic

states, and, therefore, the LIF signal is not directly proportional to the CF_2 concentration over the pressure range in Figure 3.7. The analysis of the available data on quenching of CF_2 fluorescence (see Appendix B on page 141) suggests that the quenching becomes considerable for a pressure above 20-25 mbar. We must, therefore, consider 50-60 mbar simply as a lower limit of pressure where the CF_2 yield reaches maximum. For comparison, at 50-60 mbar in a configuration with the delayed pre-excitation and dissociation pulses, the dissociation yield is essentially zero due to nearly complete relaxation of the pre-excited CF_3H [27, 28].

Because LIF detection of CF_2 does not discriminate between the carbon isotopes, it is important to know whether the signal we observe results from IRMPD of $^{13}CF_3H$ selectively pre-excited by the 1.14 μm pulse. The leading edge of CO_2 laser pulse may, for instance, pre-heat ground state $^{12}CF_3H$ molecules, shifting to the red the overtone absorption spectrum *via* hot bands and increasing the fraction of pre-excited $^{12}CF_3H$ that contribute to the dissociation yield. We have verified that this is not the case. Detuning of pre-excitation laser out of resonance with the narrow Q-branch of the 3_1 band in $^{13}CF_3H$ suppresses LIF signal as it is shown in Figure 3.8. LIF signal is proportional to CF_3H photoacoustic signal measured simultaneously, implying that the pre-excitation laser interacts only with ground state species (mainly $^{13}CF_3H$) and that the process is still highly selective.

The results of these experiments provide us with guidance how a laser isotope separation method based on the OP-IRMPD technique has to be modified to give a significantly high overall yield. The dissociation laser pulse has to be almost as short as the pre-excitation pulse, the two pulses have to be overlapped and the sample pressure has to be increased. It is, however, unclear at all to what extend isotopic selectivity of pre-excitation can be maintained at such conditions. Can it be still enhanced by collisional relaxation? To answer these questions, we have performed a series of experiments with mass-resolved detection of C_2F_4 dissociation products.

3.3.3 Mass-spectrometric study of the isotope separation process with optimized configuration

LIF detection of CF_2 is not isotopically selective. The isotopic shift in an electronic transition is determined by the difference in the isotopic shifts of the vibrational levels of the two species between the two electronic states involved in the transition. Assuming the isotopic shifts of the vibrations in CF_2 is similar to that in CF_3H [39] we have estimated the isotopic shift of the electronic transition to be around 1 cm^{-1}, which is much smaller than the 20-30 cm^{-1} width of excitation bands in the CF_2 LIF spectrum conditioned by rotational congestion [45]. For this reason we use mass-spectrometric measurements of C_2F_4 that results from recombination of the CF_2 dissociation products to monitor the dissociation yield of different isotopic species and

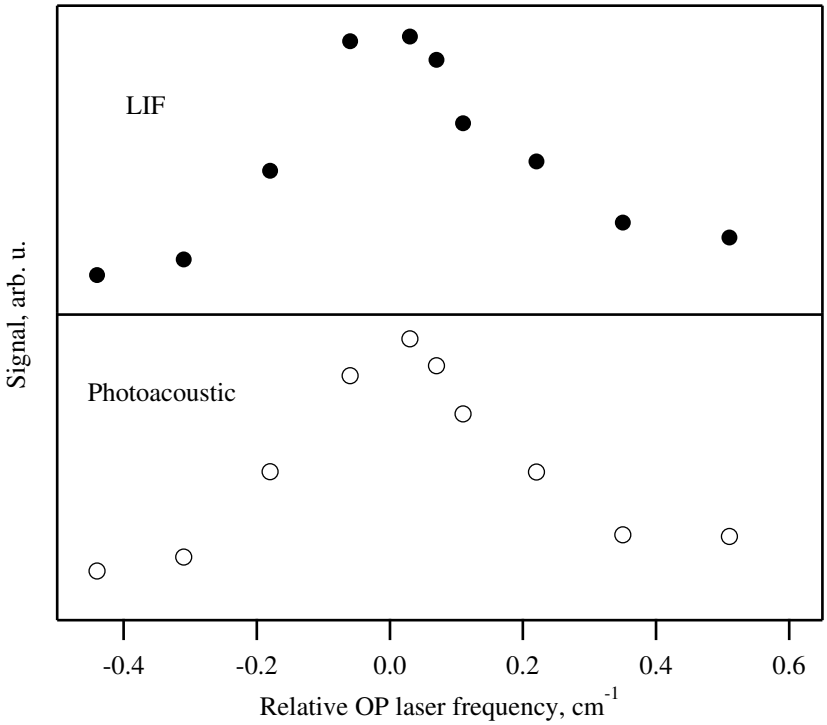

Figure 3.8: CF_2 LIF signal as a function of pre-excitation laser frequency for overlapped pre-excitation and dissociation pulses (upper panel), sample pressure 13 mbar and corresponding CF_3H photoacoustic signal (lower panel).

assess the isotopic selectivity of the separation process. In the LIF measurements we monitor the concentration of CF_2 near the focal point where the fluence of both the pre-excitation and dissociation pulses are well determined. In mass-spectrometric measurements, however, we can only determine the concentration of C_2F_4 averaged over the whole volume of the cell. Because the dissociation beam is focused, its fluence varies along our 50 cm long cell and we lose the direct relationship between the dissociation yield and the local fluence. If, however, the beam were collimated to provide the intensity in its initial spike necessary to compete with collisional deactivation, the total fluence of the pulse, which would be 10-15 J/cm^2, would be too high for the BaF_2 windows of a cell to withstand.

The LIF experiments described in Section 3.3.2 suggest that the long tail of our CO_2 pulse doesn't contribute to IRMPD of pre-excited CF_3H (see Figure 3.4), although it makes a major contribution to the total pulse fluence. If one were to cut this tail, it would lower the pulse fluence enough to allow the use of a collimated CO_2 laser beam without damaging the cell windows. To do this, we constructed a so-called "plasma shutter", the details of which are describe in Appendix C. This shutter allows the duration of the resulting tail-less pulse to be adjusted within 30-100 ns, while its peak intensity remains almost the same as in the leading

spike of the parent CO_2 laser pulse. Figure 3.9 shows the relative position of the pre-excitation and temporary modified CO_2 laser pulse resulting in the maximum OP-IRMPD yield.

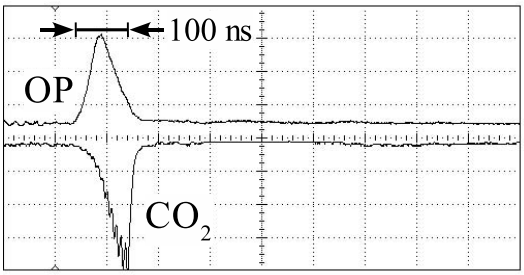

Figure 3.9: Relative positions and shapes of overtone pre-excitation laser pulse (OP) and dissociation (CO_2) laser pulse produced using the "plasma shutter" technique.

Figure 3.10 shows how the carbon-13 productivity (absolute yield) and abundance in final product depends on the sample pressure in this experimental configuration [3]. Comparison of the absolute productivity of the OP-IRMPD process measured using calibrated mass-spectrometer and the amount of pre-excited molecules estimated based on the known absorption cross-section for the pre-excitation laser radiation shows that at low pressures dissociation probability of pre-excited molecules in this experimental configuration is close to unity, as in the case of the long CO_2 laser pulse. At higher pressures dissociation probability drops also with the same rate which can be clearly seen from the similarity in the shapes of the curves representing the overall yield in the case of the long CO_2 laser pulse (Figure 3.7) and temporary modified, $\sim$ 70 ns pulse (Figure 3.10). The most important result is, however, high isotopic purity of the dissociation product obtained using the overlapped pre-excitation and dissociation pulses configuration. Carbon-13 enrichment obtained in this experiment (Figure 3.10, upper panel) is comparable with the one reported by Boyarkin *et al.* [27, 28] (up to 99%).

For consequent detailed study of the OP-IRMPD process with overlapped OP and temporary modified, short, CO_2 pulses we replaced our standard CO_2 laser with plasma shutter providing only up to 55 mJ temporary modified, short pulses (see Appendix C) by a custom made laser (PIC, model SP-7000 [44]) that allows obtaining 50-60 ns (FWHM) pulses of 400-600 mJ with almost no long tail (see Figure 3.11). The beam of this laser is weakly focused into a 2 cm reaction cell, giving a nearly constant fluence of up to 4.8 J/cm^2 along the entire axis of the cell. The maximum fluence has been kept below the optical damage threshold of the BaF_2 windows. With these modifications we can measure the isotopic selectivity and absolute yield of the isotope separation process at well determined dissociation fluence with much better

[3] We define *absolute yield* as the number of dissociated $^{13}CF_3H$ in the unit irradiated volume per unit pre-excitation laser fluence per laser pulse. The units of this quantity is the units of concentration divided by fluence: [cm^{-3}/(J cm^{-2})].

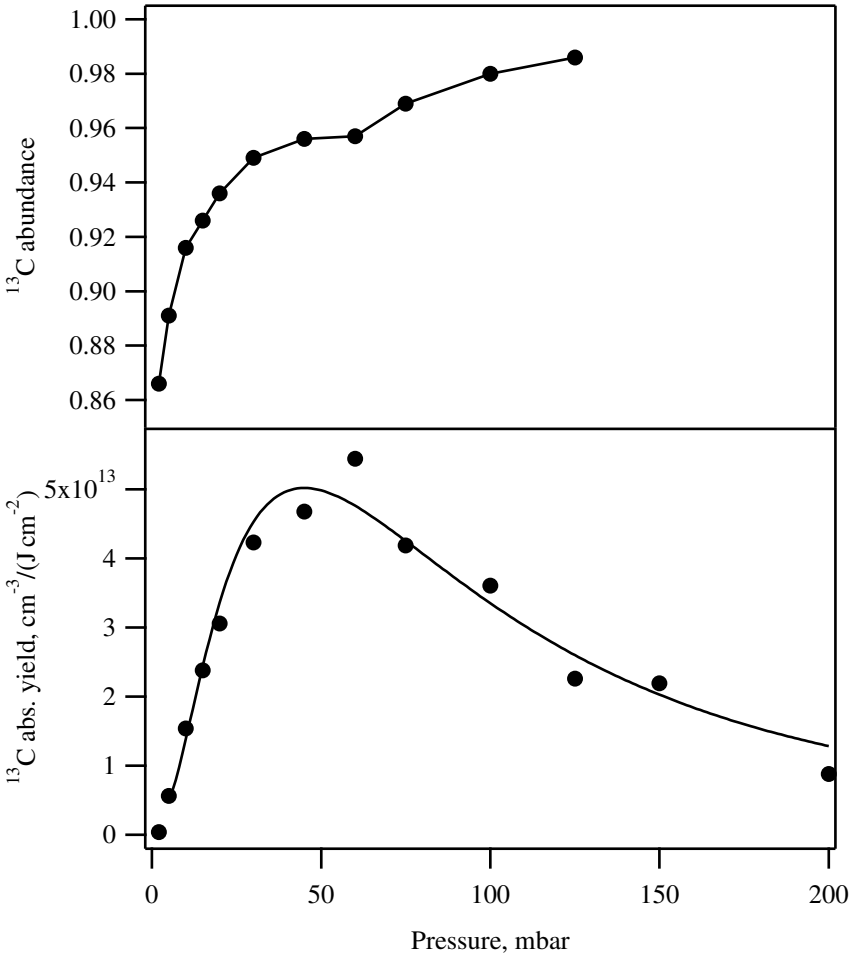

Figure 3.10: Pressure dependence of the absolute unit productivity (lower panel), and the carbon-13 isotopic abundance (upper panel) for the experiment timing shown in Figure 3.9.

accuracy.

Figure 3.11 represents the experiment timing and Figure 3.12 the pressure dependence of the isotopic abundance of carbon-13 in C_2F_4 and absolute yield of carbon-13 in the overtone pre-excitation-IRMPD process, measured by detecting C_2F_4 with a quadrupole mass-spectrometer.

The overtone pre-excitation pulses and short (50 ns) CO_2 laser dissociation pulses are overlapped as shown in Figure 3.11. The dissociation fluence was 3 J/cm^2. Each data point has been obtained after irradiation of the cell for 5 min. The yield is normalized to the irradiated volume, to the number of laser shots and to the pre-excitation fluence (the fraction of pre-excited molecules is a linear function of pre-excitation fluence in all our experiments [28]). Thus it gives the number of carbon-13 atoms in the C_2F_4 product, created per cm^3 of the irradiated volume by a single pair of laser pulses with pre-excitation fluence of 1 J/cm^2 and at a given fluence of the CO_2 laser. With a dissociation fluence of 3 J/cm^2, the absolute yield peaks at 80-100 mbar

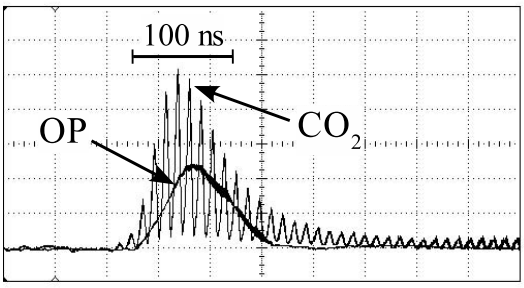

Figure 3.11: Relative positions and shapes of overtone pre-excitation laser pulse (OP) and dissociation (CO_2) laser pulse from the custom made CO_2 laser.

sample pressure. If under the same conditions at 80 mbar we shift the excitation pulse back by 100 ns ("zero" delay between the two non-overlapped pulses) the yield drops by 15 times. Such a manifold increase of the absolute yield in overlapped pulses configuration was expected based on results from our LIF experiments. However, a striking and largely unexpected feature of the data in Figure 3.12 is the significant increase of isotopic abundance with increase of pressure, a behavior that is similar to what was observed earlier with delayed pulses [27, 28]. At pressures where there is little collisional deactivation (2 mbar) the carbon-13 abundance is only 80%. At pressures of around 100 mbar, where the absolute dissociation yield is at the maximum, the carbon-13 abundance increases to 95.5% and reaches 98.2% at 265 mbar, although only at 40% of the maximum yield. This clearly demonstrates that overlap of overtone pre-excitation and IRMPD laser pulses allows a substantial increase of $^{13}C_2F_4$ yield while at the same time maintaining high isotopic selectivity. Independent of physical description of this phenomenon, it should increase significantly the practical relevance of the OP-IRMPD approach for laser isotope separation of carbon-13.

The 80% level of abundance of C_2F_4 (isotopic selectivity $S \approx 370$) at low pressure is substantially below the *ca.* 87% abundance ($S \approx 620$) of the pre-excited CF_3H, determined by the spectral overlap of the 3_1 band in the two isotopic species [28]. This fact suggests that our short, high intensity CO_2 laser pulse dissociates some ground state $^{12}CF_3H$ molecules or those warmed-up in collisions with the vibrationally excited carbon-13 species. Lowering the dissociation fluence by a factor of 2, to 1.5 J/cm^2 increases the selectivity of the process by 60-70%. The price paid for the increase of selectivity is a factor of 2.5 drop in the maximum dissociation yield. This result shows that the OP-IRMPD approach to laser isotope separation has an appreciable degree of flexibility, allowing on demand, the enhancement of selectivity or yield by adjustment of pressure and/or dissociation fluence.

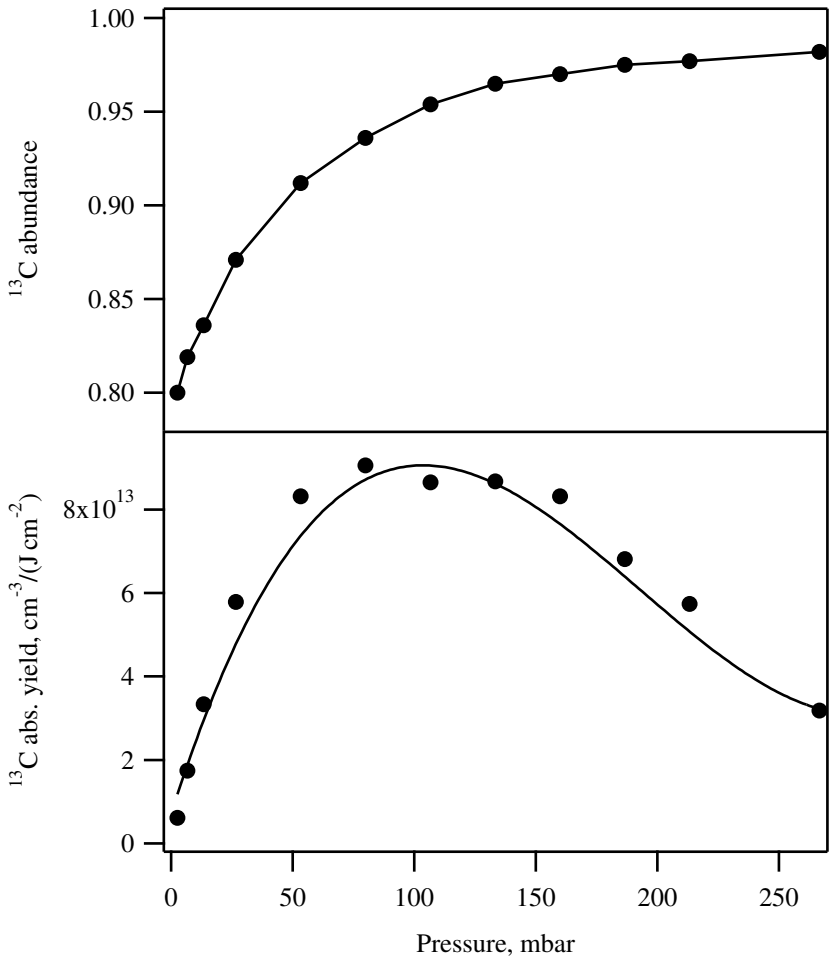

Figure 3.12: Pressure dependence of the absolute unit productivity (lower panel), and the carbon-13 isotopic abundance (upper panel) for the experiment timing shown in Figure 3.11.

3.3.4 Discussion

On the surface, the observed increase of isotopic selectivity with increasing pressure for overlapped pre-excitation and dissociation pulses may seem inconsistent with the semi-empirical model for the isotope separation process that has been suggested previously [28]. In this model, isotopic selectivity is controlled by the collisional parameter $p\Delta t$ (Δt is a delay time between pre-excitation and dissociation pulses), perhaps through isotopically selective vibrational deactivation of the pre-excited species. When the pulses are overlapped, it might seem that there is insufficient time for the deactivation. One must realize, however, that the dissociation is not an instantaneous process, as it takes some time for a pre-excited molecule to absorb the necessary number of IR photons to reach dissociation threshold. If the pressure is high enough, during this time the molecule may be relaxed through collisions in an isotopically selective manner. The dissociation time depends on both the sample pressure and the intensity of dissociation

pulse. An increase of pressure increases the collisional deactivation rate, while the up-pumping rate increases with increasing laser intensity. The overall IRMPE process is therefore governed by the difference between these two rates. In presence of deactivating collisions, a pre-excited molecule has to absorb more photons than it needs energetically to reach the dissociation limit. Each absorption-deactivation cycle improves isotopic selectivity of the process due to isotopic selectivity either in collisional deactivation and/or in IR absorption. Independent of which of the two mechanisms prevails, the isotopic selectivity of the overall process can be equally controlled by one's choice of either the sample pressure, which controls the deactivation rate, or the dissociation laser intensity, which determines the up-pumping rate. Achieving specific level of selectivity requires a sufficiently high number of absorption-deactivation cycles. Collisionally enhanced selectivity results, however, in lowering the probability of the dissociation of pre-excited molecules for the following reason. In an ensemble of molecules, each extra cycle broadens initially sharp vibrational energy distribution of the pre-excited CF_3H species due to the statistical nature of both absorption and deactivation. The broadening increases the part of the energy distribution that falls to vibrational energy levels from which the molecules have little chance to be dissociated by a given intensity of CO_2 laser. This results in a reduction in the dissociation yield. Figure 3.13 schematically illustrates the dynamics of multiphoton excitation under different sample pressures. As it can be seen from the figure, increased pressure results in slower excitation and faster broadening of the vibrational energy distribution.

Because the relative yield and the isotopic selectivity depend on the number of absorption-deactivation cycles in an opposite manner, the desired isotopic selectivity sets a limit to the dissociation yield of the overall process. The absolute dissociation yield can be increased by increasing the sample pressure with a simultaneous increase of dissociating laser intensity to maintain the relative yield and the desired isotopic selectivity. This growth has some limitations, however. First, the IRMPD yield of vibrationally ground state and warm $^{12}CF_3H$ increases rapidly with increasing dissociation intensity [47], and at some point it will degrade the isotopic selectivity. Second, at some point the spiky structure of our CO_2 laser pulse (Figure 3.11) will alter the ideal picture of excitation-deactivation kinetics considered above. Such pulse structure reflects longitudal multimode operation of our laser and it is typical for TEA lasers with a few transverse modes [48]. During the 1-2 ns high intense spikes of the pulse the pre-excited molecules have higher chance to be dissociated while experiencing only a few collisions, such that the produced CF_2 fragments are poorly enriched in carbon-13. In contrast, the isotopic purity of the pre-excited CF_3H greatly improves during the 9-10 ns intervals between the spikes, but these molecules have lower probability to be dissociated, or at least to survive in highly vibrational states before an intense spike arrives. A pulse with several transverse modes or better a smooth, single longitudal mode pulse [49] should improve the performance of the

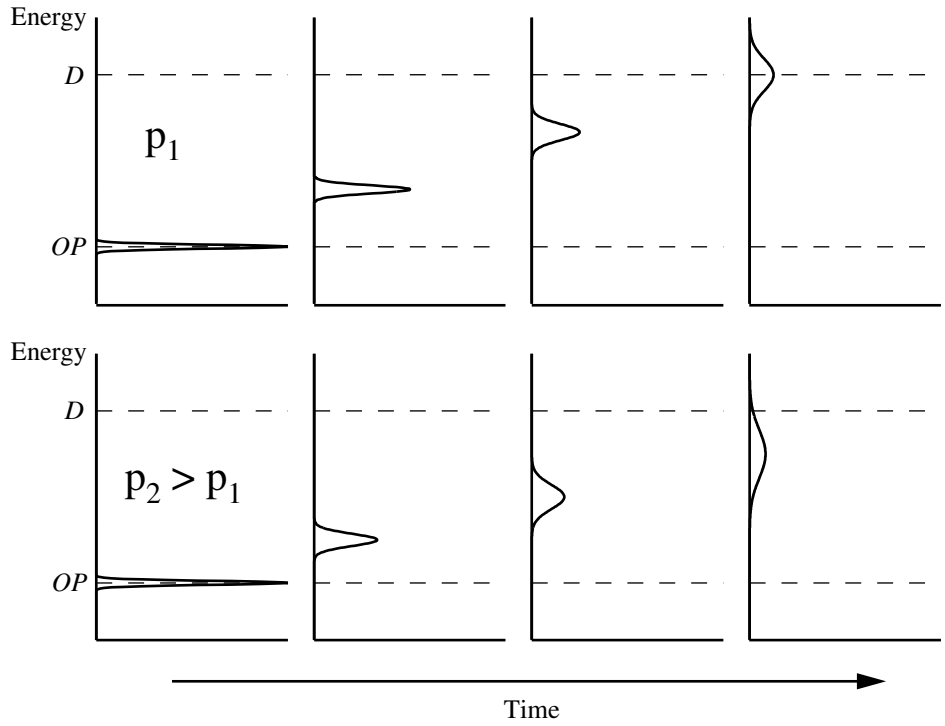

Figure 3.13: Multiphoton excitation dynamics under different sample pressures, p_1 and p_2 ($p_2 > p_1$). *OP* is the pre-excitation level and *D* is the dissociation threshold.

process.

We have drawn here only a qualitative picture of the two-laser isotopically selective collisional dissociation process in the configuration when overtone excitation and IRMPD laser pulses are overlapped. This picture is in line with our experimental observations: the increase of isotopic selectivity with increasing pressure and with decreasing dissociation laser intensity; increase of the absolute yield and simultaneous drop of the selectivity with increasing dissociation laser intensity and the weak dependence (within some limits) of the dissociation yield on the total fluence of the dissociation laser. A quantitative, semi-classical description of the process has to deal with solving numerically a master kinetic equation for IRMPD in presence of collisional vibrational deactivation, in a 3-component system (vibrationally excited $^{13}CF_3H$ and $^{12}CF_3H$ in excess of vibrationally ground state $^{12}CF_3H$) under conditions where the anharmonic shift of the absorption spectrum upon IRMPE is significant, compared with its width. This work is in progress in our laboratory, including experimental measurements of some of the spectroscopic constants in vibrationally excited CF_3H [34].

Overlapping the short pre-excitation and the dissociation pulses makes the overtone pre-excitation-IRMPD approach for MLIS of carbon-13 with CF_3H interesting from a practical point of view. First, such overlap results in a significant increase in the absolute yield of

carbon-13 atoms in the form of C_2F_4 while simultaneously achieving high isotopic selectivity for the process. The maximum dissociation yield occurs at 80-100 mbar of CF_3H, where the carbon-13 isotopic abundance is 95.5%. This is still below the 99% abundance required for most of the medical applications. A straightforward way to achieve the required isotopic selectivity is to further increase pressure of the sample and/or to reduce fluence of the dissociation laser, although this reduces the overall process yield.

A physically meaningful value that quantifies the yield of the process is the unit productivity, determined as the concentration of carbon-13 atoms converted to C_2F_4 created by a pair of laser pulses and per a unit fluence of the pre-excitation laser. We found that with a dissociation fluence of 3 J/cm^2 the maximum unit productivity is around 9×10^{14} cm^{-3}/(J cm^{-2}) (Figure 3.12). The total productivity of a separation unit scales linearly with irradiated volume, repetition rate of the lasers and the fluence of the pre-excitation laser, and thus it depends on the particular hardware employed and the details of the optical layout. Two features of the process revealed by our experiments will certainly facilitate its practical implementation. First, the relatively low dissociation fluence that we employ here allows dissociation of the pre-excited molecules by un unfocussed or slightly collimated CO_2 laser beam. This provides the opportunity to irradiate large volumes of CF_3H, which will increase the overall yield. Second, in the overlapped configuration, the length of pre-excitation pulse and the relative timing of the two pulses are less critical compared to the configuration with delayed pulses.

Whether by careful engineering one can make this process economically feasible still remains an open question. Our own evaluation suggests that the process at least merits a careful scale-up study. The experiments described below, in which we pre-excite CF_3H molecules to lower vibrational levels, make such a scale up study even more justifiable.

3.4 Pre-excitation through the first overtone of CH stretch vibration

3.4.1 Possible advantages of using lower pre-excitation levels

The study of isotopically selective collisional IRMPD of CF_3H pre-excited to the second overtone of CH stretch vibration ($3\nu_1$) has allowed us to understand the general mechanisms involved in the process. Based on this understanding, we have considerably improved the performance of the process using a properly selected combination of timing, sample pressure and dissociation laser fluence. However, the influence of the pre-excitation level on the yield and isotopic selectivity of OP-IRMPD has not yet been discussed. In order to understand the influence of this parameter, we first discuss the possible advantages and disadvantages of using pre-excitation levels different from v=3. In addition to comparing the efficiency and isotopic selectivity of the

pre-excitation step, we must evaluate the selectivity of multiphoton dissociation of pre-excited molecules vs. ground state ones at each pre-excitation level, as well as the degree of collisional enhancement of the isotopic selectivity that we might expect.

Table 3.3 summarizes the spectroscopic data for the absorption bands of interest [37,38,50].

Band in $^{13}CF_3H$	Position (cm^{-1})	Isotopic shift $[\nu(^{12}C) - \nu(^{13}C)]$ (cm^{-1})	Relative absorption intensity
3_1	8753	39.7	1
2_1	5936.6	22.8	6.7
2_2	5680.9	29.5	4.4
1_1	3024.6	10.9	4400
1_2	2695.1	15.1	210

Table 3.3: Spectroscopic data for the absorption bands of interest.

We do not consider the third overtone of the CH stretch vibration because the corresponding absorption cross section is about an order of magnitude lower than of the 3_1 absorption band [38]. Using this weak absorption line one can pre-excite about 0.1% of $^{13}CF_3H$ per typical pre-excitation laser pulse of 1 J/cm^2. Such low efficiency of the first step of OP-IRMPD limits the final dissociation yield making the overall process inefficient.

Pre-excitation through the 2_1 band is 50% more efficient than that through the 2_2 band, although the isotopic shift for the latter is larger, suggesting the possibility of higher isotopic selectivity. This suggestion, however, is not entirely clear. Figure 3.14 shows the absorption spectra of naturally abundant CF_3H in the regions of the respective Q-branches of the 2_2 and the 2_1 bands of the carbon-13 species obtained by photoacoustic spectroscopy. Because of

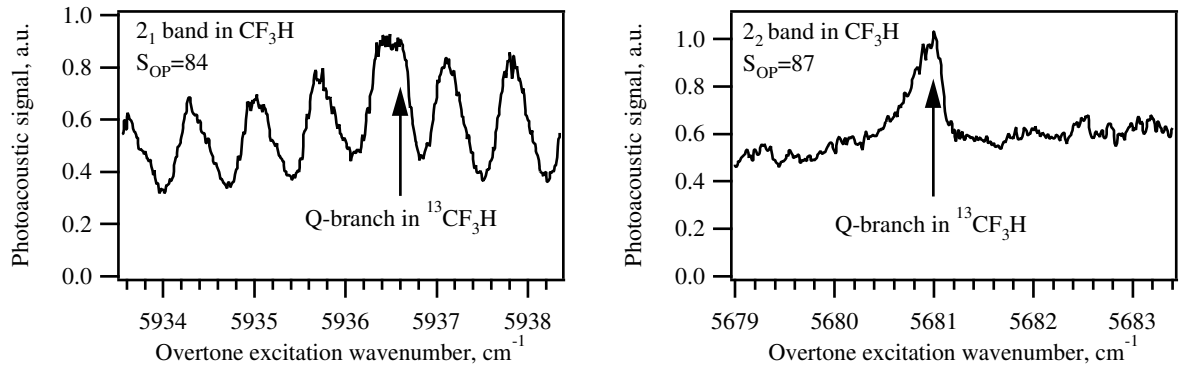

Figure 3.14: Photoacoustic spectra of the 2_1 and 2_2 absorption lines of CF_3H.

its larger isotopic shift, the 2_2 Q-branch of the carbon-13 species is overlapped with high J transitions of the P-branch in $^{12}CF_3H$. Due to the splitting of high J-states of the 2_2 level by

weak perturbations [38], these transitions appear unresolved at moderate spectral resolution of (0.08 cm^{-1}), forming a nearly continuous background. With such a spectral overlap, the maximum isotopic selectivity that one could expect to obtain upon pre-excitation of the 2_2 band is around 87. Because of its smaller isotopic shift, the Q-branch of the 2_1 band in $^{13}CF_3H$ falls into a region of more intense, but resolved moderate J-transitions. Here the 2_1 Q-branch in $^{13}CF_3H$ is just adjacent to one such transition. The maximal isotopic selectivity of the 2_1 level pre-excitation has been estimated to be about 84 by fitting the spectra represented in Figure 3.14, which is comparable to that for the 2_2 band.

On the other hand, compared to using the 3_1 level, pre-excitation to a lower energy level will result in a decreased probability of multiphoton dissociation. This is due to the low cross sections for the first steps of absorbing photons from the dissociating laser[4] as well as the higher number of absorption steps required to reach the dissociation limit. The absorption cross section, and hence the dissociation yield, can be increased by shifting of the dissociating laser frequency to the blue side towards the absorption band of the pre-excited molecules, but this will also increase the absorption cross section for ground state molecules, which reduces the selectivity. Thus, the selection of the dissociating frequency is a question of compromise between productivity (OP-IRMPD yield) and selectivity in the dissociation of pre-excited molecules. A smaller energy gap between pre-excited and ground state molecules in comparison with v=3 pre-excitation implies, correspondingly, a smaller red shift of the absorption frequency of pre-excited *v.s.* ground state molecules. Hence, finding a dissociation frequency to dissociate selectively pre-excited molecules is less probable in the case of pre-excitation *via* lower overtones or fundamentals. Our study is aimed at finding the optimal parameters (wavelength and bandwidth of pre-excitation laser, CF_3H pressure and temperature, dissociation wavelength) for isotopically selective IRMPD of CF_3H pre-excited to the first overtone of the CH stretch vibration and comparison of the performance of the OP-IRMPD approach to carbon isotope separation for the v=3 and v=2 levels of pre-excitation.

The potential advantage of using the v_{CH}=1 fundamental transition for the pre-excitation is its high absorption intensity, which is 650 times higher than that of the 2_1 band in the case of 1_1 and 31 times in the case 1_2 (see Table 3.3). Such high absorption intensity would simplify

[4]The density of vibrational states is 19 per cm^{-1} in the region of $v_{CH} = 3$ and 3 per cm^{-1} in the region of $v_{CH} = 2$ (see Figure 3.15). This implies that the $2\nu_1$ pre-excitation level lies below the limit of quasicontinuum, which is characterized by an average distance between vibrational energy levels equal to the bandwidth of the dissociation laser (~ 0.1 cm^{-1}). Such a distance between levels corresponds to a density of states of 10 per cm^{-1}. However, density of states corresponding to the energy of pre-excitation photon plus one photon of CO_2 laser ($\sim (6000 + 1000) = 7000$ cm^{-1}) is about 6 per cm^{-1}, which is close to the quasicontinuum requirement. It is hence possible that the probability of multiphoton dissociation of the molecules pre-excited to the first overtone of the CH stretch vibration is not considerably lower than the one corresponding to the pre-excitation to the second overtone if the same dissociation laser fluence is applied.

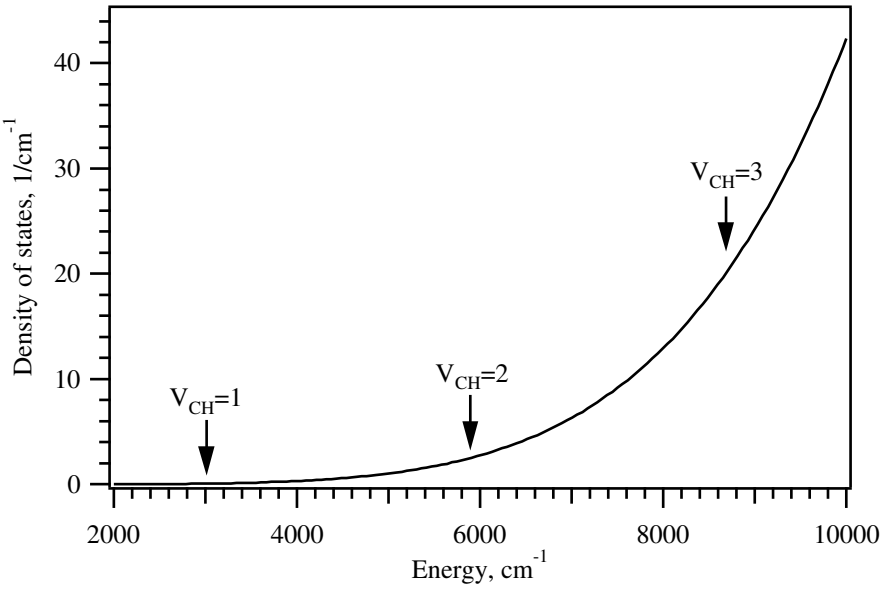

Figure 3.15: Density of vibrational states of CF_3H as a function of energy.

engineering of the MLIS process and as a result cut its production cost. A simulation of the $^{13}CF_3H$ absorption spectrum based on the available spectroscopic constants [38] and comparison with the corresponding $^{12}CF_3H$ spectrum indicates that the selectivity of pre-excitation step can be sufficiently high in spite of the smaller isotopic shift. There is, however, an associated risk created by the small difference between the absorption spectrum of the pre-excited molecules and the ground state species. For a maximum dissociation fluence of 3-4 J/cm^2 that can be used in a collimated CO_2 laser beam without damaging the windows, the IRMPD yield for molecules on the v=1 level should be considerably lower than for the molecules pre-excited to the first and second overtone levels. This is explained by the low density of vibrational states at the energy region corresponding to the fundamental frequency of CH stretch vibration which is only 0.08 per cm^{-1} (see Figure 3.15). To some extent this can be compensated by the high transition strength of the fundamental band. Slight focusing of dissociating beam is also an option, since there is no longer a need to have a long optical path. Shifting the wavelength of the CO_2 laser to a line in 9R branch instead of 9P branch used at higher pre-excitation levels will certainly increase the dissociation efficiency for molecules pre-excited to the 1_1 or 1_2 levels, but this may cause significant nonselective dissociation of the ground state species and a lost of isotopic selectivity. The proximity of the ground state and the pre-excited state on the vibrational energy scale also makes it unclear to what extent molecular collisions can be employed to enhance isotopic selectivity of the process. The main objective of our experiments concerning the IRMPD of CF_3H pre-excited to 1_1 and 1_2 levels is to check the possibility of

selective dissociation of pre-excited molecules without dissociating a considerable amount of vibrational ground state molecules. In the case selectivity could be maintained, the subsequent objective would be to estimate the productivity of the process.

3.4.2 Generation of 1.68 μm radiation for pre-excitation through the first overtone of CH stretch vibration

The experimental set-up used in these experiments is identical to that used in v=3 experiments, except for the method of generating of laser radiation for overtone pre-excitation. The system of alexandrite laser/Raman converter combination used to pre-excite molecules to the 3_1 level has been replaced with a system based upon difference frequency generation and optical parametric amplification that can generate tunable IR radiation suitable for pre-excitation *via* the 2_1, 2_2 bands. A schematics of this system is presented in the Figure 3.16. A system providing tunable radiation suitable for pre-excitation *via* the fundamental bands will be described later in the Section 3.6 on page 94.

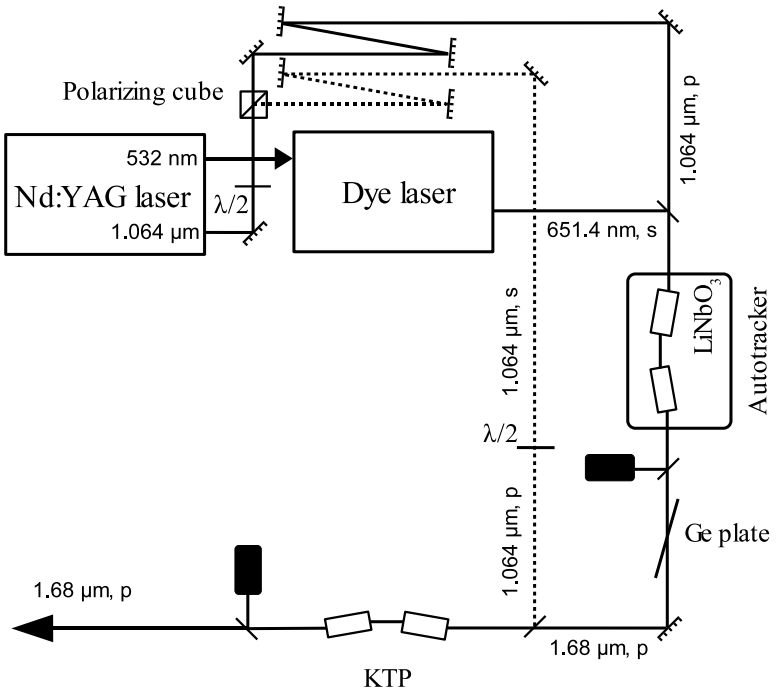

Figure 3.16: Optical layout of the system for generation of near IR tunable radiation for pre-excitation of CF_3H *via* the 2_1 and 2_2 vibrational bands (difference frequency mixing with subsequent optical parametrical amplification).

The central piece of this system is a powerful, single-mode Nd:YAG laser (Spectra-Physics GCR-250). A fraction of the 1064 nm output of this laser is frequency doubled to pump a dye laser (Lambda Physik Scanmate 2E). The 30-40 mJ output of the dye is mixed with 150

mJ of the Nd:YAG laser fundamental in a $LiNbO_3$ crystal to generate 2-4 mJ of tunable IR radiation through a difference frequency mixing (DFM) process. The phase match angle of the crystal is adjusted automatically by a commercial autotracking unit (INRAD-II) as the laser wavelength is scanned. This unit also compensates for changes in phase match angle arising from temperature variations. The output of the DFM is further amplified in a two stage optical parametric amplifier (OPA) pumped by 200 mJ of the infrared fundamental of the same Nd:YAG laser. This gives narrow bandwidth, tunable radiation up to 130 mJ per pulse at 1.68 μm. The pre-excitation radiation is slightly focused by a telescope before entering the reaction cell through a window at the Brewster angle. The dissociating CO_2 laser beam is focused by a F=100 cm lens and enters the reaction cell from the opposite side. The isotopic composition of the C_2F_4 dissociation product is measured by a computer controlled quadruple mass-spectrometer (Balzers, QMS-422).

3.4.3 Comparison of pre-excitation through the 3_1, 2_2 and 2_1 bands

Our OP-IRMPD experiments with pre-excitation of the first overtone of CH stretch vibration have been divided into two series. In the first series, we have demonstrated that the OP-IRMPD yield obtained using the v=2 pre-excitation is higher than the corresponding value for pre-excitation at v=3. At the same time isotopic selectivity of the process is conserved. The objective of the second series of the experiments is to optimize the OP-IRMPD pre-excitation at v_{CH}=2 and to study the potential of such a scheme for production of carbon-13 enriched C_2F_4.

Figure 3.17 shows the relative IRMPD yield (fraction of the pre-excited molecules dissociated) and isotopic selectivity for the OP-IRMPD process subsequent to pre-excitation to the 3_1 and 3_2 bands as a function of CF_3H pressure. In the case of 2_2 pre-excitation, the dissociation fluence has been increased to 4.5 J/cm^2 in order to get a relative IRMPD yield approximately equal to that obtained with 3 J/cm^2 when the 3_1 band is pre-excited. This allows us to compare the two processes by a single parameter (isotopic selectivity), which is more unambiguous than the simultaneous comparison of two parameters (selectivity and yield). Another option would be to choose a CO_2 laser fluence such that the isotopic selectivity of the process with 2_2 pre-excitation is equal to that using 3_1 pre-excitation and compare dissociation yields of the two processes.

In the low pressure limit, the IRMPD step is not isotopically selective (due to the saturation of the multiphoton dissociation of pre-excited molecules at the fluence of the CO_2 laser employed) and the final selectivity of OP-IRMPD process is equal to the selectivity of the overtone pre-excitation step. Thus, the isotopic selectivity of OP-IRMPD process with pre-excitation through the 2_2 band is about 3 times lower than with pre-excitation through the 3_1 band.

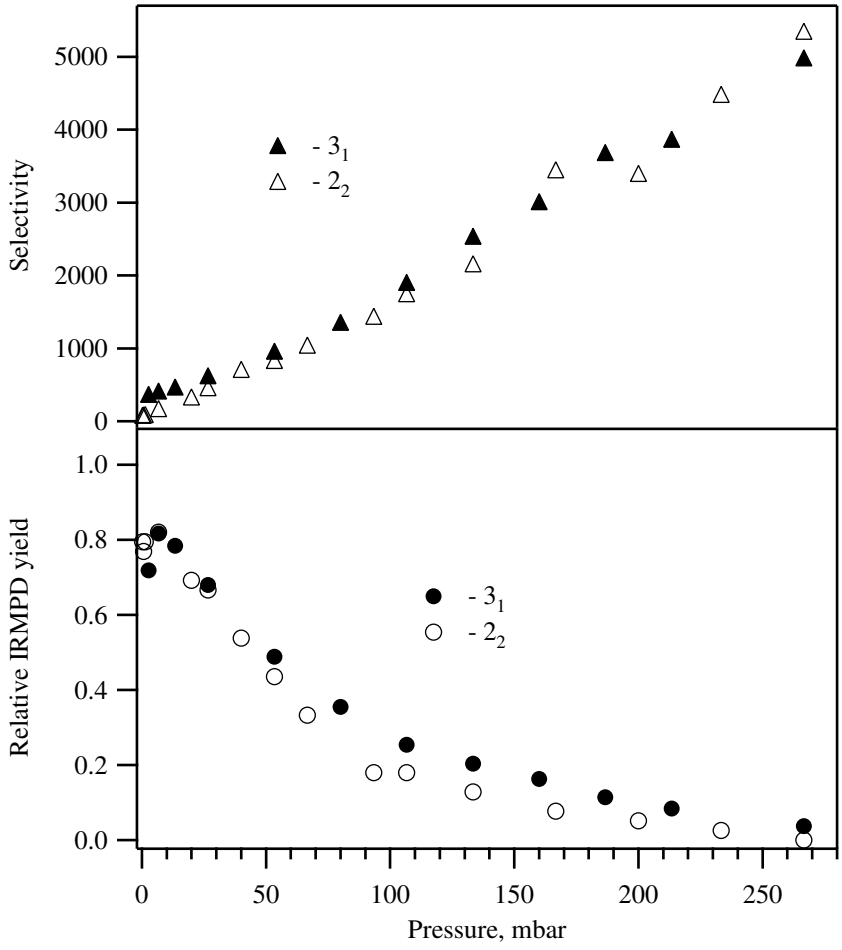

Figure 3.17: Relative IRMPD yield and overall selectivity of OP-IRMPD for different levels of pre-excitation. The dissociation fluence is 3 J/cm^2 for 3_1 and 4.5 J/cm^2 for 2_2 pre-excitation level. The relative IRMPD yield is the ratio of the numbers of dissociated and pre-excited $^{13}CF_3H$

However, at sample pressures above 50 mbar the selectivity of both processes becomes almost equal, and subsequent increase in pressure does not influence the ratio between them. This suggests that the selectivity of IRMPD step is higher in the case of pre-excitation to the lower energy level (2_2). This increase in isotopic selectivity could be explained both by isotopic selectivity in absorption of CO_2 laser photons and by different rates of collisional V-V relaxation for different isotopic species. In the first case, the difference in selectivity may result from the different number of photons required to reach the dissociation limit. In the second case, one must to consider the time required for a molecule to absorb the required number of IR photons. A longer dissociation time due to the lower pre-excitation level and the larger number of CO_2 laser photons required implies that a molecule will undergo a higher number of collisions before being dissociated, and, hence reach a higher final degree of enrichment.

Thus, using pre-excitation *via* the 2_2 band instead of the 3_1 band and increasing the fluence of the dissociation laser by a factor of 1.5, one can achieve with a sample pressure above 50 mbar approximately the same overall isotopic selectivity and the same fraction dissociated in the IRMPD step. However, as the absorption cross section of the 2_2 band is 4.4 times higher than the 3_2 band (see Table 3.3 on page 66), the overall productivity of the OP-IRMPD process for the same pre-excitation laser fluence increases by a factor of 4.4. Figure 3.18 shows the absolute yield of the processes as a function of sample pressure for two different levels of pre-excitation. One should note, however that the conservation of relative IRMPD yield is

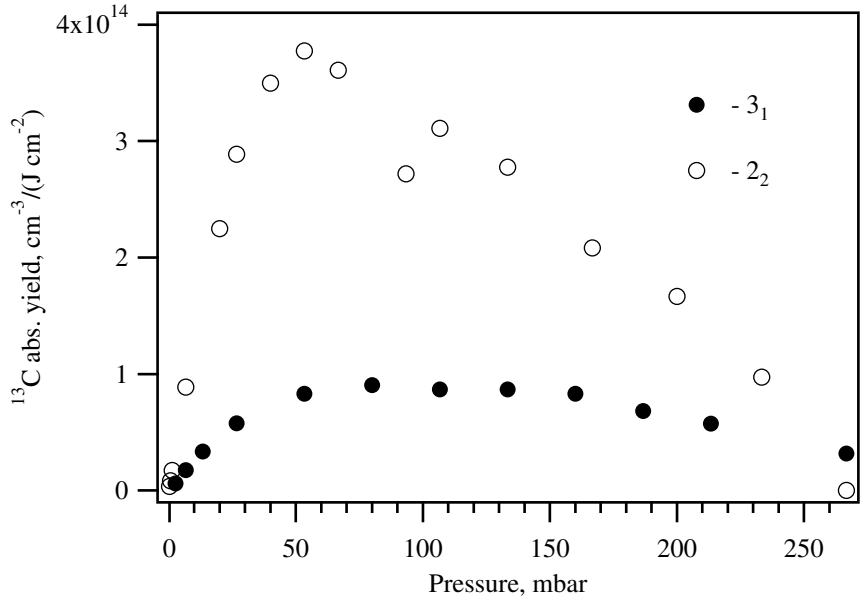

Figure 3.18: Absolute dissociation yield of OP-IRMPD for different levels of pre-excitation.

reached by increasing the CO_2 laser fluence to 4.5 J/cm^2, which is above the long-term damage threshold of IR optical materials. The BaF_2 windows used in our experiments were burned after several days of work at this fluence. However, in the multipass Heriot cell configuration, which is more appropriate for industrial-scale MLIS [19, 51], the diameter of the beam varies, reaching its maximum on the mirrors and minimum in the center in the cell. Thus, sufficiently high laser fluence can be reached in the central part of such a cell without exceeding the 3-4 J/cm^2 optics damage threshold on the mirrors and windows. Taking this into account we can consider the 2_2 band pre-excitation as more appropriate for the OP-IRMPD approach to laser isotope separation than the 3_1 one.

The next step in our experiments was to test the OP-IRMPD method with pre-excitation through the 2_1 band. Because this band is 1.5 times stronger than the 2_2 band, it is more attractive for practical implementation of the OP-IRMPD method for laser isotope separation.

The test experiment was done using 3 J/cm^2 CO_2 laser fluence and 53 mbar sample pressure. We observe an increase in the dissociation yield of a factor of 1.5 compared to the 2_2 band, which corresponds to the ratio 2_1 to 2_2 absorption cross sections. While there is a decrease in selectivity in changing the pre-excitation level from 2_2 to 2_1 of less than 10%, we have previously shown that the selectivity can be increased by increasing the sample pressure with decrease of dissociation yield. Analysis of the data represented in the Figure 3.17 shows that 10% increase in selectivity at pressures above 40 mbar is reached by increase in pressure by $\sim$ 5 mbar and results in $\sim$ 10% decrease in relative IRMPD yield. Thus, for a fixed isotopic selectivity, the process yield with pre-excitation through the 2_1 band is 1.35 times higher compare to that with pre-excitation through the 2_2 band. In the subsequent experiments we used pre-excitation through the 2_1 band.

3.4.4 Effect of the CO_2 laser pulse shape

As described in Section 3.3.4, the output beam of our free running TEA-CO_2 laser appears as a train of 1-2 ns pulses separated by intervals of 9-10 ns (see Figure 3.11 on page 61) as a result of self mode-locking [48]. This spiky structure of the CO_2 laser pulse imposes a certain time structure on the collisional multiphoton absorption process. Considering the competition between up-pumping and collisional V-V relaxation proposed earlier for the description of such a process, there should be a predominance of up-pumping during a spike and of relaxation in the trough between spikes. Thus, the entire process of multiphoton excitation consists of a number of short, alternating subprocesses. This pulse structure limits the possibility of increasing the sample pressure with simultaneous increase of dissociation laser fluence since if the collisional relaxation rate is too high, the time delay between two spikes (about 10 ns) will be sufficient for relaxation below the limit of the vibrational quasicontinuum. Increased dissociation laser fluence, in turn, will result in an increased probability for dissociation of ground state molecules. One can conclude that to effectively use the competition between up-pumping and collisional V-V relaxation during the CO_2 laser pulse, the distance between two pikes should not considerably exceed an average time between two consequent collisions. This means that at CF_3H pressures above 10-20 mbar, the spiky structure of the dissociation pulse has a considerable destructive influence on the performance of the laser isotope separation process.

A smooth temporal pulse shape can be achieved by forcing the laser to oscillate on a single longitudinal mode. There are a number of techniques to achieve this (see for example [48, 49] and references therein), among which are injection of a weak cw signal into the TEA laser cavity, the combination of the high pressure discharge region with a low pressure gain section, insertion of an etalon or an intracavity cell with a selective absorber. Quack *et al* have used the intracavity absorber approach to produce temporally modified CO_2 laser pulses for application

in multiphoton excitation experiments [49]. This technique has also been applied in the study of multiphoton excitation/dissociation of methanol pre-excited to different energies [47].

We decided, however, to use a completely different approach for the "smoothing" the CO_2 laser pulse structure. Although this approach cannot be used in a large scale apparatus, its simplicity and resulting pulse-to-pulse reproducibility makes it convenient for laboratory experiments with a small working volume. The optical configuration represented in the Figure 3.19 allows us to reduce the time delay between spikes in CO_2 laser pulse. The CO_2 laser beam

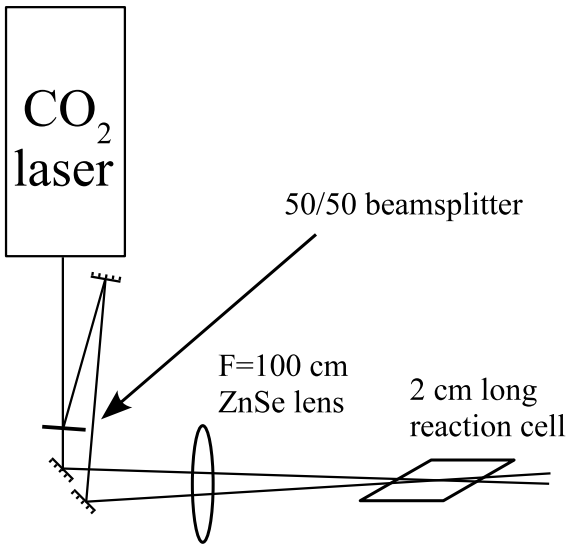

Figure 3.19: Schematics of the optical layout for producing a "doubled" CO_2 laser pulse.

is split by a 50/50 beamsplitter (a ZnSe plate the front surface of which is dielectrically coated in order to provide reflectance of 50% of laser radiation and the second surface is anti-reflective coated). One of the parts of the beam passes through a 150 cm optical delay line which gives a 5 ns delay with respect to the other part of the beam. This has the effect interposing the spikes in the second beam precisely between those of the the first beam, shortening the delay between spikes that the molecules experience from 10 ns to 5 ns. Both beams are focused by the same F=100 cm ZnSe lens and crossed in the center of the 2 cm long reaction cell. The short length of the cell allows almost complete overlap of the beams in the reaction volume. Figure 3.20 shows the temporal profile of a pulse emanating the CO_2 laser and the profile of the "doubled" pulse measured using a Ge photon drag. Although the spike structure is not resolved in the "doubled" pulse represented in the Figure 3.20 (due to the limited temporal resolution of the photon drag), we assume that this configuration does not provide complete smoothing of the pulse since typical spike width of a pulsed TEA CO_2 laser (1-2 ns [48]) is smaller than the 5

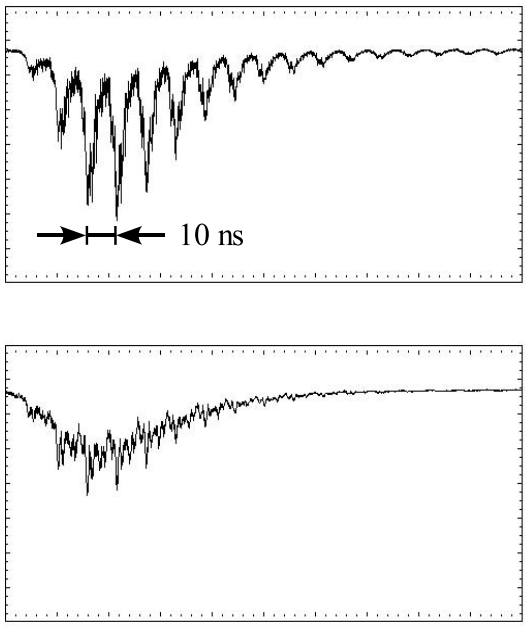

Figure 3.20: CO_2 laser pulse shape on the output of the laser (upper panel) and the "doubled" pulse (lower panel). Spikes width is determined by the 2 ns time resolution of digital oscilloscope (HP model 54615B).

ns delay between spikes in the "doubled" pulse. However, comparing the overall yield and isotopic selectivity of the OP-IRMPD process obtained using the regular and temporally modified ("doubled") CO_2 laser pulses, we can make certain conclusions about possible advantages of using a trully "smooth" dissociation laser pulse.

The yield and selectivity of the OP-IRMPD process with 2_1 pre-excitation have been measured as a function of the sample pressure using regular and "doubled" dissociation laser pulses. The dissociation laser fluence in this experiment has been reduced to 3 J/cm^2, which is below the damage threshold for BaF_2 windows. Figure 3.21 depicts the experimental results for the two CO_2 laser pulse shapes.

First of all, we have to point out a difference between the results with the regular pulse shown in the Figure 3.21 (solid lines and markers) and the results represented in the Figure 3.17 (open markers). These experiments differ by the fluence of CO_2 laser pulse (3 and 4.5 J/cm^2 respectively) and by the pre-excited vibrational band (2_1 and 2_2 respectively). As previously discussed, pre-excitation of the 2_1 and 2_2 bands results in approximately equal relative IRMPD yields and final selectivity. The dissociation laser fluence, on the other hand, has a significant influence on the process. Lower fluence results in a lower dissociation yield and higher isotopic selectivity. When 4.5 J/cm^2 fluence is applied to the molecules pre-excited to the first overtone of the CH stretch vibration, the dissociation probability (relative IRMPD yield) at low pressure is close to 1. At a dissociation fluence of 3 J/cm^2 only about 80% of the pre-excited molecules

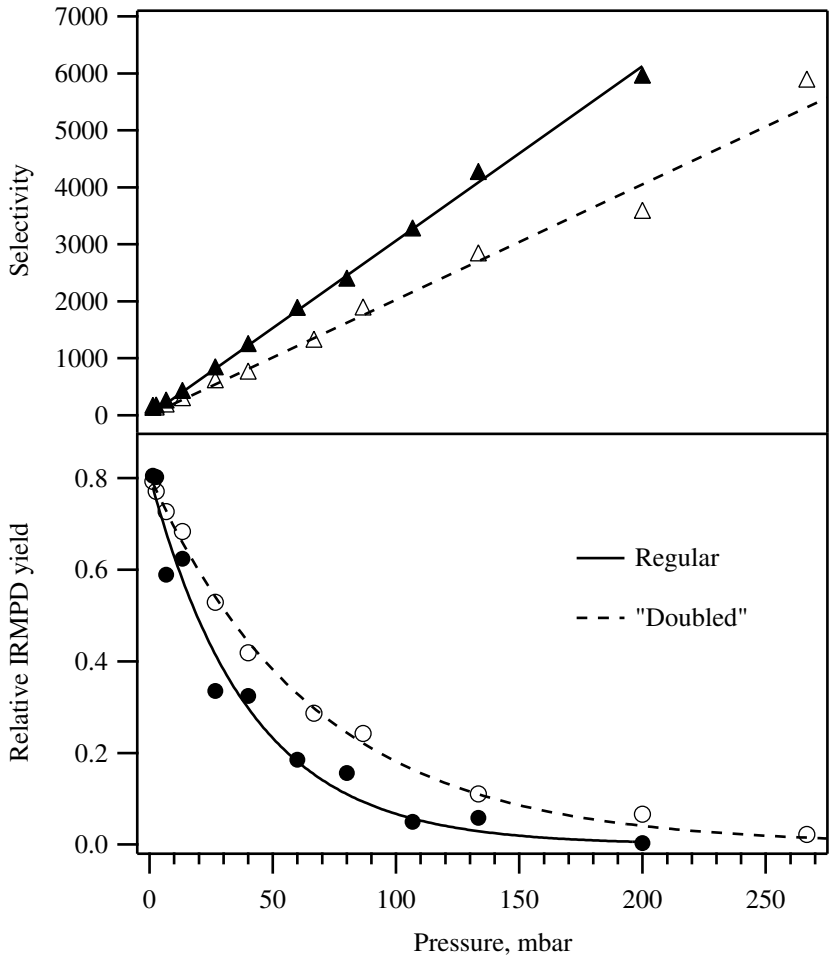

Figure 3.21: Relative IRMPD yield and selectivity of OP-IRMPD process with 2_1 pre-excitation for regular and "doubled" CO_2 laser pulses. The dissociation laser fluence was 3 J/cm^2.

dissociate at low pressure and the dissociation probability decreases faster with increasing pressure. On the other hand, the selectivity of OP-IRMPD process with 3 J/cm^2 is about 1.4 times higher than with 4.5 J/cm^2 of dissociation fluence. The absolute yield of the IRMPD with 2_1 pre-excitation at 3 J/cm^2 and sample pressure 70-100 mbar is 3-4 times larger than the yield of IRMPD with 3_1 pre-excitation under the same conditions, whereas the isotopic selectivity of the process including the first overtone pre-excitation is higher by a factor of 1.4.

Decreasing the distance between spikes in the CO_2 laser pulse leads to the result that is similar to what one can obtain by increasing the dissociation fluence (compare the curves corresponding to the regular pulse in the Figure 3.21 and the curves corresponding to the v=2 pre-excitation in the Figure 3.17). As Figure 3.21 clearly shows, "doubled" pulses cause a slower increase of isotopic selectivity and slower decrease of dissociation probability upon increase of CF_3H pressure compared to the regular CO_2 laser pulses. The effect is similar to what one

would observe by increasing the fluence of a regular pulse. A certain value of isotopic selectivity achieved either with "doubled" or with intense regular pulse corresponds to the same relative IRMPD yield. Thus, to achieve a certain level of isotopic selectivity (for example 2000, which would correspond to 95.6% of carbon-13 in the final product) one could use either regular CO_2 laser pulses and a pressure of 65 mbar or "doubled" pulses and 100 mbar. In the both cases approximately 15% of pre-excited molecules are dissociated[5]. However, working at the higher pressure is advantageous from the point of view of the absolute productivity of the process. For a selectivity of 2000, the absolute productivity with the "doubled" pulse is 1.5 times higher than for the regular (self-mode locked) CO_2 laser pulse. We assume that the use of a truly smooth pulse shape will result in even higher increase in the optimal CF_3H pressure, and, hence, in higher productivity of the isotope separation process.

3.4.5 Effect of CF_3H temperature on the selectivity and overall yield

Isotopic selectivity of our pre-excitation step is determined by spectral overlap of the Q-branch in $^{13}CF_3H$ with the P(33) transitions in $^{12}CF_3H$. Lowering sample temperature reduces population of high rotational states resulting in reducing this spectral overlap. Cooling the molecules therefore has to increase isotopic selectivity of the process. It is, however, unclear how the cooling will change its productivity, since several factors may determine this change. On one hand, cooling makes the Q-branch narrower and more intense, such as more molecules can be pre-excited through its maximum. On the other hand efficiency of dissociation of the pre-excited molecules can drop upon cooling. Indeed, pre-excitation promotes $^{13}CF_3H$ molecules only into a few rotational states that are determined by the spectral overlap of the 0.5 cm^{-1} wide Q-branch with our 0.05 cm^{-1} wide overtone laser. At typically high pressure of our experiments these molecules will quickly rotationally thermalize in collisions with the excessive bath of vibrationally ground state molecules, approaching to their thermal distribution. Cooling narrows this rotational distribution, making IRMPD, in general, more difficult.

The other factor that can influence yield of the process at low temperature is the rate of collisional deactivation. First of all, at a fixed pressure the mean rate of bimolecular collisions, $\langle z \rangle$, increases with lowering temperature T. Indeed, $\langle z \rangle$ is proportional to the concentration n and average velocity of the molecules $\langle v \rangle$. The concentration for fixed pressure is inverse proportional to the temperature, and the average velocity is proportional to the square root of temperature. Thus, the mean collision rate is inverse proportional to square root of tempera-

[5]The question about the correlation between selectivity and productivity will be discussed in more detail later on page 81.

ture:

$$\begin{cases} \langle z \rangle \propto n\langle v \rangle \\ n \propto \frac{1}{T} \\ \langle v \rangle \propto \sqrt{T} \end{cases} \qquad \Rightarrow \qquad \langle z \rangle \propto \frac{1}{\sqrt{T}}. \tag{3.11}$$

That is cooling should decrease productivity and simultaneously increase isotopic selectivity by the same way as it would be at room temperature, but at an elevated pressure that gives the same collisional rate. Second, the rate of collisional vibrational energy transfer itself changes with temperature. A several descriptions of this effect are proposed (see [52] for the overview of different theories attempting to explain the influence of temperature on the probability of V-V energy transfer in collision). Depending on the prevailing mechanism of the energy transfer (dipole-dipole or quadrupole-quadrupole interaction, for instance) and temperature range, this rate may increase or decrease [52]. One of the generally accepted theories (Sharma-Brau theory [53–55]) predicts, for instance, $1/T$ dependence of energy transfer probability for the case of the long-range dipole-dipole interaction between molecules. Thus, the overall change of the deactivation rate is difficult to predict without a comprehensive quantitative analysis. It is, therefore, difficult *a priori* to evaluate, whether cooling of CF_3H will improve the overall performance of our separation process. In order to verify this we have performed a few preliminary experiments, where isotopic selectivity and relative IRMPD yield of the process have been measured at low temperature under typical conditions of room temperature experiments (laser frequencies and fluences, pressure).

To control the temperature of CF_3H in our small (20 mm long, 22 mm internal diameter) reaction cell we employed the apparatus depicted in the Figure 3.22. The reaction cell has been placed into a foam plastic box. The laser beams passed through two 10 mm diameter holes in the opposite sides of the box. The temperature inside the box was controlled by a continuous flow of cooled dry nitrogen gas. The nitrogen was cooled by passing it through a 4 mm internal diameter copper tube placed into a liquid nitrogen dewar. Changing the gaseous nitrogen flux enables us to change the temperature inside the foam plastic shell in the range of -50°C to room temperature (+23°C). Such a configuration excludes a contact between cold cell windows and warm atmospheric air which would result in water condensation on the windows and provides homogeneous cooling of the small reaction cell.

Figure 3.23 shows the relative IRMPD yield and isotopic selectivity as a function of the sample temperature after pre-excitation of CF_3H to the 2_1 level. The bandwidth of the pre-excitation laser was reduced in this experiment to 0.03 cm^{-1} by an intracavity etalon, and a "doubled" CO_2 laser pulse was used for dissociation. The sample pressure was 80 mbar. As it can be seen from the figure, a decrease of the temperature results in an increase of isotopic

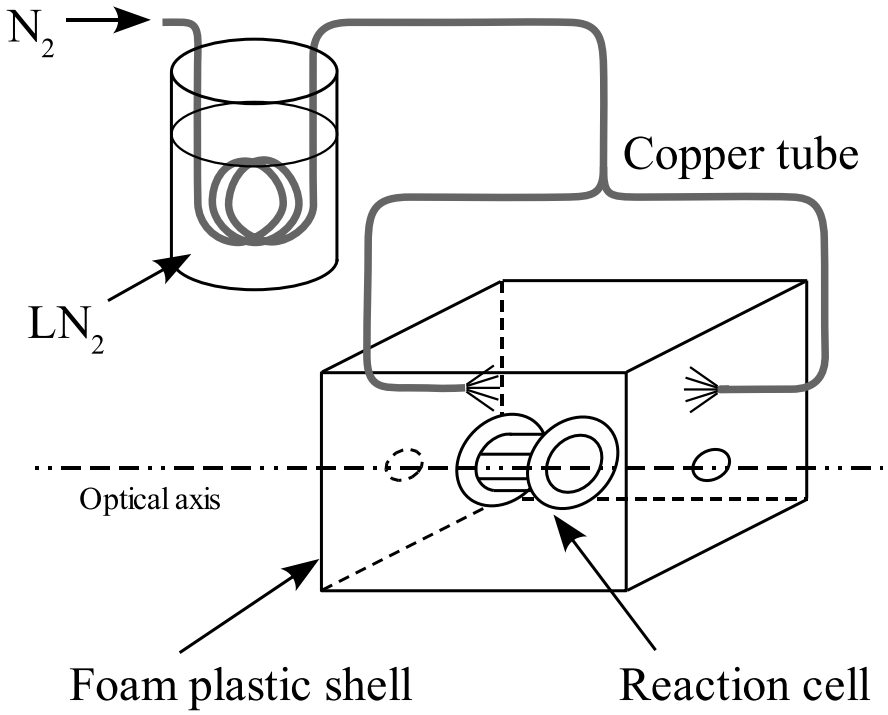

Figure 3.22: Apparatus for cooling the small reaction cell.

selectivity with simultaneous drop of the yield. While the increase of selectivity is expected and can be explained by the smaller spectral overlap of carbon-12 and carbon-13 bearing species and/or by higher collision rate, the nature of the relative IRMPD yield (fraction of pre-excited $^{13}CF_3H$ dissociated) drop by a factor 1.7 is not obvious. The increase of collisional rate by a factor of 1.14 (3.4.5) for a decrease of temperature from +15°C (288K) to -50°C (223K) may account only for 18% out of 70% of the total drop of the yield in this temperature interval, which follows from the results of the experiments where the dissociation probability was measured as a function of sample pressure (as can be seen from Figure 3.21, increase of pressure by a factor of 1.14 from 80 to 91.2 leads to the relative IRMPD yield drop by a factor of 1.18).

In the case if the residual decrease in the dissociation yield is explained by the depopulation of the high rotational states participating in the multiphoton excitation process, a small change in the dissociation laser frequency to the blue side could result in multiphoton excitation of lower rotational states and, hence, compensate the decrease of the yield resulted from the decrease of temperature. Such experiments carried out earlier by Boyarkin *et al.* [56] for the pre-excitation of the second CH stretch overtone where the analogous selectivity and yield dependence on the sample temperature were observed did not show any considerable change in the OP-IRMPD yield when the CO_2 laser frequency was varied within the 9P branch (1025 -

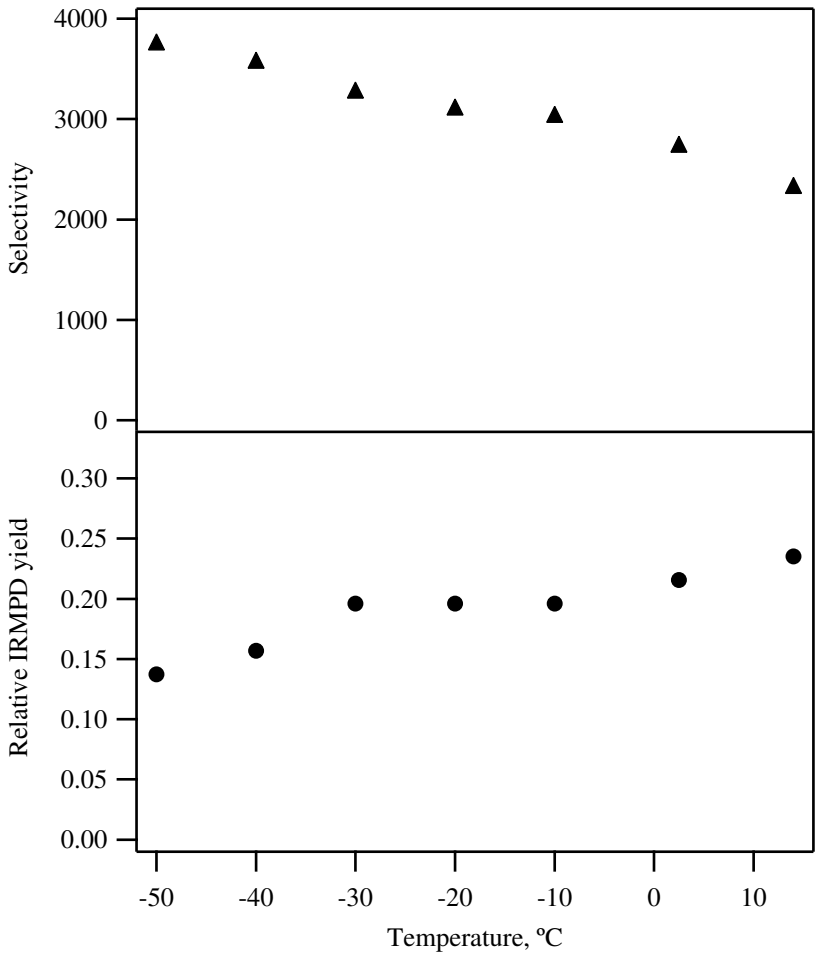

Figure 3.23: Relative IRMPD yield and selectivity of OP-IRMPD with 2_1 pre-excitation as a function of sample temperature. Pre-excitation laser bandwidth was 0.03 cm^{-1}. "Doubled" CO_2 laser pulses, 3 J/cm^2 used. Sample pressure was 80 mbar.

1060 cm^{-1}). Using other branches resulted in considerable decrease either of the dissociation yield or of the isotopic selectivity. The ongoing research in the Laboratory of molecular physical chemistry [34] is aimed in the study of the collisional processes in the OP-IRMPD approach to laser isotope separation and should result in particular in better understanding the influence of temperature on the isotopic selectivity and the overall yield of the separation process.

The behavior of the isotopic selectivity and overall yield with decrease temperature (an increase of the selectivity is accompanied by a decrease of the yield) is similar to that with increase sample pressure (Figure 3.21). From the point of view of practical realization of the OP-IRMPD based approach to carbon isotope separation it is useful to compare these two possible ways of controlling the productivity and selectivity of the MLIS process from the point of view of their efficiency. To do this we have to compare the "price" paid, expressed in the

drop of absolute OP-IRMPD yield, for a certain gain in isotopic selectivity.

As the temperature decreases from +14°C to -50°C at a sample pressure of 80 mbar, the selectivity increases by a factor of 1.6 and the relative IRMPD yield decreases by a factor of 1.7. Taking into account the factor of 1.3 increase in density, one gets 1.3 for the drop of absolute yield.

To reach an increase of isotopic selectivity by the same factor of 1.6 at room temperature, the sample pressure has to be increased from 80 to 125 mbar, which would result in a decrease in the relative IRMPD yield by a factor of 2 (Figure 3.21). However, the increased working pressure partially compensates the decrease of relative IRMPD yield, giving a factor of 1.3 for the absolute yield drop.

Thus, an equal increase of isotopic selectivity of the OP-IRMPD process reached either by reducing the temperature or by increasing the pressure leads to an equal drop of the absolute yield[6]. However, each of these approaches to improving the isotopic selectivity have certain advantages and disadvantages. Increasing the pressure at room temperature is preferential from the point of view of experimental complexity, since no cooling system is needed. On the other hand, the increase of selectivity by working at a higher pressure is reached by increasing a number of absorption-collisional relaxation cycles, which results in an increased number of CO_2 laser photons required for the dissociation of a pre-excited molecule. Apart from that loss of dissociation laser radiation in ground state CF_3H absorption also increases with pressure. Thus, the final choice between the ways of selectivity improvement will be a question of compromise between complexity of a set-up (and, hence, maintenance cost) and energy cost of isotope production. In our opinion, a combination of reduced temperature and increased pressure should be the most effective way of selectivity increase.

3.4.6 Correlation between selectivity and relative IRMPD yield

We have observed an interesting correlation between the overall isotopic selectivity of OP-IRMPD process and relative dissociation yield of IRMPD step. Figure 3.24 shows the relative IRMPD yield as a function of corresponding isotopic selectivity. These data have been obtained from experiments where we use different methods of controlling the isotopic selectivity of the process:

1. increasing the sample pressure in overlapped pre-excitation and dissociation laser pulses;

[6]This correlation is not fulfilled if a very different initial pressure is used, for example at low pressures the absolute yield increases with increase of pressure. However, in the region of practically interesting sample pressure corresponding to near maximum absolute OP-IRMPD yield (60-100 mbar) this correlation of yield and selectivity will stay approximately correct.

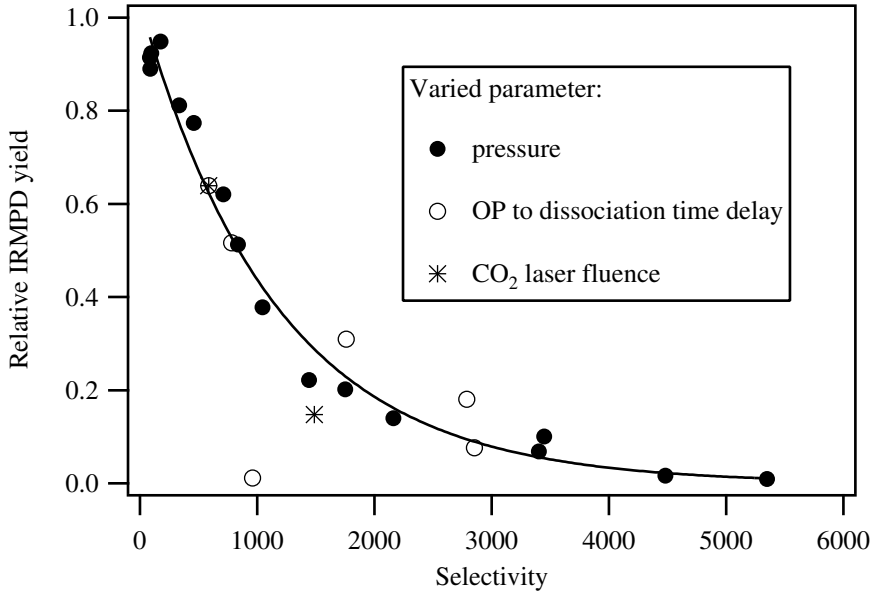

Figure 3.24: Relative IRMPD yield as a function of required selectivity. Different parameters used for control over the process. Pre-excitation at 2_2 line, dissociation fluence 4.5 J/cm^2, sample pressure for "time delay" and "fluence" experiments 53 mbar.

2. increasing the time-delay between pre-excitation and dissociation pulses when the sample pressure is fixed;

3. reducing the dissociation laser fluence.

In all cases the data points lie approximately on the same curve. Considerable deviation is observed only in the case of using a long time-delay between the overtone pre-excitation pulse and the CO_2 dissociation laser pulse where the dissociation probability drop is accompanied by a decrease of isotopic selectivity (this is explained by dissociation of ground state molecules [27, 28]). However, within a certain range of experimental conditions that are relevant for practical implications of the process, such simple correlation between selectivity and relative IRMPD yield is fulfilled with a high degree of accuracy. As we have mentioned earlier, this correlation is valid also for the switch between "spiky" and "doubled" dissociation laser pulses.

Such a behavior is explained by the same mechanism of selectivity gain in all cited experiments. This gain is reached by increasing the number of collisions with ground state molecules (V-V relaxation) and, correspondingly, the number of CO_2 laser photons required to reach the dissociation threshold.

In the experiments with reduced sample temperature, we observed, within certain pressure range, correlation between *absolute* OP-IRMPD productivity and isotopic selectivity in "pressure" and "temperature" approaches to selectivity increase. However, the last correlation has to be considered as a coincidence, because in this case the mechanism of selectivity increase is

different from that suggested above.

A simple correlation between the isotopic selectivity of the OP-IRMPD process and the relative IRMPD yield discussed in this section can be helpful for the evaluation of practical relevance of an isotope separation process aimed in a certain level of enrichment and for selection of experimental conditions for such a process.

3.5 Evaluation of practically attainable overall productivity

A complete analysis of industrial applicability of OP-IRMPD approach to carbon-13 isotope separation has to include a detailed economical study of the market and production cost of enriched carbon-13 by different methods. The production cost includes the cost of equipment (lasers, optics, reaction cells, gas system, *etc.*), cost of consumed materials (parent gas (CF_3H), gas mixture for CO_2 laser, cooling water, electricity, *etc.*), cost of maintaining the equipment, cost of labor *etc.* In this work we did not aim in such an analysis that would require a separate economical research. We performed, however, a detailed study of the OP-IRMPD process itself which allows us to estimate the laser energy consumption (that determines the productivity of the OP-IRMPD process for a given laser energy) and the required characteristics of an industrial-scale setup. This information is independent on the current market situation and can be used later in the marketing study of the applicability of the OP-IRMPD approach.

In Sections 3.5.1 and 3.5.2 we introduce the parameters which determine the laser energy consumption and the overall yield of the OP-IRMPD process and establish the correlations between these parameters. One of the parameters that determine the energy consumption of the separation process is the number of CO_2 laser photons absorbed by pre-excited molecule. Section 3.5.3 describes the experimental measurement of the absorption of CO_2 laser photons by pre-excited CF_3H. Finally, in the Section 3.5.4 we show an example of estimation of the optimal setup characteristics and the isotope separation process overall yield for a given isotopic selectivity, assuming certain realistic values for laser energies, repetition rate and laser energy loses on optical elements.

3.5.1 Quantum efficiency of OP-IRMPD process

The laser energy consumption in a single-laser isotope separation process is determined by the efficiency η of using the available laser photons (quantum efficiency) [57]:

$$\eta = \frac{\text{Number of C-13 atoms separated}}{\text{Number of photons}}. \tag{3.12}$$

In the case of the two-step OP-IRMPD process the quantum efficiencies of overtone pre-excitation (η_{op}) and multiphoton dissociation (η_{irmpd}) steps have to be considered separately:

$$\begin{cases} \eta_{op} = \frac{\text{Number of pre-excited molecules}}{\text{Number of OP laser photons}}, \\ \eta_{irmpd} = \frac{\text{Number of dissociated molecules}}{\text{Number of IRMPD laser photons}}, \end{cases} \tag{3.13}$$

where 'Number of OP laser photons' and 'Number of IRMPD laser photons' are the numbers of photons in pre-excitation and dissociation laser pulses, 'Number of pre-excited molecules' the number of molecules pre-excited by each pre-excitation pulse and 'Number of dissociated molecules' the number of molecules dissociated by each dissociation pulse.

Several parameters determine η_{op} and η_{irmpd}. First of all, only a fraction of all the available photons is absorbed by parent molecules. This fraction is determined by the construction of optical system and quality of optical elements. We will use η'_{op} for fraction of pre-excitation photons and η'_{irmpd} for fraction of IRMPD photons absorbed by CF_3H molecules.

Some of the pre-excitation photons are absorbed by $^{12}CF_3H$ and, hence, do not participate in dissociation of carbon-13 bearing molecules. The number of OP laser photons absorbed by $^{13}CF_3H$ molecules relative to the total number of the absorbed pre-excitation photons ϑ_{op} can be expressed by the following equation:

$$\vartheta_{op} = \frac{n_{13}\sigma_{13}^{op}}{n_{12}\sigma_{12}^{op} + n_{13}\sigma_{13}^{op}} = \frac{S_{op}}{\frac{n_{12}}{n_{13}} + S_{op}}, \tag{3.14}$$

where n_i ($i = 12$ or 13) are the concentrations of ground state carbon-12 and carbon-13 bearing molecules, σ_i^{op} the absorption cross-sections of the two isotopic species on the wavelength of pre-excitation laser and $S_{op} = \sigma_{13}^{op}/\sigma_{12}^{op}$ the isotopic selectivity of the pre-excitation step.

Thus, we can write for η_{op}:

$$\boxed{\eta_{op} = \eta'_{op}\vartheta_{op} = \eta'_{op}\frac{S_{op}}{\frac{n_{12}}{n_{13}} + S_{op}}} \tag{3.15}$$

The dissociation laser photons are absorbed by both excited and unexcited $^{12}CF_3H$ and $^{13}CF_3H$. In our experiments only the pre-excited molecules can reach the dissociation limit in the multiphoton excitation process, therefore, the photons, absorbed by the ground state CF_3H reduce the quantum efficiency of IRMPD step η_{irmpd}. The fraction of absorbed by CF_3H molecules CO_2 laser photons participating in the dissociation of $^{13}CF_3H$ ϑ_{irmpd} can be approximately determined as:

$$\vartheta_{irmpd} = \frac{n_{13}^*\sigma_{13}^*}{n_{12}\sigma_{12} + n_{13}\sigma_{13} + n_{12}^*\sigma_{12}^* + n_{13}^*\sigma_{13}^*}, \tag{3.16}$$

where n_i and n_1^* ($i = 12$ or 13) are the concentrations of ground state and pre-excited molecules and σ_i and σ_i^* the absorption cross-sections of ground state and pre-excited CF_3H respectively.

Taking into account the relative IRMPD yield Y_{irmpd} (fraction of pre-excited molecules dissociated) and the average number of CO_2 laser photons absorbed by a pre-excited carbon-13 bearing molecule $\langle N_{h\nu} \rangle$ one get for overall quantum efficiency of IRMPD step:

$$\begin{aligned} \eta_{irmpd} &= \eta'_{irmpd} Y_{irmpd} \frac{1}{\langle N_{h\nu} \rangle} \vartheta_{irmpd} = \\ &= \eta'_{irmpd} Y_{irmpd} \frac{1}{\langle N_{h\nu} \rangle} \frac{n^*_{13}\sigma^*_{13}}{n_{12}\sigma_{12} + n_{13}\sigma_{13} + n^*_{12}\sigma^*_{12} + n^*_{13}\sigma^*_{13}} \end{aligned} \tag{3.17}$$

The formula (3.17) can be considered only as approximation because the absorption cross-section changes with excitation of the molecule due to unharmonic shift and inhomogenous statistical broadening of absorption spectra. Thus, σ^*_i is an averaged value of the absorption cross-section for the molecules undergoing the multiphoton excitation process. For an accurate calculation of the quantum efficiency of IRMPD step a detailed numerical modelling of the multiphoton excitation process under collisional conditions has to be done. This work is currently in the progress in our laboratory [34]. In our estimation of productivity of OP-IRMPD isotope separation in Section 3.5.4 we use the known absorption cross-section for ground state CF_3H and average number of CO_2 laser photons absorbed per one pre-excited $^{13}CF_3H$ molecule measured experimentally for a particular process conditions (Section 3.5.3).

3.5.2 Characteristics of an industrial scale setup

Below we list the parameters which have to be taken into account in the development of an industrial scale setup for OP-IRMPD laser isotope separation process and in estimation of its productivity and show how they are linked to each other.

- Required overall selectivity of the process S which determines the relative IRMPD yield (see Section 3.4.6) and, hence, the overall productivity of the process.
- Pulse energies E_{op} and E_{irmpd} and repetition rate Ω of laser systems;
- Fractions of laser energies absorbed by CF_3H η'_{op} and η'_{irmpd}.
- Fluences of pre-excitation and dissociation lasers Φ_{op} and Φ_{irmpd}.
- Parent gas pressure and temperature, p and T, which have to be selected based on required selectivity and available fluence and pulse shape of CO_2 laser (see Sections 3.4.4, 3.4.5 and 3.4.6).

- Concentration of pre-excited $^{13}CF_3H$ molecules in the irradiated volume[7]:

$$n_{13}^{*} = n_{13}\frac{\Phi_{op}}{h\nu_{op}}\sigma_{13}^{op} \tag{3.18}$$

- Characteristic absorption length for pre-excitation laser radiation:

$$L_{op} = \frac{1}{n_{12}\sigma_{12}^{op} + n_{13}\sigma_{13}^{op}} = \frac{1}{n_{13}\sigma_{13}^{op}\left(1 + \frac{n_{12}}{n_{13}} \cdot \frac{1}{S_{op}}\right)}; \tag{3.19}$$

- Volume irradiated by pre-excitation laser. If OP laser fluence is kept constant, this volume will be determined as:

$$V_{op} = \frac{E_{op}}{h\nu_{op}} \cdot \frac{\eta'_{op}}{n_{12}^{*} + n_{13}^{*}} = \frac{E_{op}}{h\nu_{op}} \cdot \frac{\eta'_{op}}{\frac{\Phi_{op}}{h\nu_{op}}(n_{12}\sigma_{12}^{op} + n_{13}\sigma_{13}^{op})} = \frac{E_{op}}{\Phi_{op}}\eta'_{op}L_{op}; \tag{3.20}$$

- Relative IRMPD yield Y_{irmpd}.

  Having this information and assuming that the entire volume containing the pre-excited molecules is irradiated by the dissociation laser we can calculate the overall yield of the process during the time t;

$$Y_{abs} = n_{13}^{*}V_{op}Y_{irmpd}\Omega t \tag{3.21}$$

- Characteristic absorption length L_{irmpd} and volume V_{irmpd} irradiated by CO_2 laser. In an ideal case $L_{irmpd} \approx L_{op}$ and $V_{irmpd} \approx V_{op}$, that would simplify the task of spatial and temporal overlap of the pre-excitation and dissociation laser pulses.

  Evaluation of these parameters assumes using of absorption cross-sections of ground state and pre-excited molecules containing both isotopes. However, as we have mentioned in Section 3.5.1, absorption cross-section of pre-excited CF_3H depends on the energy deposited in the molecule and, therefore, its direct use is hampered. To avoid using of σ_i^{*} (i=12 or 13) we can estimate separately characteristic absorption length of CO_2 laser radiation for the hypothetical cases of absorption exclusively by ground state molecules $L_{irmpd}^{gr.state}$ and exclusively by pre-excited molecules L_{irmpd}^{*}. In the first case we can use the known absorption cross-section, in the second case we have to measure the average number $\langle N_{h\nu}\rangle$ of CO_2 laser photons absorbed per one pre-excited $^{13}CF_3H$ molecule under particular conditions which supposed to be used in the set-up. The resulting absorption characteristic length L_{irmpd} can then be calculated using the following expression:

$$\frac{1}{L_{irmpd}} = \frac{1}{L_{irmpd}^{gr.state}} + \frac{1}{L_{irmpd}^{*}}. \tag{3.22}$$

[7]Equations 3.18, 3.19 and 3.20 are valid for linear absorption regime, where only a few percent of molecules pre-excited.

The characteristic absorption length $L_{irmpd}^{gr.state}$ for ground state absorption can be determined as:

$$L_{irmpd}^{gr.state} = \frac{1}{(n_{12} + n_{13})\sigma}, \tag{3.23}$$

where σ is the CF_3H absorption cross-section measured using a sample with natural isotopic abundance. Equation 3.23 assumes a linear absorption regime at CO_2 laser wavelength fluence used in our OP-IRMPD process which is justified by the results of O'Neill and coworkers [58] who did not observe multiphoton absorption at CO_2 laser fluences up to 26 J/cm^2 using a CO_2 laser line in the 9P branch.

The absorption by multiphoton excitation of pre-excited molecules does not obey the exponential Beer-Lambert law because each pre-excited molecule absorbs a certain average number of laser photons. Instead, the number of absorbed photons is determined by the number of the pre-excited molecules in the irradiated volume multiplied by the average number of photons absorbed by each pre-excited molecule. Assuming that CO_2 laser fluence is kept constant in entire irradiated volume (by reducing the laser beam area s as the beam propagates through the sample) we can write:

$$\begin{cases} \frac{E}{h\nu_{co_2}} = \frac{E_0}{h\nu_{co_2}} - \langle N_{h\nu} \rangle \cdot n_{13}^* \cdot l \cdot s \\ \frac{E}{s} = \Phi_{irmpd} = const \end{cases} \quad \Rightarrow \quad \frac{E_0}{E} = 1 + \frac{\langle N_{h\nu} \rangle \cdot n_{13}^* \cdot l \cdot h\nu_{co_2}}{\Phi_{irmpd}},$$

where E_0 is the initial laser pulse energy and E the pulse energy after passing the distance l through the sample.

And, for the characteristic absorption length (the length at which the laser pulse energy drops by a factor of e) we have:

$$L_{irmpd}^* = \frac{(e-1) \cdot \Phi_{irmpd}}{\langle N_{h\nu} \rangle \cdot h\nu_{co_2} \cdot n_{13}^*}, \tag{3.24}$$

- Using the ratio of characteristic absorption length L_{irmpd} and L_{irmpd}^* which determines the fraction of photons absorbed by pre-excited molecules and knowing the average number of photons absorbed per each pre-excited $^{13}CF_3H$ we can write another expression for quantum efficiency of IRMPD step which does not include explicitly the absorption cross-section of pre-excited molecules:

$$\boxed{\eta_{irmpd} = \eta'_{irmpd} Y_{irmpd} \frac{1}{\langle N_{h\nu} \rangle} \frac{L_{irmpd}}{L_{irmpd}^*}}. \tag{3.25}$$

3.5.3 Measurement of the absorption of CO_2 laser radiation by pre-excited molecules

Since the OP-IRMPD isotope separation process consists of two steps (overtone pre-excitation and multiphoton dissociation of pre-excited molecules) we have to consider the number of photons required for each of these steps. The answer to this question for pre-excitation of one molecule is straightforward, since overtone pre-excitation is a single-photon process. The question about the number of CO_2 laser photons absorbed by each pre-excited molecule, however, is not simple. Although the energy which has to be deposited into the pre-excited molecule can be easily calculated as the difference between the dissociation threshold and the energy of pre-excitation photon, collisional energy transfer occurring in the time between the pre-excitation and dissociation laser pulses as well as during the multiphoton excitation process results in loss of energy, increasing the number of CO_2 laser photons required to dissociate a molecule (see Figure 3.1 on page 41).

In order to estimate the number of the CO_2 laser photons absorbed by each pre-excited molecule under the typical conditions of the OP-IRMPD process, we measured the CO_2 laser energy absorbed by $^{13}CF_3H$ molecules pre-excited through the 2_1 band using the set-up depicted in Figure 3.25. The CO_2 laser beam was collimated using a telescope system, resulting in a

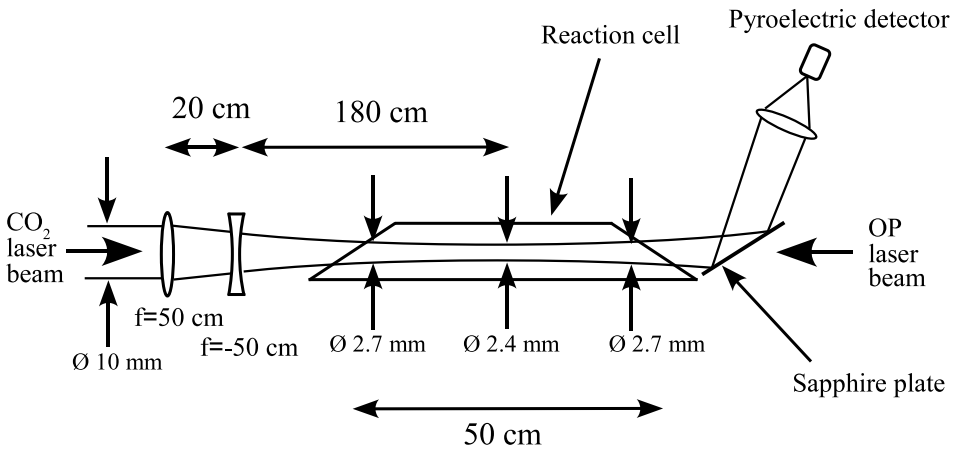

Figure 3.25: Apparatus applied for measurement of the absorption of CO_2 laser radiation by pre-excited CF_3H molecules.

beam diameter that varied only slightly along the 50 cm long reaction cell filled with 100 mbar of CF_3H. The CO_2 laser fluence varied in this configuration from ~ 2 J/cm^2 on the cell windows to ~ 3 J/cm^2 in the center of the cell. The CO_2 laser was tuned to the 9P(14) line at 1052.2 cm^{-1}, where the absorption cross-section of ground state CF_3H has a minimum [58]. The pre-excitation laser beam enters the cell from the opposite side through a sapphire plate

and on the output of the cell is decoupled from the CO_2 laser beam by a Pellin-Broca prism (not in the figure). A small fraction of the CO_2 laser beam reflected from the Sapphire plate is focused by a F=7.62 cm ZnSe lens onto a pyroelectric photodetector. The photodetector signal is measured using a digital oscilloscope (HP model 54615B). Measuring the difference between the signals with and without the pre-excitation pulse, together with information about the density of pre-excited $^{13}CF_3H$ in the irradiated volume, allows us to estimate the number of CO_2 laser photons absorbed by each pre-excited molecule.

The calculation of the number of CO_2 laser photons absorbed by each pre-excited molecule based on the results of the described experiment gives 36 ± 6 (which corresponds to the absorption of $\sim 2\%$ of CO_2 laser pulse energy in our reaction cell). This value is about twice higher than that required to provide the pre-excited molecules with energy equal the difference between the dissociation threshold and the energy of the pre-excitation photon. It is much smaller, however, than the number of photons required for dissociation of ground state molecules to achieve a similar degree of isotopic selectivity. For example, isotopically selective IRMPD of ground state CF_2HCl, which possesses a lower dissociation threshold than CF_3H, requires ~ 2000 photons, resulting in selectivity of 1000 [14], whereas the selectivity that can be reached using the OP-IRMPD approach under conditions used in the described experiment exceeds 3000 (see Figure 3.21 on page 76, upper panel, solid line). We must consider, however, that not all the pre-excited molecules are dissociated by the CO_2 laser radiation. Under conditions used in the discussed experiment, the fraction of pre-excited molecules dissociated (i.e., the relative IRMPD yield) is only about 7% (Figure 3.21, lower panel, solid line), which gives ~ 510 CO_2 laser photons per dissociated molecule, which is still considerably less than the value for ground state molecules from the Reference [14]. Moreover, isotopic selectivity of 1000 reported in [14] is achieved with the OP-IRMPD approach at higher relative IRMPD yield: $\sim 33\%$, or 110 photons per each dissociated $^{13}CF_3H$.

3.5.4 Example of estimation of industrial scale setup characteristics

In order to illustrate the possibility of using the results obtained in this work for the development of an industrial carbon-13 isotope separation process we will show an example of determination of the setup parameters required for the optimal use of the available laser power and calculation of the overall yield of the separation process for a given isotopic selectivity. The order of operations which will be done is shown in the Table 3.4 and we will explicitly describe below these operations step by step.

I. First of all we have to specify the required overall isotopic selectivity and chose the basic parameters of the process which would allow reaching the specified level of selectivity: the sample pressure, the temperature, the pre-excitation level and the fluence of the dissociation

I	S	$\longrightarrow$	$p,\ T,\ \Phi_{irmpd},\ Y_{irmpd}$
II	Assumptions:		$\eta'_{op},\ \eta'_{irmpd},\ \Omega$
III	p	$\xrightarrow{Eq.\ (3.19),(3.23)}$	$L_{op},\ L_{irmpd}^{gr.state}$
IV	$L_{irmpd} \equiv L_{op}$	$\xrightarrow{Eq.\ (3.22),(3.24)}$	$n_{13}^*,\ L_{irmpd}^*$
V	$\Phi_{irmpd} = const$ over L	$\longrightarrow$	s
VI	n_{13}^*	$\xrightarrow{Eq.\ (3.18)}$	Φ_{op}
VII	$s,\ \Phi_{op}$	$\longrightarrow$	E_{op}
	$s,\ \Phi_{irmpd}$	$\longrightarrow$	E_{irmpd}
VIII	$E_{op},\ \Phi_{op},\ \eta'_{op},\ L$	$\xrightarrow{Eq.\ (3.20)}$	V_{op}
IX	$n_{13}^*,\ V_{op},\ Y_{irmpd},\ \Omega$	$\xrightarrow{Eq.\ (3.21)}$	Y_{abs}/t
X	$S_{op},\ \eta'_{irmpd}$	$\xrightarrow{Eq.\ (3.15)}$	η_{op}
XI	$L,\ L_{irmpd}^*,\ \eta'_{irmpd},\ Y_{irmpd}$	$\xrightarrow{Eq.\ (3.25)}$	η_{irmpd}

Table 3.4: Order of steps for estimation of industrial scale setup characteristics.

laser. We will assume that the required carbon-13 enrichment is 95-96% ($S \approx 2000$). As we have shown earlier such a selectivity is achieved at the maximum absolute productivity of the OP-IRMPD process (number of produced carbon-13 species in unit volume per unit time). In order to reach this level of selectivity we will use a fluence of $\Phi_{irmpd} = 3$ J/cm^2 of CO_2 laser in the temporary modified pulses (see Section 3.4.4), 100 mbar CF_3H pressure and room temperature. The chosen values are not the only possible values providing the specified selectivity (see, for example Figure 3.24). They, however, provide the highest possible working pressure for the dissociation laser fluence limited by the optics breakdown threshold and, hence, provide the highest absolute productivity of the process. For the pre-excitation of $^{13}CF_3H$ we will use the Q-branch of 2_1 band at 5936.6 cm^{-1} which provides a pre-excitation selectivity $S_{op} \approx 85$. The relative IRMPD yield Y_{irmpd} in this configuration will be approximately 0.2 (see Figure 3.21, lower panel, dashed line).

II. A reasonable assumption about the laser repetition rate and the loss of laser photons on the optical elements and due to the setup geometry has to be done. We will consider a very simple setup configuration where the pre-excitation and dissociation laser beams propagate collinearly through the reaction cell. In order to keep the laser fluence constant along the absorption path, the beams are focused by long focal length lenses providing the decrease of beam area proportional to the decrease of pulse energy due to absorption. Such a single-pass configuration cannot provide a complete utilization of available laser photons because this would require a very long cell. We will consider a cell length equal to the characteristic absorption length, assuming that $1/e$ fraction of laser energy is not absorbed by the parent molecules. We will assume $\Omega = 100$ Hz and $\eta'_{op} = \eta'_{irmpd} = 0.3$. The 0.3 value includes the 0.5 factor for the fraction of energy contained in the active central part within the FWHM diameter of the Gaussian beam (See Appendix E) and 30% of loses in optics and due to not complete use of laser energy in the suggested setup configuration.

III. Knowing the concentration of $^{13}CF_3H$ and $^{12}CF_3H$ at the working pressure p ($n_{13} = 2.8 \times 10^{16}$ cm^{-3}, $n_{12} = 2.65 \times 10^{18}$ cm^{-3} at 100 mbar) and the absorption cross-sections for the pre-excitation radiation $\sigma_{13}^{op} = 1.2 \times 10^{-20}$ cm^2 [27, 38] and for the dissociation radiation $\sigma = 0.47 \times 10^{-22}$ cm^2 (at 9P(14) line (1052.2 cm^{-1}) [58]) we can calculate the characteristic absorption length for the pre-excitation and dissociation laser radiation by ground state molecules using Equation (3.19) and (3.23):

$$L_{op} = \frac{1}{2.8 \times 10^{16} \cdot 1.2 \times 10^{-20} \left(1 + \frac{98.93\%}{1.07\%} \cdot \frac{1}{85}\right)} = 1430\,[\text{cm}] = 14.3\,[\text{m}],$$

$$L_{irmpd}^{gr.state} = \frac{1}{2.65 \times 10^{18} \cdot 0.47 \times 10^{-22}} = 8000\,[\text{cm}] = 80\,[\text{m}].$$

IV. The effective use of both the pre-excitation and the dissociation laser photons can be reached only under the condition of good spatial and temporal overlap of the two laser pulses.

Such an overlap can be provided by using the collinear beams which have an equal absorption length. Using the condition $L_{op} \equiv L_{irmpd}$ for the known L_{op}, $L_{irmpd}^{gr.state}$, Φ_{irmpd}, $\langle N_{h\nu} \rangle = 36$ (see Section 3.5.3) and CO_2 laser photon energy $h\nu_{co_2} = 2.1 \times 10^{-20}$ J (at 1052.2 cm^{-1}) and using the equations (3.22) and (3.24) we get:

$$L^*_{irmpd} = \left(\frac{1}{L_{irmpd}} - \frac{1}{L^{gr.state}_{irmpd}} \right)^{-1} = \left(\frac{1}{1430} - \frac{1}{8000} \right)^{-1} = 1740\,[\text{cm}] = 17.4\,[\text{m}],$$

$$n^*_{13} = \frac{(e-1) \cdot \Phi_{irmpd}}{\langle N_{h\nu} \rangle \cdot h\nu_{co_2} \cdot L^*_{irmpd}} = \frac{(e-1) \cdot 3}{36 \cdot 2.1 \times 10^{-20} \cdot 1740} = 3.9 \times 10^{15} \text{cm}^{-3},$$

i.e. about 14% of $^{13}CF_3H$ has to be pre-excited.

V. To keep the laser fluence constant while the beam propagates through the sample, its size has to gradually decrease. The minimum laser beam diameter is limited by the divergency of the beam. This is especially important in the case of the long wavelength of CO_2 laser radiation. Assuming that CO_2 laser operates at TEM_{00} mode (fundamental Gaussian mode) and the beam is focused by a lens with a focal length $f = L_{irmpd}$ we can estimate the initial area of the beam s which will provide a beam waist area in the focal point $s_f = s/e$. Using the formula for the beam waist spot size ω_f of the focused gaussian beam with initial spot size ω_1 (see Appendix E), we get:

$$\begin{cases} \omega_f = f\frac{\lambda}{\pi\omega_1} \\ f = L_{irmpd} \\ \frac{s}{s_f} = e \;\Rightarrow\; \frac{\omega_1}{\omega_f} = \sqrt{e} \end{cases} \quad \Rightarrow \quad \omega_1 = \sqrt{\frac{L_{irmpd}\lambda\sqrt{e}}{\pi}},$$

$$\omega_1 = \sqrt{\frac{1430 \cdot 9.5 \times 10^{-4} \cdot \sqrt{e}}{\pi}} \approx 0.84\ [\text{cm}],$$

$$(FWHM) = 2 \cdot 0.59 \cdot \omega_1 \approx 1\ \text{cm},$$

$$\text{s} = \frac{\pi(FWHM)^2}{4} \approx 0.8\ \text{cm}^2.$$

Assuming that the divergency of the pre-excitation laser is smaller than the divergency of the CO_2 laser we can assert that it is always possible to focus the pre-excitation laser beam such a way that the pre-excitation and dissociation laser beams are almost completely overlapped on the characteristic absorption length (see Figure 3.26 for a schematics of a possible optical configuration).

VI. Using Equation (3.18), the calculated earlier value $n^*_{13} = 3.9 \times 10^{15}$ cm^{-3}, the known $\sigma^{op}_{13} = 1.2 \times 10^{-20}$ cm^2, $n_{13} = 2.8 \times 10^{16}$ cm^{-3} and pre-excitation photon energy $h\nu_{op} = 1.18 \times 10^{-19}$ J we get for the required fluence of the pre-excitation laser:

$$\Phi_{op} = \frac{n^*_{13} \cdot h\nu_{op}}{n_{13} \cdot \sigma^{op}_{13}} = \frac{3.9 \times 10^{15} \cdot 1.18 \times 10^{-19}}{2.8 \times 10^{16} \cdot 1.2 \times 10^{-20}} = 1.37\ [\text{J/cm}^2].$$

VII. For known laser beam cross-sections and laser fluences we can calculate the required laser pulse energies. We have to take into consideration that only 50% of the pulse energy is concentrated in the active part of the beam within the FWHM diameter (see Appendix E), resulting in the factor 2 in the following equations:

$$E_{op} = 2s\Phi_{op} \approx 2 \cdot 0.8 \cdot 1.37 \approx 2.2 \text{ [J]},$$
$$E_{irmpd} = 2s\Phi_{irmpd} \approx 2 \cdot 0.8 \cdot 3 = 4.8 \text{ [J]}.$$

Figure 3.26 shows a setup configuration possessing the calculated characteristics. The pre-excitation and dissociation laser beams are shown separately in order to simplify the figure. In a real setup these two beams can be combined, for example, by a Pellin-Broca prism. A curved rear mirror can be used to reflect the non-absorbed pre-excitation laser photons and thus increase the quantum efficiency η'_{op}.

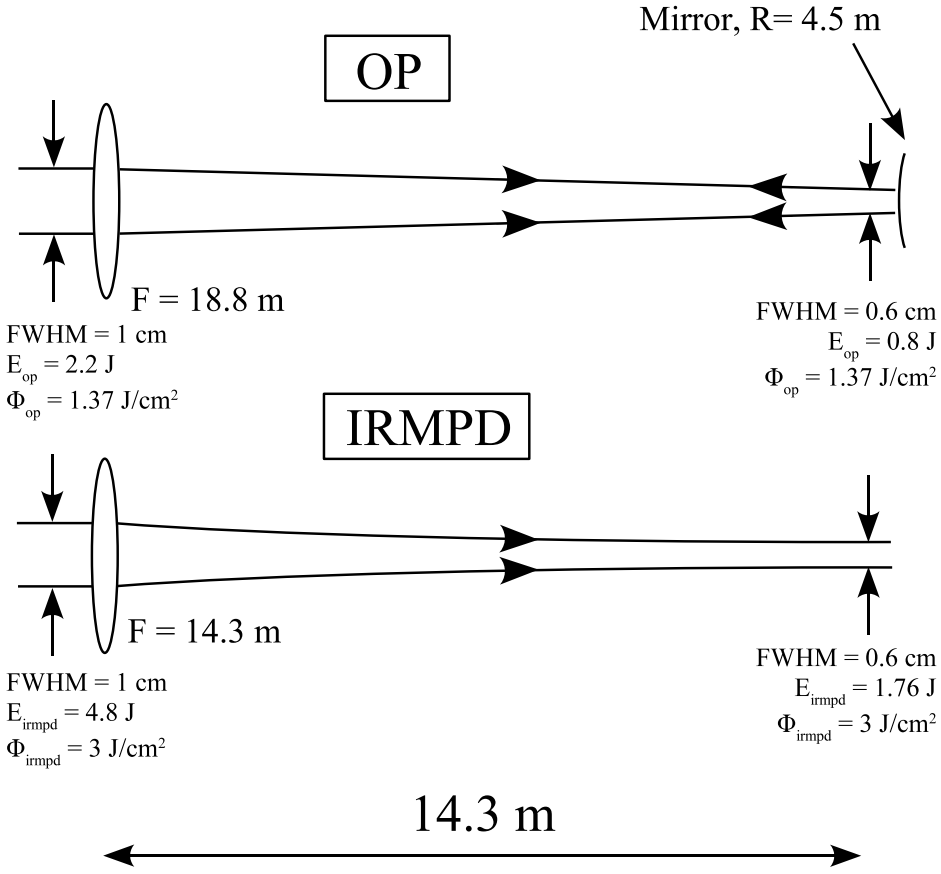

Figure 3.26: Possible configuration of an industrial-scale setup.

VIII. Using 3.20 we get for the active volume:

$$V_{op} = \frac{2.2}{1.37} \cdot 0.3 \cdot 1430 \approx 700 \,[\text{cm}^3].$$

IX. Using 3.21, and assuming 2000 hours (7.2×10^6 seconds) per year operation (40 hours per week, 50 weeks per year):

$$\boxed{Y_{abs} = 3.9 \times 10^{15} \cdot 700 \cdot 0.2 \cdot 100 \cdot 7.2 \times 10^6 \approx 3.8 \times 10^{26} \left[\frac{\text{C-13 atoms}}{\text{year}}\right] \approx 8.3 \left[\frac{\text{kg}}{\text{year}}\right]}$$

X. Using Equation 3.15 we get:

$$\eta_{op} = 0.3 \frac{85}{\frac{98.93\%}{1.07\%} + 85} = 0.15$$

XI. Finally, for the quantum efficiency of IRMPD (Equation 3.25) we get:

$$\eta_{irmpd} = 0.3 \cdot 0.2 \cdot \frac{1}{36} \cdot \frac{14.3}{17.4} \approx 0.0014.$$

Thus, the number of CO_2 laser photons required for the dissociation of one $^{13}CF_3H$ ($1/\eta_{irmpd}$) under the conditions specified in the beginning of this section is approximately 700.

The estimation of an industrial-scale setup configuration presented in this section should be considered only as an example of application of formula end experimental data describing the OP-IRMPD process to an arbitrary selected isotopic selectivity, setup configuration (single pass cell), and the criteria of completeness of utilization of available laser photons. Other criteria can be more important in certain cases. For instance, the pulse energies of available lasers can be considered as fixed parameters as opposite to what we did in our calculations, where the pule energies have been selected to satisfy the condition of equal absorption lengths and beam diameters for pre-excitation and dissociation lasers, or the multipass configuration of reaction cell can be considered. Nevertheless, we hope that the presented example can serve as a guideline for the calculations of setup parameters in different particular cases.

3.6 Remark about the possibility of using the fundamental frequency of CH stretch vibration at the pre-excitation step

While pre-excitation at the fundamental frequency of the CH stretch vibration is no longer an "overtone pre-excitation", we will use the term "OP-IRMPD" nonetheless. We have performed several qualitative test measurements aimed to check the possibility of efficient selective dissociation of CF_3H pre-excited at fundamental CH stretch vibration frequency.

The apparatus that we used to generate the 3.3 μm radiation for v=1 pre-excitation is depicted in Figure 3.27. This setup is similar to the that used for 1.68 μm radiation generation (Figure 3.16). The main difference is that the amplification stage is replaced by a second stage of different frequency mixing in a $LiNbO_3$ crystal. This system provides up to 6 mJ/pulse at 3.3 μm, which is, taking to account a high absorption cross-section of the v= $1 \leftarrow 0$ transition

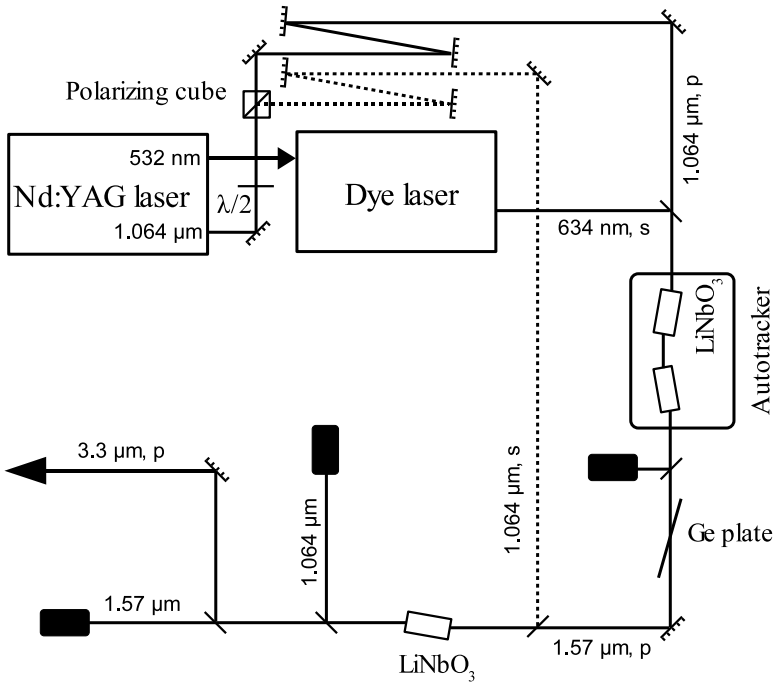

Figure 3.27: Schematic of the generation of 3.3 μm radiation for ν_1 fundamental pre-excitation.

(see Table 3.3), sufficient for pre-excitation of a substantial fraction (typically about 10%) of the $^{13}CF_3H$ molecules in the irradiated volume.

We found, that the relative IRMPD yield that can be reached using the same CO_2 laser fluence and frequency is at least an order of magnitude lower if v=1 instead of v=2 pre-excitation is used. A higher IRMPD efficiency can be obtained either by an increase of the CO_2 laser fluence or by using a higher frequency line. Both these solutions result, however, in an increase in the absorption by ground state CF_3H (see, for example, [58]). This, in its turn, limits the number of dissociation laser photons that participate in multiphoton excitation of pre-excited $^{13}CF_3H$ and reduces the isotopic selectivity of the process. An example of the mass-spectrum of C_2F_4 produced in the OP-IRMPD process with pre-excitation through the 1_1 band is shown in the Figure 3.28 (upper panel). The frequency of the CO_2 laser has been changed to 1077 cm^{-1} (9R(18) line) in order to increase the dissociation yield, however, the overall C_2F_4 concentration is still several times smaller than in the case of CF_3H pre-excitation through 2_1 band. The lower panel of the Figure 3.28 shows the mass-spectrum of C_2F_4 produced by IRMPD of ground state CF_3H using the same CO_2 laser fluence and frequency. As it can be clearly seen from the comparison of these mass-spectra, dissociation of ground state $^{12}CF_3H$ makes a considerable contribution to the overall yield of the OP-IRMPD process, in spite of the large fraction ($\sim$ 10%) of $^{13}CF_3H$ molecules pre-excited. Thus, laser isotope separation of

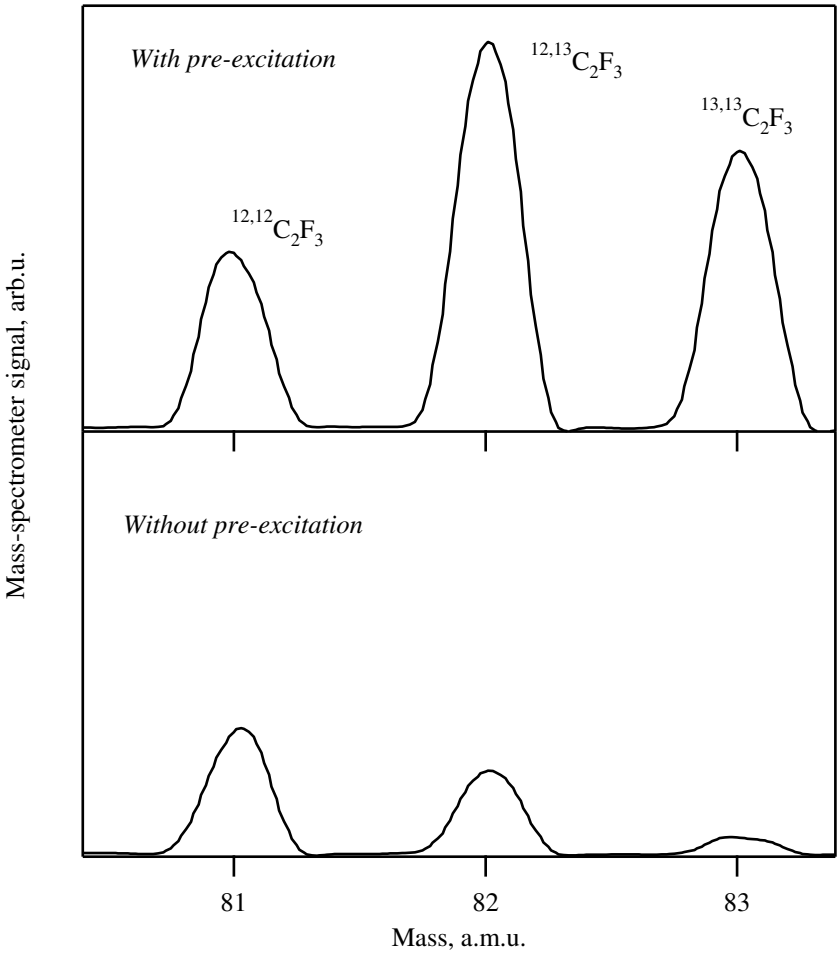

Figure 3.28: Comparison of the C_2F_4 yield and isotopic composition for IRMPD with 1_1 band pre-excitation (upper panel) and without pre-excitation (lower panel). The CO_2 laser fluence was 3 J/cm^2, and its frequency 1077 cm^{-1} (9(R)18 line). The pre-excitation laser fluence was 2.4 mJ/cm^2 and the CF_3H pressure 6.5 mbar.

carbon-13 using v_{CH}=1 pre-excitation of CF_3H followed by IRMPD is unfavorable comparison with the corresponding process with 2_1 pre-excitation.

3.7 Conclusions

With a view towards developing a method for highly selective isotope separation of carbon-13, we have investigated the details of IRMPD of CF_3H molecules pre-excited to different levels in the CH stretch bands.

Using pre-excitation to 3_1 level we gained the general understanding of the OP-IRMPD process under collisional conditions that allowed us to considerably enhance the carbon-13 yield compared to earlier experiments [27,28] while keeping high isotopic selectivity. We found that in

the absence of collisional vibrational deactivation between the pre-excitation and dissociation laser pulses, the dissociation by a 50-100 ns laser pulse has a very low threshold of 0.2-0.3 J/cm^2, compared with a threshold fluence of 30-40 J/cm^2 for IRMPD of ground state species. The dissociation yield approaches 100% already at a fluence of 1.5-2 J/cm^2. At higher pressure (above 4 mbar) when collisional deactivation becomes important, efficient IRMPD occurs only during the intense leading spike of a long dissociation pulse delivered by our conventional CO_2 laser.

Overlapping the overtone pre-excitation pulse with the leading spike of the pulse from the CO_2 laser results in a manifold increase of the relative IRMPD yield at elevated pressures. The process of IR multiphoton excitation of the pre-excited molecules is governed by the dissociation laser pulse intensity rather than by its fluence through a competition with collisional vibrational deactivation. With a 50 ns dissociation pulse of 3 J/cm^2 fluence, the maximum absolute IRMPD yield occurs at 80-100 mbar of CF_3H. Under these conditions, and when the pre-excitation laser is tuned to the Q-branch of the 3_1 band in $^{13}CF_3H$, the C_2F_4 final product is enriched to 95.5% in carbon-13. This high isotopic selectivity increases further upon increasing the sample pressure, reaching, for instance, 98.2% at 265 mbar. The opportunity to control the isotopic selectivity of our process by pressure in a configuration with overlapped pulses is similar to what we have earlier observed in an arrangement with the pre-excitation and dissociation pulses delayed. Despite the difference in these arrangements, in both cases the isotopic selectivity is governed essentially by the number of collisions that a molecule has before it is dissociated. This may arise from either isotopic selectivity in collisional vibrational deactivation or in the IR multiphoton excitation process. Which of these is the dominant mechanism for isotopically selectivity is still an open question.

A study of isotopically selective OP-IRMPD of CF_3H pre-excited to the first overtone and fundamental frequency of CH stretch vibration has been performed based on the understanding gained from the analysis of the data obtain with pre-excitation to the 3_1 level. Pre-excitation to the first overtone of the CH stretch vibration allows us to increase the maximum overall unit volume productivity of our MLIS process by a factor of 3-5 compare to the productivity obtained using the second overtone while conserving high isotopic selectivity. Pre-excitation of the 2_1 instead of the 3_1 band has the additional advantage that the 1.68 μm radiation that is needed can be efficiently generated by an all-solid-state laser system included Nd:YAG laser and optical parametrical oscillator (OPO). A use of well developed Nd:YAG lasers seems to be more convenient and less costly than a use of low efficient Alexandrite laser with Raman shifter system required for generation of 1.14 μm for the 3_1 band excitation.

We have also demonstrated a substantial improvement of the process performance by reducing the sample temperature and by use of temporary modified ("doubled") CO_2 laser pulse.

Our estimate shows that the optimal process configuration involves pre-excitation *via* the 2_1 band, overlapped pulses, reduced sample temperature, 80-120 mbar sample pressure, ~3 J/cm^2 pre-excitation and 3-4 J/cm^2 dissociation laser fluences, and use of smooth 50-60 ns dissociation laser pulses. Under these conditions, the process should allow, for instance, production of C_2F_4 enriched to 95-96% in carbon-13 at a rate of about 4 g/h with 2.2 J pre-excitation and 4.8 J dissociation pulses at 100 Hz repetition rate.

Bibliography

[1] Commission on Atomic Weights and Isotopic Abundances report for the International Union of Pure and Applied Chemistry, *Pure and Applied Chemistry*, 1998, **70**, 217–235.

[2] M. M. Ivanenko, H. Handreck, J. Göthel, W. Fuß, K.-L. Kompa, and P. Heiring, *Appl. Phys. B*, 1997, **65**, 577–582.

[3] V. Parthasarathy, S. Sethi, L. M. Gantayet, P. Nilaya, D. J. Biswas, N. V. Iyer, K. A. Rao, and S. K. Sarkar, *J. Photochem. Photobiol. A*, 1997, **110**, 11–15.

[4] N. Hansen and A. M. Wodtke, *Chem. Phys. Lett.*, 2002, **356**, 340–346.

[5] S. Mori, H. Akatsuka, and M. Suzuki, *J. Nucl. Sci. Technol.*, 2002, **39**, 637–646.

[6] V. M. Apatin, V. P. Laptev, and E. A. Ryabov, *High Energy Chemistry*, 2003, **37**, 101–107.

[7] V. S. Letokhov, *Laser und Optoelektronik*, 1998, **30**, 29–33.

[8] Gas-Oil JSC, http://www.c13.ru.

[9] R. V. Ambartsumyan, V. S. Letokhov, E. A. Ryabov, and N. V. Chekalin, *JETP Lett.*, 1974, **20**, 273–274.

[10] J. L. Lyman, R. J. Jensen, J. Rink, C. P. Robinson, and S. D. Rockwood, *Appl. Phys. Lett.*, 1975, **27**, 87–89.

[11] M. Droun, M. Gauthier, R. Pilon, P. A. Hacket, and C. Willis, *Chem. Phys. Lett*, 1978, **60**, 16–18.

[12] V. N. Bagratashvili, V. S. Doljikov, V. S. Letokhov, and E. A. Ryabov, *Appl. Phys.*, 1979, **20**, 231–235.

[13] G. N. Makarov, D. E. Malinovsky, and D. D. Ogurok, *Laser Chem.*, 1998, **17**, 205–218.

[14] M. Gauthier, C. G. Cureton, P. A. Hackett, and C. Willis, *Appl. Phys. B*, 1982, **28**, 43–50.

[15] A. V. Evseev, V. S. Letokhov, and A. A. Puretzky, *Appl. Phys. B*, 1985, **36**, 93–103.

[16] I. Deac, V. Cosma, and V. Tosa, *J. Mol. Structure*, 1992, **266**, 405–410.

[17] W. Fuß, J. Göthel, M. Ivanenko, K. L. Kompa, and W. E. Schmid, *Z. Phys D*, 1992, **24**, 47–56.

[18] A. N. Ezubchenko, A. I. Ilyukhin, A. I. Karchevskii, N. S. Krasnikov, A. V. Merzlyakov, and A. B. Soloukhin, *High Energy Chemistry*, 1993, **27**, 161–163.

[19] W. Fuß, J. Göthel, M. Ivanenko, K. L. Kompa, W. E. Schmid, and K. Witte, *Z. Phys. D*, 1994, **29**, 291–298.

[20] C. L. Sigüenza and P. F. González-Díaz, *Spectrochimica Acta*, 1994, **50A**, 813–817.

[21] V. N. Lokhman, G. N. Makarov, E. A. Ryabov, and M. V. Sotnikov, *Quantum Electron.*, 1996, **26**, 79–86.

[22] J. V. Magill, K. M. Gough, and W. F. Murphy, *Spectrochimica Acta*, 1986, **42A**, 705–715.

[23] R. I. Martinez, R. E. Huie, J. T. Herron, and W. Braun, *J. Phys. Chem.*, 1980, **84**, 2344–2347.

[24] M. Quack and G. Seyfang, *Chem. Phys. Lett.*, 1982, **93**, 442–447.

[25] P. Kolodner, C. Winterfeld, and E. Yablonovich, *Optics Commun.*, 1977, **20**, 119–122.

[26] S. Koletzko, M. Haisch, I. Seeboth, B. Braden, K. Hengels, B. Koletzko, and P. Hering, *The Lancet*, 1995, **345**, 961–962.

[27] M. Kowalzcyk *Highly Selective Molecular Laser Isotope Separation of Carbon-13* PhD thesis, Ecole Polytechnique Fédérale de Lausanne, Switzerland, 2000.

[28] O. V. Boyarkin, M. Kowalzcyk, and T. R. Rizzo, *J. Chem. Phys.*, 2003, **118**, 93–103.

[29] J. Makowe *Isotopically Selective Infrared Multiphoton Dissociation of Vibrationally Pre-excited Silane* PhD thesis, Ecole Polytechnique Fédérale de Lausanne, Switzerland, 2000.

[30] J. Makowe, O. V. Boyarkin, and T. R. Rizzo, *J. Phys. Chem. A*, 2002, **106**, 5221–5229.

[31] J. C. Stephenson, R. E. Wood, and C. B. Moore, *J. Chem. Phys.*, 1968, **48**, 4790–4791.

[32] C. Coletti and G. D. Billing, *J. Chem. Phys.*, 2000, **113**, 4869–4875.

[33] C. Coletti and G. D. Billing, *Chem. Phys. Lett.*, 2002, **356**, 14–22.

[34] R. Bossart PhD thesis, Ecole Polytechnique Fédérale de Lausanne, Switzerland, to be published.

[35] F. W. Dalby, *J. Chem. Phys.*, 1964, **41**, 2297–3203.

[36] F. Battin-Leclerc, A. P. Smith, G. D. Hayman, and T. P. Murrells, *J. Chem. Soc., Faraday Trans.*, 1996, **92**, 3305–3313.

[37] H. Hollenstein, M. Lewerenz, and M. Quack, *Chem. Phys. Lett.*, 1990, **165**, 175–183.

[38] H.-R. Dübal and M. Quack, *J. Chem. Phys.*, 1984, **81**, 3779–3791.

[39] H. F. Chambers, R. W. Kirk, J. K. Thompson, M. J. Warner, and P. M. Wilt, *J. Mol. Spec.*, 1975, **58**, 76–86.

[40] J. P. Champion and G. Graner, *Mol. Phys.*, 1986, **58**, 475–484.

[41] G. Graner, R. Antilla, and J. Kauppinen, *Mol. Phys.*, 1979, **38**, 103–128.

[42] S. Sofue, K. Kawaguichi, E. Hirota, and T. Fujiyama, *Bull. Chem. Soc. Jpn.*, 1981, **54**, 897–900.

[43] S. Sofue, K. Kawaguichi, E. Hirota, and T. Fujiyama, *Bull. Chem. Soc. Jpn.*, 1981, **54**, 3546–3550.

[44] Physics Instrumentation Center, Troitsk, Russia, http://www.lasersys.ru.

[45] D. King, P. Schenck, and J. C. Stephenson, *J. Mol. Spect.*, 1979, **78**, 1–15.

[46] K. Sugita, Y. Ishikawa, and S. Arai, *Appl. Phys. B*, 1985, **36**, 111–113.

[47] O. V. Boyarkin, T. R. Rizzo, D. Rueda, M. Quack, and G. Seyfang, *J. Chem. Phys.*, 2002, **117**, 9793–9805.

[48] W. J. Witteman, *The CO_2 laser*, Springer-Verlag, Berlin, Heidelberg, 1987.

[49] M. Quack, C. Rüede, and G. Seyfang, *Spectrochimica Acta*, 1990, **46A**, 523–536.

[50] H.-R. Dübal and M. Quack, *Chem. Phys. Lett.*, 1981, **80**, 439–444.

[51] G. T. Fraser, J. Domenech, M.-L. Junttila, and A. S. Pine, *J. Mol. Spec.*, 1992, **152**, 307–316.

[52] J. T. Yardley, *Introduction to Molecular Energy Transfer*, Academic Press: New York, 1980.

[53] R. D. Sharma and C. A. Brau, *Phys. Rev. Lett.*, 1967, **19**, 1273–1275.

[54] R. D. Sharma and C. A. Brau, *J. Chem. Phys.*, 1969, **50**, 924–930.

[55] R. D. Sharma, *Phys. Rev.*, 1969, **177**, 102–107.

[56] O. V. Boyarkin, Private communications.

[57] V. S. Letokhov, *Science*, 1973, **180**, 451–458.

[58] J. A. O'Neill, L. Pateopol, and B. Pogue, *J. Phys. B: At. Mol. Opt. Phys.*, 1992, **25**, 3335–3344.

Chapter 4

Overtone pre-excitation - infrared multiphoton dissociation of trichlorosilane in view of silicon isotope separation

4.1 Introduction

The large increase in thermal conductivity of silicon upon isotopic purification [1] and the predicted unique properties of silicon isotope superlattices [2] suggest significant improvement of semiconductor devices upon use of isotopically enriched Si. Producing isotopically pure semiconductors is, however, currently limited by the high cost of enrichment. The development of economically feasible approaches for isotopic enrichment of these materials would facilitate exploring their potential in practical devices. The method of molecular laser isotope separation (MLIS) based on infrared multiphoton dissociation (IRMPD) has been investigated for the last three decades and applied to many isotopes, and recently it has been implemented for commercial production of carbon-13 [3, 4]. While isotope separation of silicon by IRMPD of naturally abundant (92.1% ^{28}Si, 4.7% ^{29}Si, 3.2% ^{30}Si) samples of $Si(OCH_3)_4$ and $((CH_3)_3Si)_2O$ [5], CH_3SiF_3, and $C_6H_5SiF_3$ [6] has achieved a maximum enrichment in ^{30}Si of only 5-15%, this approach has shown some promise for laboratory-scale separation of silicon isotopes using Si_2F_6 as a working molecule [7–10], with a reported enrichment of ^{30}Si to 46% in the SiF_4 dissociation product [7] and 20% ^{29}Si in the SiF_2 fragment [10]. Although this is currently the most advanced laser-based technique for silicon isotope separation, the present level of enrichment is still far below that required for electronic applications.

A new highly selective MLIS approach based on overtone pre-excitation of a high frequency vibration followed by IRMPD of the pre-excited molecules has been recently proposed and studied in view of separating carbon [11] and silicon [12] isotopes. In both cases, this approach has achieved high isotopic selectivity, allowing enrichment of minor isotopes up to 99% in a single stage process. For carbon isotope separation, this new technique has been applied to CF_3H, which as a symmetric top has a sharp, prominent Q-branch in the CH stretch overtone bands, allowing efficient pre-excitation of the parent molecules. In the case of silicon, this approach has been tested with SiH_4, a spherical top with a broad Q-branch in the SiH overtone bands and a low density of vibrational states [12]. These characteristics, along with the low pressure used in these experiments, resulted in a fairly low estimate for the productivity. To separate silicon isotopes successfully using the overtone-pre-excitation infrared multiphoton dissociation (OP-IRMPD) approach, one must find a more suitable parent compound.

We report here our investigation of the applicability of the OP-IRMPD technique to the molecule trichlorosilane ($SiHCl_3$). This molecule is a good candidate for such an approach in that it has a light atom stretch vibration for overtone pre-excitation (ν_1) that exhibits a sharp, $\sim$1 cm^{-1}, Q-branch [13,14]. In the minor isotopic species the Q-branch has been assigned only for the fundamental transitions [15]. Extrapolation of these data to the first overtone suggests $\sim$2.6 cm^{-1} isotopic shift per mass unit. The $2\nu_1$ Q-branch in the $^{29}SiHCl_3$ may partially overlap with a "hot" band, while the position of this branch in the ^{30}Si species should allow a significant isotopic selectivity in the pre-excitation step, especially at low temperatures, when the "hot" bands are substantially suppressed. The particular selectivity figures for different pre-excitation conditions have to be determined experimentally, perhaps with isotopically enriched $SiHCl_3$. In this work we use IRMPD of naturally abundant $SiHCl_3$ molecules vibrationally pre-excited to the first SiH stretch overtone to determine optimal parameters for selective dissociation of these species relative to the ground-state molecules, since this puts an upper limit for the isotopic selectivity of the process.

4.2 Experimental approach

Studies of $SiHCl_3$ dissociation by thermal [16–18] and laser [19] pyrolysis suggest that the lowest energy decomposition channel for trichlorosilane in the electronic ground state is the production of $SiCl_2$ and HCl:

$$SiHCl_3^{\dagger\dagger} \longrightarrow SiCl_2 + HCl \tag{4.1}$$

Under certain conditions, the $SiCl_2$ radicals polymerize to form $(SiCl_2)_n$ [17,18]. We measure *in situ* the relative dissociation yield of reaction (4.1) after IRMPD using laser-induced fluorescence (LIF) detection of $SiCl_2$ immediately after the dissociation laser pulse.

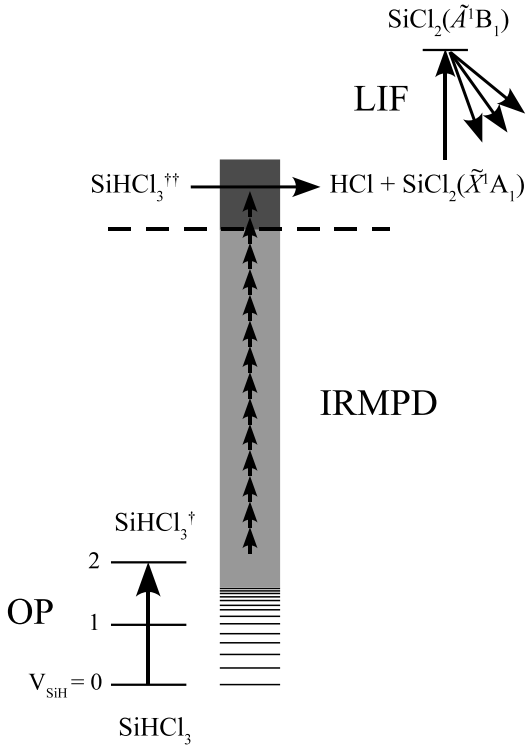

Figure 4.1: Schematic energy level diagram for infrared multiphoton dissociation of vibrationally excited $SiHCl_3$ followed by LIF detection of $SiCl_2$.

Figure 4.1 shows a schematic energy level diagram for IRMPD of vibrationally excited $SiHCl_3$ followed by LIF detection of $SiCl_2$. First, an IR laser pulse excites the first overtone band ($2\nu_1$) of the SiH stretch vibration. Approximately 400 ns later, a pulse from an NH_3 laser promotes some fraction of the vibrationally excited molecules to energies above the dissociation threshold via infrared multiphoton excitation of the ν_4 bending vibration. The $SiCl_2$ dissociation fragments are then detected by a third laser via LIF 600 ns after the pre-excitation pulse. By choosing properly the dissociating frequency and fluence, one can dissociate selectively the pre-excited molecules without significant dissociation of the ground-state species.

The apparatus we employ for these experiments depicted schematically in Figure 4.2. We generate 3-4 mJ of infrared radiation at 4450.5 cm^{-1} for excitation of the first SiH stretch overtone by difference frequency mixing the output of a Nd:YAG pumped dye laser with the fundamental of the same pump laser in a $LiNbO_3$ crystal. As a dissociating laser we use either a homebuilt NH_3 laser [20] pumped by a pulsed CO_2 laser or the CO_2 laser directly. The dissociating pulse from the NH_3 laser largely resembles the pumping pulse, exhibiting a 150-200 ns initial peak and a 3-4 μs long tail. Because we probe the $SiCl_2$ dissociation products by LIF after only the first 600 ns of the dissociating pulse, the parent molecules that we investigate have experienced only 32% of the total fluence.

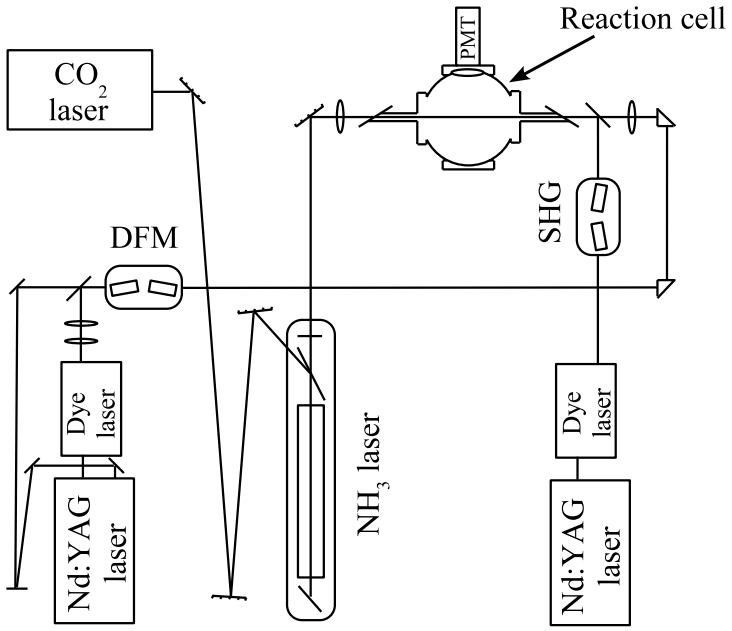

Figure 4.2: Apparatus for experiments on IRMPD of pre-excited $SiHCl_3$.

For LIF detection of the $SiCl_2$ fragments at 325.084 nm (*via* the $\tilde{A}^1B_1(050) \leftarrow \tilde{X}^1A_1(000)$ transition [21]), we use the second harmonic of another Nd:YAG-pumped dye laser. The probe laser beam is combined with the pre-excitation beam on a dichroic mirror. The latter is focused by an F=60 cm lens, resulting in 1.5 J/cm^2 fluence in the beam waist. The two beams are overlapped with the counter-propagating NH_3 laser beam, which is focused by an F=50 cm lens to the center of the vacuum chamber. Semiconductor grade $SiHCl_3$ (Aldrich) slowly flows through the chamber at constant pressure.

4.3 Results and discussion

Our first attempt at IRMPD of $SiHCl_3$ used excitation of the overlapped $2\nu_2$ and $\nu_4+\nu_6$ bands [13] centered at 986 cm^{-1} by a CO_2 laser tuned to the 10R(20) and 10P(20) lines at 982.02 cm^{-1} and 944.18 cm^{-1}, respectively. Under these conditions, we detected a product LIF signal only when the effective dissociation fluence exceeded 20-30 J/cm^2 for a sample pressure in the range of 0.15-3 mbar. Such high dissociation threshold fluence is likely due to the low absorption intensity of the pumped band, making this scheme unsuitable for a practical isotope separation process. This led us to use an ammonia laser for pumping the strong ν_4 fundamental at 810.8 cm^{-1}.

The overall IRMPD efficiency of $SiHCl_3$ by the ammonia laser is significantly higher than that by the CO_2 laser. Despite the fact that the output energy of our ammonia laser on weak

red lines (780, 773 cm^{-1}) is only 8-10% of the CO_2 laser energy, the dissociation yield is more than an order of magnitude higher than for direct dissociation of trichlorosilane by the latter. This suggests that infrared multiphoton excitation of trichlorosilane is 2 orders of magnitude more efficient when pumping through the ν_4 fundamental than that via the $2\nu_2/(\nu_4+\nu_6)$ band. We thus concentrate on NH_3 laser induced dissociation of $SiHCl_3$ in studying its suitability for isotope separation.

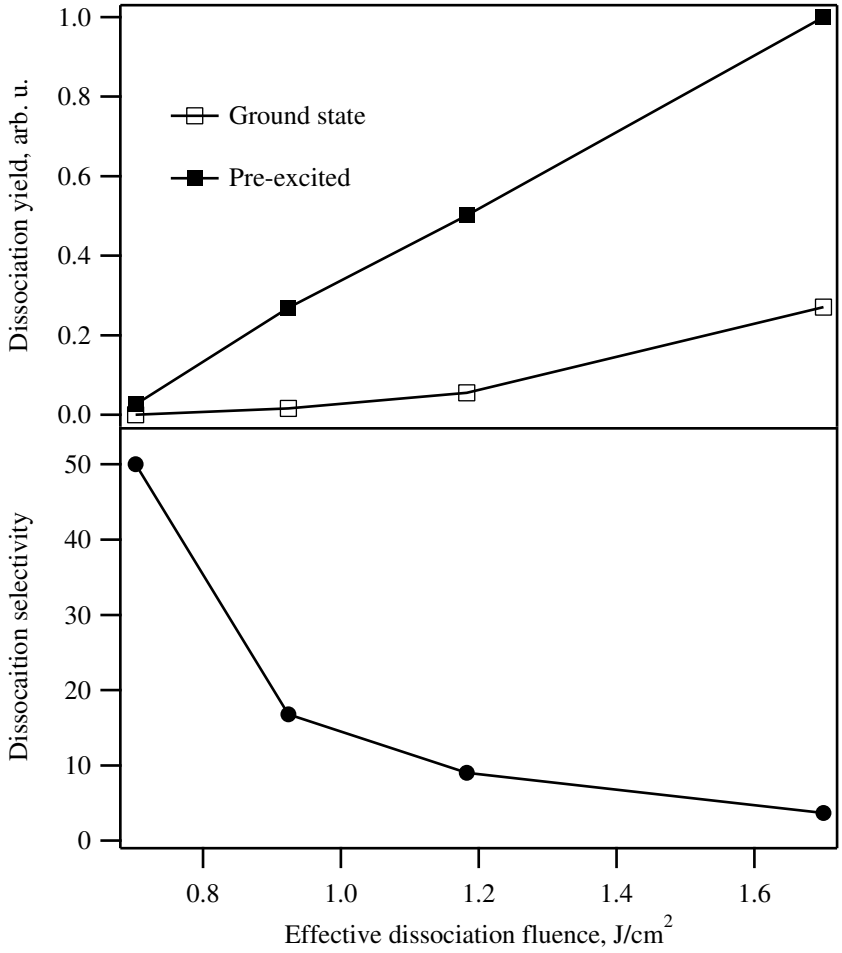

Figure 4.3: IRMPD yield as a function of effective dissociation fluence for room-temperature $SiHCl_3$ (upper panel, open squares) and for $SiHCl_3$ pre-excited to the $2\nu_1$ level (upper panel, solid squares). The dissociation selectivity, which is the ratio of the two yields, is also plotted as a function of the fluence (lower panel). The NH_3 dissociation laser is tuned to 780 cm^{-1}, and the sample pressure is 0.7 mbar.

Figure 4.3 shows the dissociation yield, measured by LIF detection of $SiCl_2$, as a function of the effective dissociation fluence for both vibrationally unexcited $SiHCl_3$ and for $SiHCl_3$ molecules pre-excited to the $2\nu_1$ vibrational level. Dissociation of molecules in both vibrational states increases significantly with increasing fluence over the range investigated, but the increase

is faster for the pre-excited species, in line with our expectations [22]. An appreciable number of pre-excited molecules dissociate at fluence below 1 J/cm^2, where the dissociation yield from the room-temperature species is still small. The ratio of these two dissociation curves, which we call the dissociation selectivity, is plotted on the same figure (right-hand scale). It represents the ratio of the dissociation probability for the pre-excited and ground state molecules at the same CO_2 laser fluence and frequency. Along with the isotopic selectivity of the pre-excitation step, the dissociation selectivity as defined here limits the overall isotopic selectivity of the OP-IRMPD approach. We expect infrared multiphoton dissociation of the pre-excited molecules to be isotopically selective, since the vibration that we use for IRMPE, ν_4, should also have some isotopic shift. We do not expect this selectivity to be significant, however, because the ν_4 absorption spectra of the two isotopic species in vibrationally pre-excited room temperature molecules are strongly overlapped due to both rotational structure and vibrational statistical (inhomogeneous) broadening [23–25]. We can thus consider the dissociation selectivity plotted in Figure 4 as an estimate for the upper limit of isotopic selectivity in the overall OP-IRMPD process. At an NH_3 laser fluence of ∼1.5 J/cm^2, where the dissociation yield of the pre-excited $SiHCl^3$ is significant, this selectivity is only a factor of 5-6. This can be increased if one pre-excites a higher fraction of molecules, but for an optical scheme with unfocused laser beams, which would be best from a practical point of view, the pre-excitation fluence is limited to a few J/cm^2 because of the damage threshold of IR optical materials. Another way to increase the selectivity is to suppress the dissociation of the ground-state molecules and to favor that of the pre-excited species by shifting the dissociation frequency further to the red from the ν_4 fundamental. Using the lowest frequency line available from our NH_3 laser (773 cm^{-1}) results in an almost 2-fold increase in dissociation yield of the pre-excited molecules compared to a 25-30% drop in the dissociation yield of the ground-state species. As a result, this change of dissociation frequency increases the selectivity by a factor of ∼2.5.

Figure 4.4 shows the dependence of the $SiCl_2$ LIF signals on $SiHCl_3$ pressure for both pre-excited and room-temperature species dissociated by 1.5 J/cm^2 pulses of the ammonia laser tuned to 773 cm^{-1}. Because of collisional quenching of electronically excited $SiCl_2$, the LIF signal increases more slowly with pressure than the dissociation yield (see Appendix B). The measured curves thus provide a lower limit for dissociation yield, especially for high pressure. However, since the change of LIF detection efficiency with pressure is the same for $SiCl_2$ produced by dissociation of ground-state and pre-excited species, collisional quenching should not influence our measurements of dissociation selectivity, plotted in the lower panel of Figure 4.4. The selectivity reaches a maximum at ∼0.7 mbar and then slowly drops with further increase of pressure, which is likely due to collisional vibrational deactivation of pre-excited molecules. The initial increase of the selectivity can be explained by collisional rotational relaxation of a few

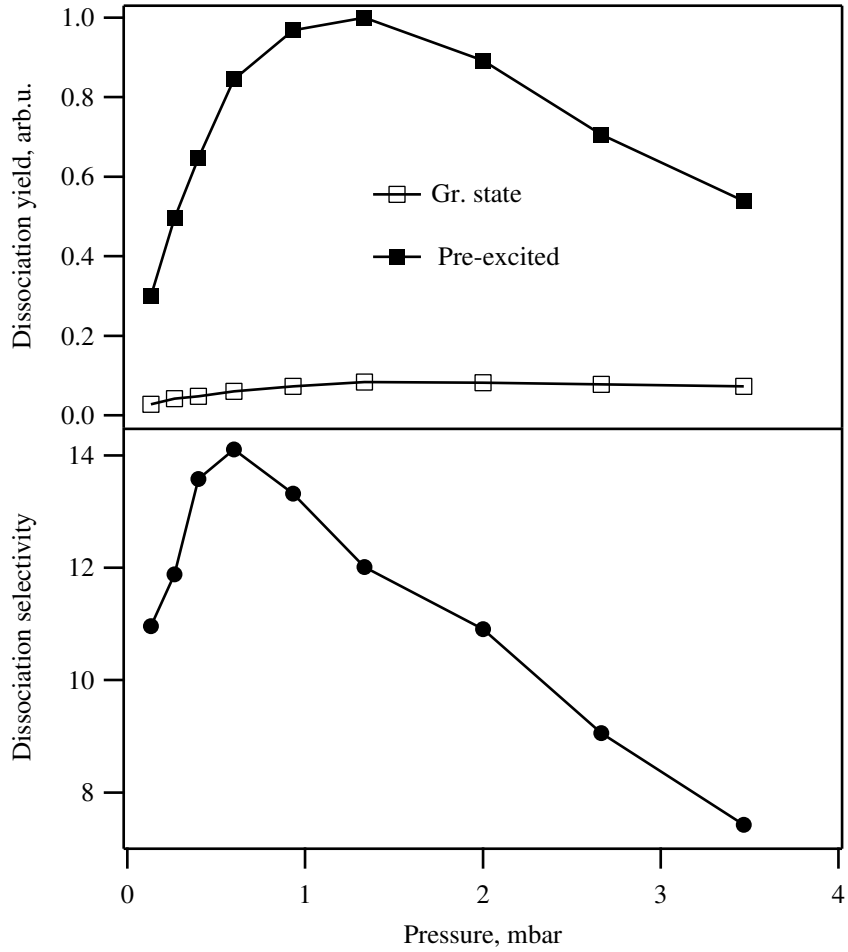

Figure 4.4: IRMPD yield as a function of $SiHCl_3$ pressure for the room temperature molecules (upper panel, open squares) and for the species pre-excited to the $2\nu_1$ level (upper panel, solid squares), left-hand scale. Dissociation selectivity, which is the ratio of the two yields, is also plotted as a function of pressure (lower panel, dots). The NH_3 laser is tuned to 773 cm^{-1}, and the dissociation fluence is 1.5 J/cm^2.

states initially prepared by pre-excitation. This thermalization may populate rotational states that are favored for IRMPD by the 773 cm^{-1} laser line, leading to an increased dissociation yield for the pre-excited species. A selectivity of around 10 for the sample pressure of 1.5-3 mbar implies, for example, a maximum possible isotopic enrichment of ^{29}Si species to 35%. If the pre-excitation fluence were doubled, it will be still below the damage threshold for IR optics and this would increase the level of enrichment to 50%.

The dissociation selectivity can be improved by cooling the molecules. Indeed, at room temperature, 82% of $SiHCl_3$ molecules have thermal excitation in low-frequency vibrations (ν_3 = 257.7 cm^{-1}, ν_6 = 175.5 cm^{-1}), giving rise to "hot" bands in the IR absorption spectrum of the ν_4. Multiphoton excitation through these "hot" bands may contribute significantly to

dissociation of $SiHCl_3$ molecules without pre-excitation. Lowering the working temperature will suppress this contribution and substantially increase the dissociation selectivity.

4.4 Conclusions

With a view toward applying the overtone pre-excitation - IRMPD approach for highly selective laser isotope separation of silicon, we have studied IRMPD of $SiHCl_3$. The dissociation of room temperature $SiHCl_3$ by a CO_2 laser *via* the weak $2\nu_2/(\nu_4+\nu_6)$ band turns out to be inefficient, with a high (20-30 J/cm^2) dissociation fluence threshold. The dissociation becomes 2 orders of magnitude more efficient and the fluence threshold drops below 1 J/cm^2 if one pumps the strong ν_4 fundamental by an ammonia laser. The spectral maximum of the IRMPD yield appears at $\sim$795 cm^{-1}.

The dissociation efficiency increases even further when $SiHCl_3$ molecules are pre-excited to the $2\nu_1$ overtone level. At sample pressures of 1.5-3 mbar, and pre-excitation fluence of $\sim$1.5 J/cm^2 the dissociation yield of the pre-excited molecules is an order of magnitude higher than that of the room temperature species. This result, if scaled to practically realistic laser parameters of lasers, should result in an enrichment of the minor Si isotopes in the $SiCl_2$ dissociation fragments of up to 50%. Lowering the temperature will suppress the ν_4 "hot" bands and may significantly improve this number.

Bibliography

[1] W. S. Capinski, H. S. Maris, E. Bauser, I. Silier, M. Asen-Palmer, T. Ruf, M. Cardona, and E. Gmelin, *Appl. Phys. Lett.*, 1997, **71**, 2109–2111.

[2] E. E. Haller, *J. Appl. Phys.*, 1995, **77**, 2857–2878.

[3] V. S. Letokhov, *Laser und Optoelektronik*, 1998, **30**, 29–33.

[4] Gas-Oil JSC, http://www.c13.ru.

[5] V. B. Laptev, L. M. Tumanova, and E. A. Ryabov, *High Energy Chemistry*, 1998, **32**, 108–113.

[6] V. Y. Baranov, A. P. Dyad'kin, and V. A. Kuz'menko, *Sov. J. Quantum Electron.*, 1990, **20**, 450–452.

[7] M. Kamioka, S. Arai, Y. Ishikawa, S. Isomura, and N. Takamiya, *Chem. Phys. Lett.*, 1985, **119**, 357–360.

[8] K. Tanaka, S. Isomura, H. Kaetsu, Y. Yatsurugi, M. Hasimoto, K. Togashi, and S. Arai, *Bull. Chem. Soc. Jpn.*, 1996, **69**, 493–498.

[9] T. Noda, H. Suzuki, and H. Araki, *Fusion Engineering and Design*, 1998, **41**, 173–179.

[10] Y. Okada and K. Takeuchi, *J. Nucl. Sci. Technol.*, 1997, **34**, 413–415.

[11] O. V. Boyarkin, M. Kowalzcyk, and T. R. Rizzo, *J. Chem. Phys.*, 2003, **118**, 93–103.

[12] J. Makowe, O. V. Boyarkin, and T. R. Rizzo, *J. Phys. Chem. A*, 2002, **106**, 5221–5229.

[13] H. Bürger and A. Ruoff, *Spechtrochimica Acta*, 1970, **26A**, 1449–1458.

[14] Y. Ding, S.-G. He, J.-J. Zheng, S.-M. Hu, X.-H. Wang, and Q.-S. Zhu, *Mol. Phys.*, 2001, **99**, 1669–1678.

[15] W. Fuß and S. Weizbauer, *Ber. Busenges. Phys. Chem.*, 1995, **99**, 289–295.

[16] R. A. Abramovich, *Reactive Intermediates*, Vol. 2, Plenum Press, New York, London, 1982.

[17] G. H. Kruppa, S. K. Shin, and J. L. Beauchamp, *J. Phys. Chem.*, 1990, **94**, 327–331.

[18] M.-D. Su and H. B. Schlegel, *J. Phys. Chem.*, 1993, **97**, 9981–9985.

[19] B. B. Lavrushenko, A. V. Baklanov, and V. P. Strunin, *Spechtrochim. Acta*, 1990, **46A**, 479–481.

[20] J. Makowe, O. V. Boyarkin, and T. R. Rizzo, *Rev. Sci. Instr.*, 1998, **69**, 4041–4043.

[21] M. Suzuki, N. Washida, and G. Inoue, *Chem. Phys. Lett.*, 1986, **131**, 24–30.

[22] O. V. Boyarkin, T. R. Rizzo, D. Rueda, M. Quack, and G. Seyfang, *J. Chem. Phys.*, 2002, **117**, 9793–9805.

[23] O. V. Boyarkin, S. I. Ionov, and V. N. Bagratashvili, *Chem. Phys. Lett.*, 1988, **146**, 106–112.

[24] G. N. Makarov, D. E. Malinovsky, and D. D. Ogurok, *Laser Chem.*, 1998, **17**, 205–218.

[25] A. Stuchebrukhov, S. Ionov, and V. J. Letokhov, *J. Phys. Chem.*, 1989, **93**, 5357–5365.

Chapter 5

Overtone pre-excitation - infrared multiphoton dissociation of ammonia

5.1 Introduction

The stable nitrogen-15 isotope (natural abundance 0.368(7)% [1]) is widely used in biochemical and agricultural research [2] and in medicine, in particular for the so-called N-15 urea urine test [3]. Low cost methods of nitrogen isotope separation are therefore of particular interest. We have undertaken test experiments with an objective to evaluate the OP-IRMPD approach for separation of nitrogen isotopes. In these experiments, ammonia was used as a parent molecule because it meets the main spectroscopic requirements for the applicability in OP-IRMPD isotope separation method (see Section 2.3). Namely, NH_3 posses a high frequency NH stretch vibration that is suitable for the overtone pre-excitation step, and the NH bending "umbrella" vibration, whose frequency is within the tuning range of the CO_2 laser and therefore suitable for the multiphoton dissociation step.

The NH_3 molecule is smaller, however, than other molecules previously studied for application in the OP-IRMPD process and hence poses a lower density of vibrational states. Moreover, the structure of the ammonia vibrational energy levels is irregular due to the inversion doubling and numerous resonances between vibrations. This could result in lower efficiency for the multiphoton excitation process. Indeed, the multiphoton dissociation of ground state ammonia requires a much higher CO_2 laser fluence in comparison with larger molecules with a more regular energy level spacing [4–10]. On the other hand, the low efficiency of IRMPE of ground state ammonia can be exploited in the OP-IRMPD approach to ensure the selective dissociation of only the pre-excited molecules. Overtone pre-excitation should bring the molecule to the energy region of higher density of vibrational states and help to overcome the difficulty of pumping the molecule through the region of irregular energy level spacing. This should result in

a considerable lowering of the CO_2 laser fluence required for the dissociation of the pre-excited compared to ground state molecules. The study of the influence of the overtone pre-excitation on the IRMPD yield is the main purpose of this research.

5.2 Basis of vibrational spectroscopy and multiphoton excitation of ammonia

The NH_3 molecule has a symmetrical pyramidal structure with the N atom at the top and it is a classical example of a molecule with an inversion barrier [11]. This molecule has four vibrational modes: one symmetric and one antisymmetric stretch vibration (ν_1 and ν_3 respectively) and one symmetric and one antisymmetric bending vibration (ν_2 and ν_4). The potential corresponding to the symmetric bending (umbrella) vibrational mode, ν_2, is represented by a double minima well (Fig 5.1). The two equilibrium positions corresponding to the two different orientations

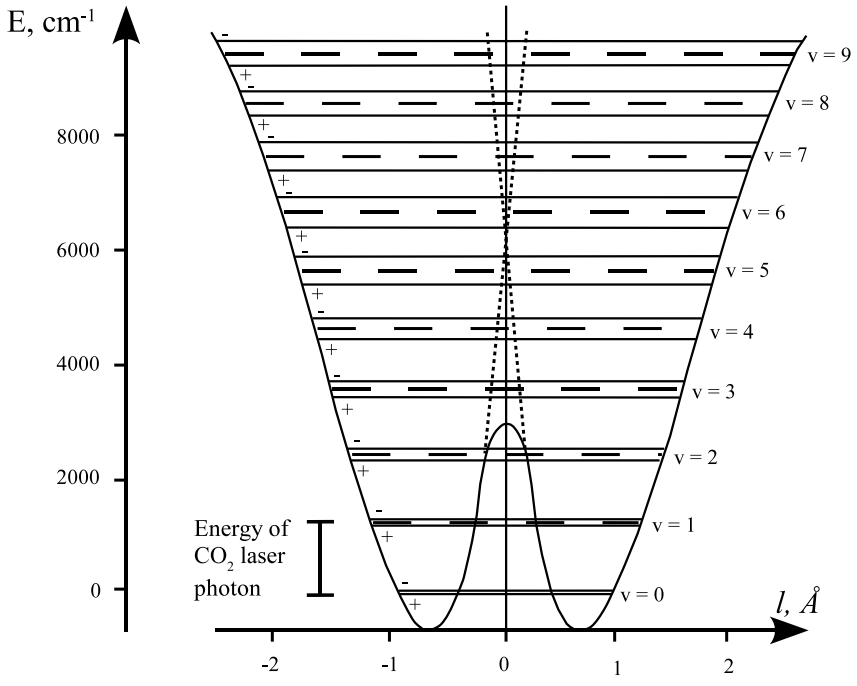

Figure 5.1: Potential and vibrational energy levels of ν_2 vibration in ammonia. Coordinate l of the potential curve plot is the distance between the nitrogen atom and the plane of the hydrogen atoms in Ångstrems.

of the N atom with respect to the H_3 plane are separated by a potential barrier of about 1800 cm^{-1} [12–17]. Due to the tunnelling effect, the wave functions for the low amplitude umbrella vibrations are not localized in one of the two wells but rather distributed between them. As a consequence, the mutual interaction of the vibrational states corresponding to the

two orientations of the molecule results in level splitting that is related to the time scale for an ammonia molecule to tunnel from one side of the barrier to the other (and hence the term *inversion doubling*). The value of the tunnelling splitting for the lowest energy level is 0.79 cm^{-1} [18]. At higher energies the value of splitting increases reaching a half the separation of successive unperturbed levels. In other words, far above the potential barrier, we have a simple series of levels with roughly half the spacing that one would have if there were only one minimum in the potential curve. Table 5.1 lists the fundamental frequencies of the vibrational modes in ammonia and of the first and second overtones of ν_2 vibration. As it can be seen from

	Vibration	ν_{vacuum}, cm^{-1}	$\Delta\nu_{inv}$, cm^{-1}
ν_1	symm. stretch (A_1)	3336.02 / 3337.08 [12]	1.06
ν_2	umbrella bend (A_1)	932.43 / 968.12 [19]	35.69
$2\nu_2$		1597.47 / 1882.18 [20]	284.71
$3\nu_2$		2384.15 / 2895.52 [21]	511.37
ν_3	a.s. stretch (E)	3443.63 / 3444.00 [12]	0.37
ν_4	a.s. bend (E)	1626.30 / 1627.30 [20]	1.00

Table 5.1: NH_3 vibrational fundamentals, ν_2 overtones and inversion splitting values.

the Table 5.1, the energy levels corresponding to ν_1, ν_3 and ν_4 vibrational modes are also split due to tunnelling effect, although the values of these splittings are much smaller than for the umbrella vibration.

In zero approximation, the two wave functions corresponding to a pair of split levels are a symmetric and an antisymmetric combination of the wave functions $\Psi_v(\xi)$ corresponding to each minimum of the potential curve, where ξ is the displacement from the minimum (counted

positive towards the potential hill):

$$\begin{aligned} \Psi_s &= \Psi_{\mathrm{v}}(\xi) + \Psi_{\mathrm{v}}(-\xi), \\ \Psi_a &= \Psi_{\mathrm{v}}(\xi) - \Psi_{\mathrm{v}}(-\xi), \end{aligned} \tag{5.1}$$

where v is the vibrational quantum number. The energy levels corresponding to the symmetric and antisymmetric functions are denoted by " + " and " − " respectively (Figure 5.1). The selection rule for the infrared absorption is $+ \leftrightarrow -$ and $- \leftrightarrow +$, thus, for example $\mathrm{v}_{\nu_2} = 1 \leftarrow 0$ transition has two subbands at 629.37 cm^{-1} and 949.75 cm^{-1}, $\mathrm{v}_{\nu_2} = 2 \leftarrow 1$ has two subbands at 471.97 cm^{-1} and 1298.05 cm^{-1} (as calculated using the values represented in Table 5.1).

From the above discussion, the data represented by Table 5.1 and the Figure 5.1, we can conclude that at low excitation energies only one vibrational transition (the one between symmetric $\mathrm{v}_{\nu_2} = 0$ and antisymmetric $\mathrm{v}_{\nu_2} = 1$) in ammonia can be effectively pumped by CO_2 laser, whose photon energy is in order of 1000 cm^{-1}. This situation is completely different from the case of CF_3H molecule (Chapter 3), where excitation of CF stretch vibration by absorption of CO_2 photons results in relatively small gradual shift of absorption frequency such as absorption is possible at several consequent vibrational transitions.

Another important feature of the ammonia molecule that determines the complexity of its IR absorption spectrum is the presence of several anharmonic resonances. Since ν_1 and ν_3 are close in frequency, vibrations $\nu_1 + \nu_3$ and $2\nu_3$ are in resonance with $2\nu_1$; $2\nu_1 + \nu_3$, $\nu_1 + 2\nu_3$ and $3\nu_3$ are in resonance with $3\nu_1$, and so on. Taking into account the symmetry of the interacting vibrations, it can be shown [11] that the region of 6600 cm^{-1} ($2\nu_1$) has two parallel and two perpendicular bands[1], the region of 9800 cm^{-1} ($3\nu_1$) - three parallel and three perpendicular bands, the region of 12600 cm^{-1} ($4\nu_1$) - four parallel and five perpendicular bands, and so on. In addition, Fermi-resonance between $n\nu_1$ and $(n-1)\nu_1 + 2\nu_4$ and the resonance between $m\nu_1$ and $(m-1)\nu_1 + 3\nu_2$ (where n and m are integers) are substantial at certain n and $m > 1$. The influence of the latter resonance is especially strong in the energy region of the third NH stretch overtone ($m = 4$) which we have chosen for the study.

The inversion doubling, together with numerous resonances perturbs the vibrational energy levels in ammonia making the level spacing essentially irregular. Considerable efforts in the assignment of the NH_3 spectral lines corresponding to overtone and combinational vibrations have not yet led to the complete understanding of the rovibrational spectroscopy of this molecule. One of the most comprehensive studies of this question has been reported by Lehmann and Coy [22–24], who fulfilled a detailed analysis of highly excited vibrational states of ammonia resulted in rotational assignment of substantial number of NH_3 absorption lines. A certain suc-

[1] $2\nu_1$ is a parallel band, $\nu_1 + \nu_3$ is a perpendicular band and $2\nu_3$ has two sub-bands, a perpendicular and a parallel one.

cess has been achieved recently in the field of *ab inito* calculations of the ammonia vibrational spectroscopy [13–17].

It is the irregularity of the energy level structure that makes ammonia a promising candidate for using the OP-IRMPD approach to nitrogen isotope separation. Indeed, one of the requirements for the molecule to be a good candidate for this method is the possibility of the selective multiphoton dissociation of the pre-excited molecules without dissociation of the ground state molecules (see Section 2.3). The multiphoton dissociation of ground state ammonia is hampered not only by the low density of vibrational states at low excitation levels, but also by the irregularity of their spacings inhibiting the resonant stepwise excitation process. Previous work on multiphoton excitation and dissociation of the ammonia [4–10] has shown that the dissociation occurs only at extremely high fluence (> 1000 J/cm^2 at typical CO_2 laser pulse duration of 100-200 ns) or at high ammonia pressure (~ 100 mbar at CO_2 laser fluence of several tens of J/cm^2). The pressure dependence of the NH_3 IRMPD yield was explained by the thermal mechanism of the dissociation process, when the laser radiation is resonantly absorbed only by the ground state molecules, such as the excitation of the high energy states is due to the energy pooling collisions between the excited molecules. Once the molecule has reached the region of high states density (*quasicontinuum*) it can more easily be excited up to the dissociation threshold by subsequent absorption of the CO_2 laser photons. It has been found, however, that the quasicontinuum limit in ammonia is above 10000 cm^{-1} [10], which is considerably higher than in other molecules studied for the multiphoton dissociation, which means that the requirement for the resonance with the CO_2 laser field is not easily satisfied even, for highly excited NH_3 molecules. To some extent, multiphoton excitation through the region below the quasicontinuum is facilitated by the rich rotational structure of the molecule. In this case, a fast collisional rotational relaxation overcomes the so-called *rotational bottleneck* (see page 23) by compensating the lack of resonances between vibrational transitions and laser.

5.3 Experimental set-up

Figure 5.2 depicts the experimental apparatus we employ for application of the OP-IRMPD approach to ammonia. The pre-excitation laser pulse is generated by a dye laser (Lumonics HD-500) pumped by the 2^{nd} harmonic of the Nd:YAG laser (Spectra-Physics). The dye laser operates with LDS-795 dye and delivers 45-60 mJ per pulse when pumped with 450 mJ pulses at 532 nm from the Nd:YAG laser. The duration of the generated pulses is 5-6 ns and their bandwidth is 0.05 cm^{-1}. The pre-excitation laser pulse is focused into the center of the 50 cm stainless-steel reaction cell by a 50 cm focal length lens through a BaF_2 window. After passing through the cell the pre-excitation laser beam is blocked by a 4x4 mm absorption plate (beam

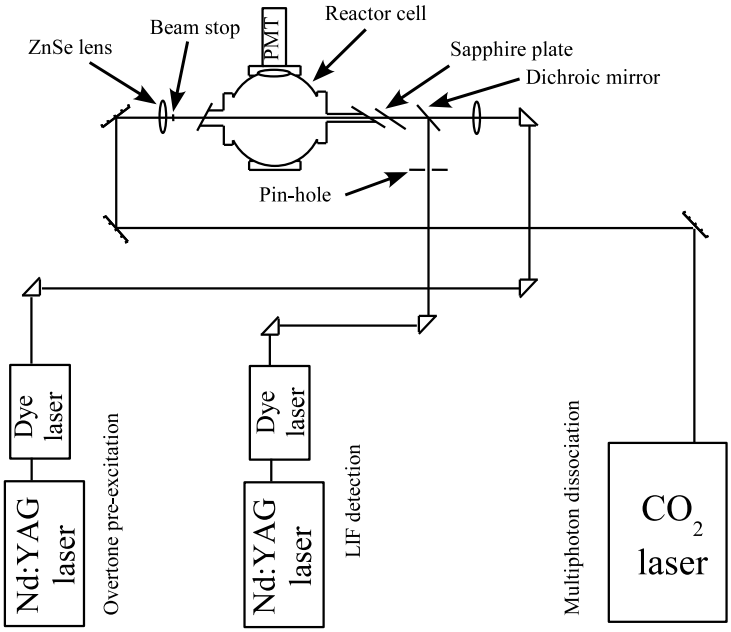

Figure 5.2: Experimental setup.

stop).

The dissociation laser pulse is generated by a line-tunable TEA CO_2 laser (PIC, model SP-7000 [25]). This laser delivers up to 600 mJ per pulse (80% within the first 100 ns) in a near TEM_{00} beam. The CO_2 laser beam is expanded to the diameter of about 2.5 cm and then focused by an AR coated ZnSe lens of 50 mm diameter and 50 cm focal length. Due to the relatively large initial diameter of the CO_2 laser beam, the energy loss on the pre-excitation laser beam stop does not exceed 15%. This configuration provides about 50 J/cm^2 dissociation laser fluence at the focal point. After exiting the cell, the CO_2 laser beam is blocked by a 2 mm thickness sapphire plate (which passes the pre-excitation laser).

For LIF detection of the NH_2 dissociation fragments we employ a third laser pulse at 597.72 nm, which corresponds to the strong $\Sigma(0,9,0)\longleftarrow(0,0,0)$ vibronic band between the $\tilde{A}(^2A_1)$ and $\tilde{X}(^2B_1)$ electronic states. The probe laser pulse is generated by a dye laser (Lumonics HD-500) with the Rhodamine-610 dye pumped by the 2^{nd} harmonic of the Nd:YAG laser (Spectra-Physics). The laser beam is truncated by a 0.5 mm pin-hole and combined with the pre-excitation laser beam on an AR-coated dichroic mirror. The fluorescent light is collected by 1:1 condensor lens through a rectangular 2x5 mm slit, filtered by a combination of 1 mm BG-40 and RG-610 filters and detected by an infrared-sensitive photomultiplier (PMT). The PMT signal is integrated within a 270 ns window after the LIF laser pulse and transmitted into the PC computer *via* a CAMAC interface.

5.4 Experimental results

5.4.1 Comparison of photoacoustics and action spectra of NH_3 at different sample pressures

As the absorption spectrum of ammonia in the region of the third overtone of the symmetric NH stretch vibration has not been published, the first step in our study was to measure this spectrum. Using the photoacoustic technique, we recorded the absorption spectra of NH_3 at the 70 mbar pressure in the range between 12450 and 12800 cm^{-1} with a resolution of 0.1 cm^{-1}. A part of the recorded spectra containing the strongest absorption lines is shown in the upper panel of Figure 5.3.

In subsequent experiments, we investigated the multiphoton dissociation of ammonia molecules pre-excited to different energy levels. The dissociation yield as a function of pre-excitation laser frequency represents an *action spectrum*, which can be considered as an overtone excitation spectrum measured using the IRLAPS detection technique. This action spectrum in the spectral range covering the most intense absorption lines appearing in the photoacoustics spectrum has been recorded under different sample pressures using different frequencies of the dissociation laser. The maximum dissociation yield (and hence the maximum signal to noise ratio) was observed when lines from the 10P branch of the CO_2 laser (920 - 960 cm^{-1}) were used for multiphoton excitation of pre-excited molecules. The frequencies of the 10P branch are close to the ν_2 frequency of ground state NH_3. Despite the proximity of the IRMPD laser to this band, we did not detect any signal corresponding to the dissociation of ground state ammonia molecules when the sample was exposed only to the CO_2 laser.

Figure 5.3 (lower panels) depicts a portion of such an action spectrum measured using the several CO_2 laser lines in the 10P and 10R branches.

As can be clearly seen from Figure 5.3, the general structure of the action spectra is conserved independent of the frequency and the pressure and corresponds to the structure of the absorption (photoacoustic) spectrum. Relative intensities of the particular lines in the action spectra depend, however, on both the sample pressure and the dissociation laser frequency. At pressures above 10 mbar, the relative intensities of the lines in the action spectra correspond to those determined from the photoacoustic spectrum, except the strong line at 12658.6 cm^{-1}, which appears only in the photoacoustic spectrum. Below 10 mbar, the relative intensities of some of the lines in the action spectra differ markedly from the corresponding absorption intensities. Using the 10P(20) CO_2 laser line at 943.9 cm^{-1} and a pressure of 0.8 mbar, the strongest feature is observed at the pre-excitation frequency of 12696.9 cm^{-1}. This feature is almost 5 times higher than its relative intensity in the photoacoustic spectrum.

In order to distinguish the spectral lines whose relative intensities differ from the correspond-

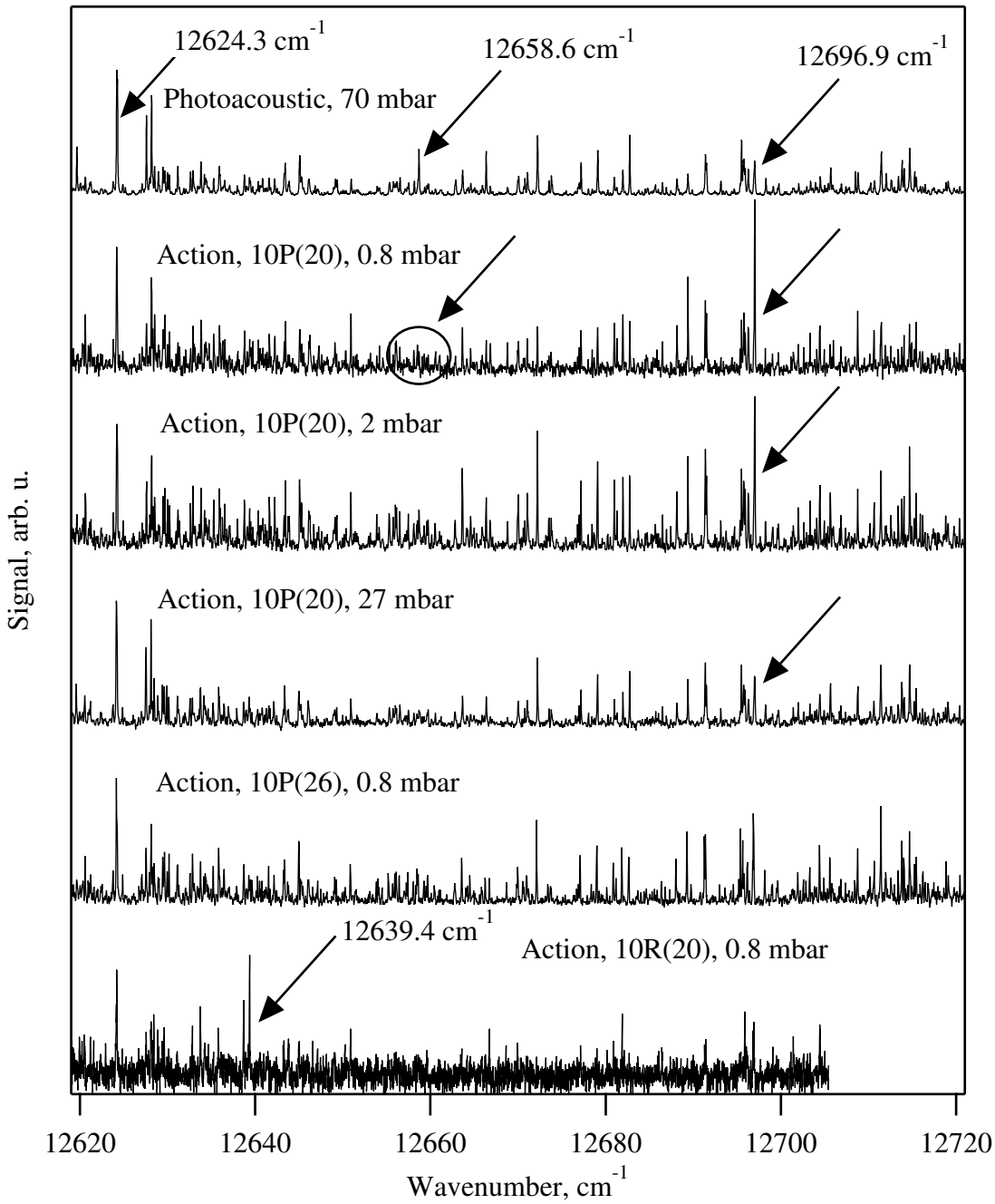

Figure 5.3: Part of the photoacoustic spectrum of NH_3 in the region of the 3^{rd} NH stretch overtone (top) and corresponding region of the ammonia action spectra under different sample pressures, obtained using the 10P(20), 10P(26) and 10R(20) CO_2 laser lines (943.9 cm^{-1}, 938.5 and 975.6 cm^{1-} respectively). The spectra are normalized to the intensity of the strongest absorption line at 12624.3 cm^{-1}

ing absorption intensities under certain experimental conditions, we will call them *"unusual"* lines. Correspondingly, for the lines with the "usual" behavior (the line intensity corresponds to the absorption intensity) we will use the term *"usual"* lines. The most prominent *usual* spectral line is at 12624.3 cm^{-1}. The most interesting *unusual* lines are the lines at 12696.9 cm^{-1} (strong dependence of relative intensity on the sample pressure) and 12658.6 cm^{-1} (does not appear in the action spectra at any pressure and at any dissociation laser frequency).

The nature of the *unusual* line observed in the photoacoustic spectra and not observed in the IRLAPS spectra at all various experimental conditions (12658.6 cm^{-1}) is not completely clear. We assume that the wave function of the eigenstate corresponding to this absorption line has no (or very small) component corresponding to a $\nu_2 = 0$. As only the transition between symmetric $v_{\nu_2} = 0$ and antisymmetric $v_{\nu_2} = 1$ states can be effectively pumped by CO_2 laser (see Section 5.2), the absence of a $\nu_2 = 0$ component should dump the consequent excitation of pre-excited NH_3 molecules.

To understand the nature of the *unusual* line at 12696.9 cm^{-1} we have performed several additional experiments. The idea of these experiments is to compare the influences of different experimental parameters on the dissociation yield from the two different pre-excitation levels. The first of these levels corresponds to the *usual* spectral line at 12624.3 cm^{-1}, the second one to the *unusual* line at 12696.9 cm^{-1}. The results of these experiments are described in the following sections.

5.4.2 IRMPD yield of pre-excited NH_3 as a function of pressure

The NH_2 LIF signal has been measured as a function of NH_3 pressure for pre-excitation at frequencies corresponding to *usual* and *unusual* lines[2] followed by dissociation by the 10P(20) CO_2 laser line at 943.9 cm^{-1}. The efficiency of the LIF detection of NH_2 decreases with pressure due to collisional electronic quenching. An estimation of the quenching effect on our experimental results, and a calculation of the corresponding correction coefficient are given in Appendix B. The correction factor, which has to be applied to the LIF signal as a function of sample pressure, is shown in Figure 5.4. Applying this correction factor to our experimental data allows us to extract a quantity proportional to the ratio of the number of NH_2 dissociation fragments to the number of NH_3 molecules in the irradiated volume (i.e. the dissociation probability):

$$\frac{S_{LIF}}{\epsilon_q \mathrm{p}} \sim \frac{[\mathrm{NH_2}]}{[\mathrm{NH_3}]}, \tag{5.2}$$

where S_{LIF} is the LIF signal, p the pressure and $\epsilon_q p$ the LIF correction factor.

[2]From here on in the text we will use the term *"usual"* for the line at 12624.3 and *"unusual"* at 12696.9 cm^{-1} if nothing else is mentioned.

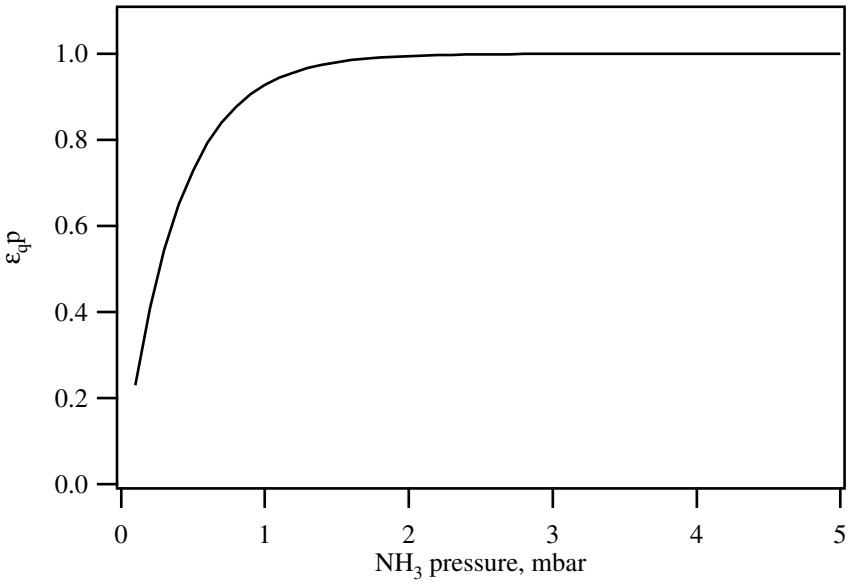

Figure 5.4: LIF correction factor as a function of pressure. The LIF signal has to be divided by the ϵ_qp value in order to obtain a value that is proportional to the dissociation probability.

The dissociation probability as a function of ammonia pressure is shown in Figure 5.5 for molecules pre-excited at the frequencies of both *usual* and *unusual* lines and for ground state NH_3. Figure 5.6 shows the dissociation probability for pre-excited molecules normalized on the corresponding pre-excitation cross-sections determined from the photoacoustic spectrum (or IRMPD probability) as a function of pressure.

Up to pressures of about 50 mbar we do not detect any signal from the molecules dissociated from the vibrational ground state. This is consistent with the results of earlier experiments where IRMPD of ground state NH_3 at low pressure was observed only with, at least, 10 times higher CO_2 laser fluences [4–10]. At the same time, dissociation of the pre-excited molecules occurs already at pressures below 1 mbar, reaching its maximum efficiency at 11 mbar for pre-excitation at *usual* and 4 mbar at *unusual* line frequencies. Thus, the selectivity of the OP-IRMPD process at low NH_3 pressures and CO_2 laser fluence ~ 50 J/cm^2 is extremely high. We attribute this high selectivity to the high level of irregularity in the ammonia absorption spectra, caused mostly by inversion splitting of energy levels, which inhibits the IRMPD of vibrational ground state molecules.

The increase of the relative dissociation yield with ammonia pressure has been observed earlier for dissociation of ground state molecules, but at higher CO_2 laser fluences [6, 7, 9]. Campbell *et al.* proposed two possible explanations of this effect [6]. The first one is collisional refilling of rotational levels depleted by the IRMPD process. We attribute the increase of the relative dissociation yield of the pre-excited NH_3 in our experiments to this effect (see below).

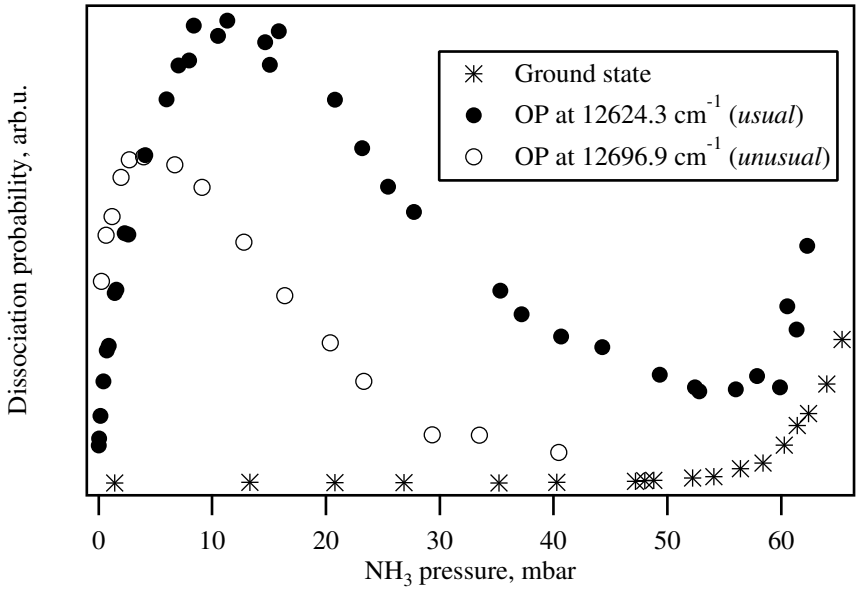

Figure 5.5: Dissociation probability as a function of ammonia pressure for molecules pre-excited *via* the *usual* and *unusual* lines and for ground state NH_3.

Another process suggested by Campbell and coworkers that could increase the relative dissociation yield at high ammonia pressures is up-pumping by energy-pooling collisions between highly vibrationally excited NH_3 molecules. This process does not seem to be of high importance in our experiments, science the concentration of pre-excited molecules is low as compared with the concentration of ground state molecules and, hence, most collisions occur between excited and ground state molecules.

To explain the observed pressure dependance of IRMPD probability of ammonia pre-excited at *usual* and *unusual* lines frequencies we apply the model illustrated by Figure 5.7. If pre-excitation occurs at an *usual* line frequency, the multiphoton excitation goes exclusively through the channel **A**, shown on the left side of Figure 5.7. The pre-excitation populates one (or a few) rovibrational energy states that is *not in resonance* with the dissociation laser field. Collisional rotational relaxation creates a Boltzmann like energy distribution between the rotational levels of a given vibrational state. If at least one of these levels is in resonance with the CO_2 laser field, the first step of multiphoton absorption will occur from this level. Absorption of the first CO_2 laser photon will populate one (a few) rovibrational state(s) and rotational relaxation is needed again for subsequent excitation. Thus, fast rotational relaxation increases the efficiency of the multiphoton excitation process.

If pre-excitation occurs at an *unusual* line frequency, the resonant transition is possible directly from the pre-excited rovibrational state (double resonance). In this case, the first step of multiphoton excitation does not require rotational relaxation (channel **B** in the figure), that

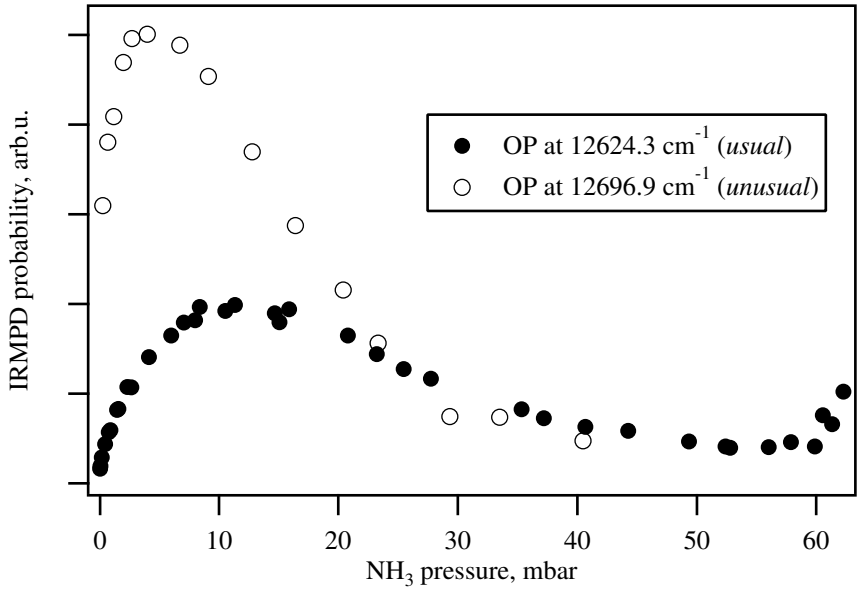

Figure 5.6: IRMPD probability as a function of ammonia pressure for molecules pre-excited *via* the *usual* and *unusual* lines.

results in higher IRMPD probability at low ammonia pressures (see Figure 5.6). At increased pressure, a partial collisional rotational relaxation occurs before the resonant absorption of the first CO_2 laser photon. This leads to the dissociation of a fraction of the molecules pre-excited at an *unusual* line frequency through the channel **A**. With increasing pressure the probability of dissociation through channel **A** increases resulting in the observed disappearance of the difference between *usual* and *unusual* lines at high pressures.

Thus, rotational energy transfer can both enhance and inhibit the OP-IRMPD process in ammonia. On one hand it helps molecules to fulfill the resonance conditions at each step of multiphoton excitation and in this sense it enhances dissociation. On the other hand, if the molecule is already in resonance with the dissociation laser field, rotational energy transfer can inhibit dissociation by depopulating the resonant level. In the case of pre-excitation at the frequency corresponding to a *usual* line of the NH_3 action spectrum, rotational energy redistribution plays only an enhancing role, refilling the resonant rovibrational states, whereas in the case of *unusual* line excitation the enhancing and inhibiting effects are in competition with one another, resulting in faster initial growth of the relative dissociation yield at low pressure and shifting the maximum of the curve representing the relative dissociation yield as a function of NH_3 pressure to lower pressures.

The described above model can be simplified in order to obtain approximate analytical solutions describing the collisional IRMPD process for pre-excitation at *usual* and *unusual* lines. Such a simplified model is illustrated in Figure 5.8. Ammonia molecule pre-excited to

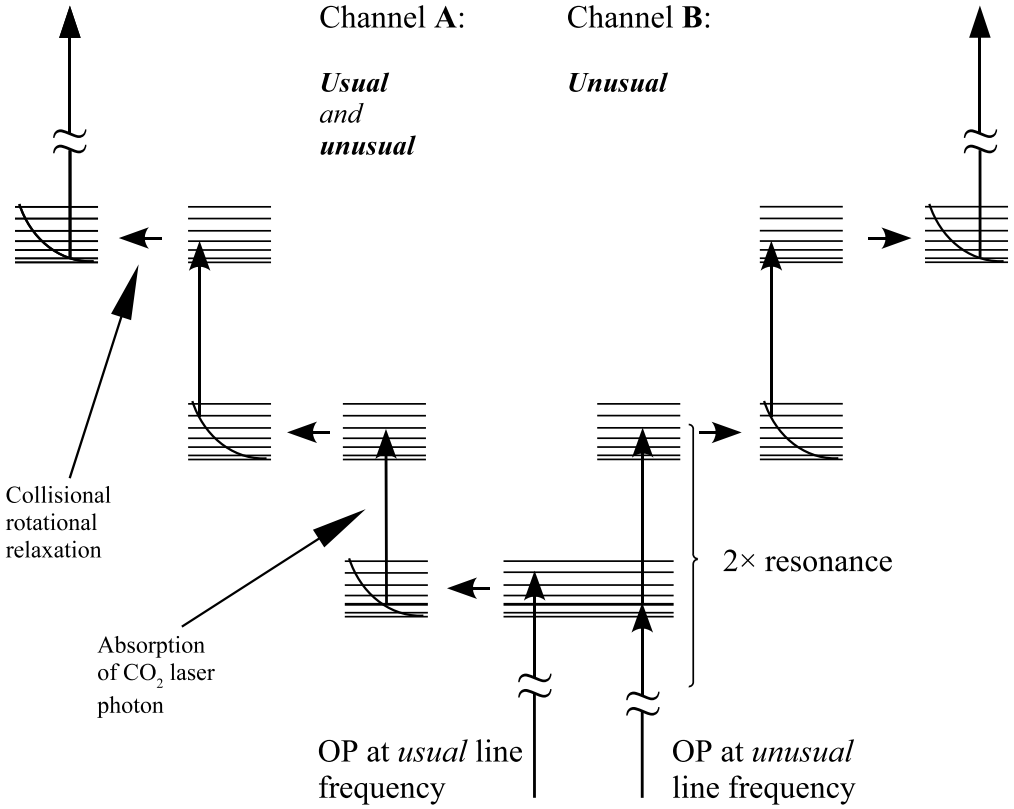

Figure 5.7: Dissociation channels for pre-excitation at *usual* and *unusual* lines.

the level *1* (*usual*) or *2* (*unusual*) can be dissociated without collisions with probabilities β_A and β_B respectively. Collisions lead to depopulation of levels *1* and *2* by vibrational relaxation with rate k_{v} and by rotational relaxation. Enhancement of IRMPD yield by rotational energy transfer is taken to account by introduction of levels *3* and *4* populated by rotational relaxation with rate k_r from levels *1* and *2* respectively. Dissociation probabilities for levels *3* and *4* are $B_A > \beta_A$ and $B_B > \beta_B$ respectively. Transition from the resonant channel **B** to the channel **A** has rate k_{BA}.

Although both the k_r and k_{BA} constants describe the rotational relaxation of excited NH_3 molecule, a substantial difference between them exists. The depopulation of the resonant level *2* is a single step process, whereas multiphoton dissociation of NH_3 from levels *3* and *4* requires rotational relaxation at each step of the IRMPE process. Thus, k_r describes the rotational relaxation at several consequent levels populated during the IRMPE. Consequently, the population of the effective levels *3* and *4* is slower than the depopulation of the level *2*, and $k_r < k_{BA}$.

According to the simplified model, the IRMPD probability for NH_3 molecules pre-excited

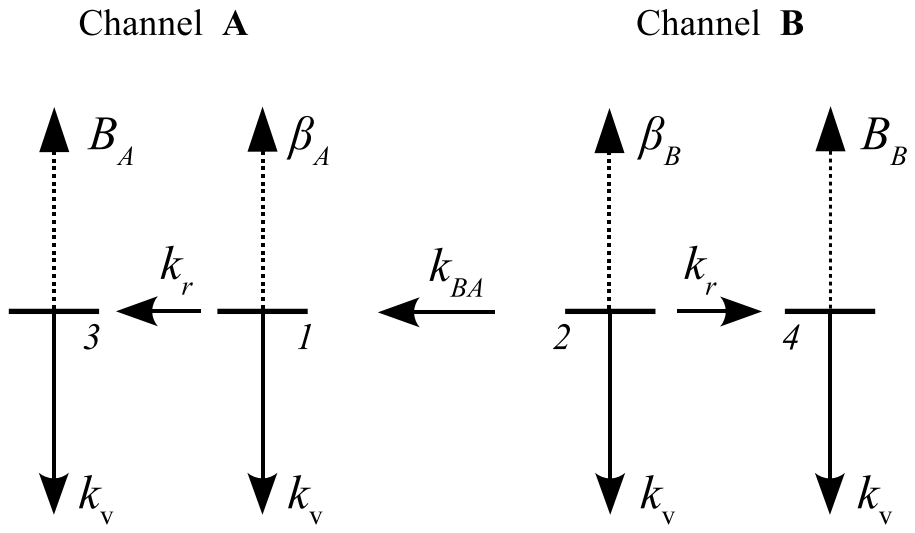

Figure 5.8: Dissociation channels for pre-excitation at *usual* and *unusual* lines - simplified model.

through the *usual* line is described by the following equation:

$$Y_{usual} = e^{-k_v p\tau}\left(\beta_A e^{-k_r p\tau} + B_A(1 - e^{-k_r p\tau})\right), \tag{5.3}$$

where τ is the characteristic time of the IRMPD process determined by the temporal profile of the part of the CO_2 laser pulse located after the pre-excitation pulse. In our experiments τ is 20-30 ns. Using β_A, B_A, $k_v\tau$ and $k_r\tau$ as the fitting parameters we can fit the experimental data representing the IRMPD probability as a function of pressure for pre-excitation at the *usual* line frequency. Figure 5.9 (dots, solid line) shows the experimental data and the fitting curve respectively. The values of the fitting parameters with their standard deviations are also shown in the figure. Although the number of fitting parameters is high, the different parts of the curve are described by different parameters (for example, the tail of the curve described by k_v and B_A), thus the accuracy of the fit is reasonably good, which confirmed by the relatively small values of standard deviations of the fitting parameters.

The IRMPD probability for NH_3 molecules pre-excited through the *unusual* line is described by the following equation:

$$\begin{aligned} Y_{unusual} = e^{-k_v p\tau}\Big(e^{-k_{BA} p\tau'}\left(\beta_B e^{-k_r p\tau} + B_B(1 - e^{-k_r p\tau})\right) + \\ + (1 - e^{-k_{BA} p\tau'})\left(\beta_A e^{-k_r p\tau} + B_A(1 - e^{-k_r p\tau})\right)\Big), \end{aligned} \tag{5.4}$$

where τ' is the average time required for the absorption of one CO_2 laser photon by the molecule on the resonant level *2*. Using the values of β_A, B_A, $k_v\tau$ and $k_r\tau$ obtained from the

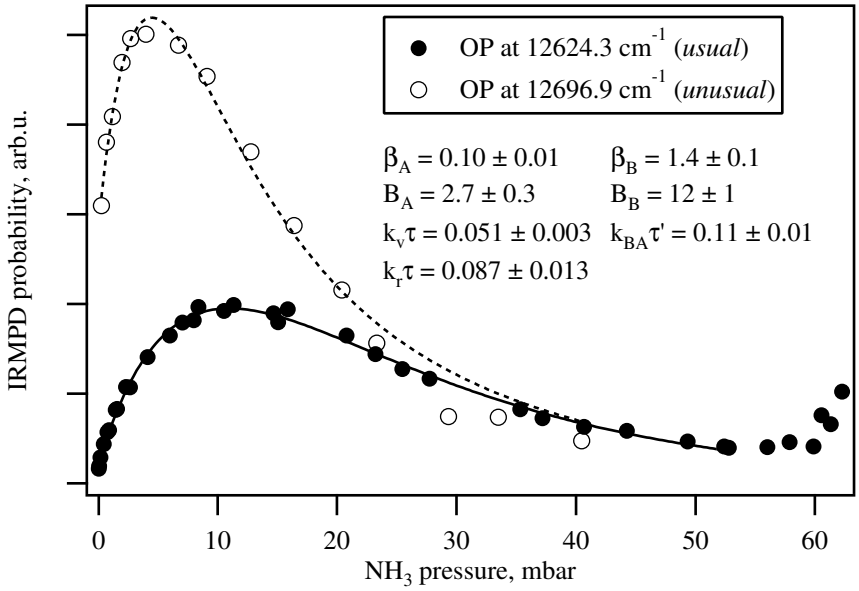

Figure 5.9: IRMPD probability as a function of ammonia pressure for molecules pre-excited *via* the *usual* and *unusual* lines.

fit of the curve corresponding to the pre-excitation at *usual* line, and using β_B, B_B, $k_{BA}\tau'$ as fitting parameters we can fit the experimental data corresponding to the pre-excitation at the *unusual* line. The fitting curve and the fitting coefficients with standard deviations are shown by the dashed line in the Figure 5.9.

A good correlation between the experimental data and the fitting curves obtained using the equations based on the model assuming the double resonance in the absorption of pre-excitation and first dissociation photons supports the suggested model. The other experimental results confirming the double resonance model are described in the following section.

5.4.3 Verification of the double resonance model

As the first check of the double resonance model we can compare the low pressure action spectra measured using different CO_2 laser lines for the dissociation of pre-excited ammonia molecules. If the double resonance description of the *unusual* lines nature is correct, then even a slight shift of the dissociation laser frequency has to result in the disappearing of this spectral feature and, perhaps, appearance of an *unusual* line (lines) at different frequencies. As we expect, the spectral feature at 12696.9 cm^{-1} disappears when the 9P(26) (938.5 cm^{-1}) and 10R(20) (975.6 cm^{-1}) CO_2 laser lines are employed (see Figure 5.3). Moreover, a considerable increase of intensity of the line at 12640.6 cm^{-1} is observed in the low pressure action spectra when the 10R(20) CO_2 laser line is employed. These observations support the double resonance model describing the nature of intense *unusual* spectral lines detected in the low pressure action

spectra of ammonia.

Another result which confirms the double resonance model is the dependence of the dissociation probability on the time delay between the pre-excitation and the dissociation laser pulses. The results of these experiments for excitation at the *usual* and *unusual* lines are represented in Figure 5.10.

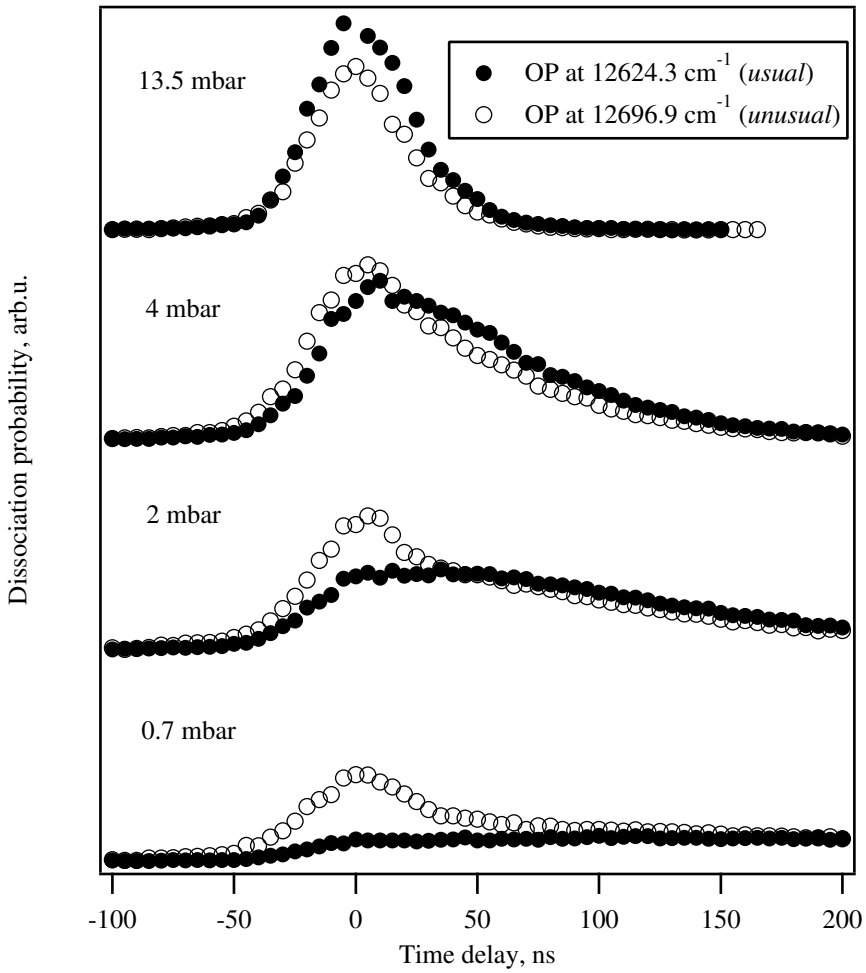

Figure 5.10: Dissociation yield as a function of time delay between pre-excitation and dissociation laser pulses.

Similarly to the experiments where the dissociation probability was measured as a function of the ammonia pressure, the tails of the curves corresponding to the pre-excitation at *usual* and *unusual* line frequencies tend to have a ratio corresponding to the corresponding absorption intensities. The behavior of the curves corresponding to the pre-excitation at *usual* line is well understood in our previous experiments on CF_3H molecule (Chapter 3): the initial rise corresponds to the increase of the effective fluence of the CO_2 laser[3], and the subsequent

[3] *Effective fluence* is the fluence of the part of the CO_2 laser pulse located after the pre-excitation laser pulse.

decrease of the signal arises from collisional V-V relaxation of pre-excited molecules during the time delay between pre-excitation and dissociation laser pulses. At low pressures (0.7 mbar), collisional V-V relaxation is slow compared to the time scale of the experiment, and therefore the corresponding curve does not show a significant decrease. In contrast to the behavior after pre-excitation at the *usual* line frequency, the experimental curves corresponding to the pre-excitation at the *unusual* line frequency have a strong peak when the overtone excitation and CO_2 laser pulses are overlapped, even at 0.7 mbar sample pressure. This behavior is explained below in the terms of the double resonance model.

The initial rise of the dissociation probability upon pre-excitation of an *unusual* line frequency is faster as compared to the pre-excitation at the *usual* line frequency due to a resonance with the CO_2 laser field (channel **B** dissociation is preferential). However, when the time delay between the pre-excitation and the dissociation pulses increases, the pre-excited, resonant rovibrational state is depopulated before the beginning of the IRMPE process, and the absorption of the first CO_2 laser photon takes place under the conditions analogous to the those where the *usual* line frequency is used for the pre-excitation (channel **A**)[4]. At increased pressures the collisional V-V relaxation effect becomes important, leading to the decrease of the dissociation probabilities for the NH_3 molecules pre-excited at the both *usual* and *unusual* line frequencies.

5.4.4 Dissociation probability as a function of CO_2 laser fluence and productivity of the OP-IRMPD process.

The ammonia dissociation probability has been measured as a function of the dissociation laser fluence for pre-excitation of *usual* and *unusual* lines and for different ammonia pressures. We found that within the experimental error bars, the normalized experimental curves are the same for all the applied conditions. Figure 5.11 represents the experimental results for both usual and unusual lines and for NH_3 pressures between 0.7 and 27 mbar.

The shape of the curve representing the relative dissociation yield as a function of CO_2 laser fluence does not depend on the ammonia pressure. This indicates that the shape of the curves describing relative dissociation yield as a function of NH_3 pressure will remain unchanged for different fluences of the dissociation laser. Combining the results represented in Figure 5.5 and 5.11, one can obtain a 3-dimensional graph representing the relative dissociation yield as a function of ammonia pressure and CO_2 laser fluence. The corresponding graph is shown in Figure 5.12 for the case of pre-excitation at an *usual* line frequency (12624.3 cm^{-1}).

[4]However, if the resonance occurs not in the first step but in one of the subsequent steps of multiphoton excitation, such a resonance will still exist independently on the time delay between the pre-excitation and dissociation laser pulses resulting in an increased dissociation probability for the molecules pre-excited at the *unusual* line frequency.

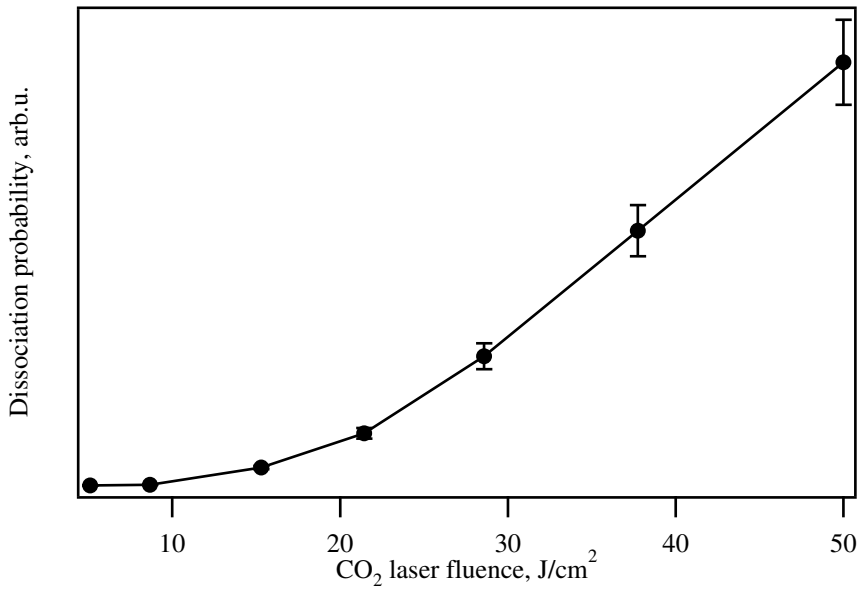

Figure 5.11: Dissociation probability as a function of CO_2 laser fluence. Sample pressure 0.7 to 27 mbar, excitation at *usual* (12624.3 cm^{-1}) and *unusual* (12696.9 cm^{-1}) lines.

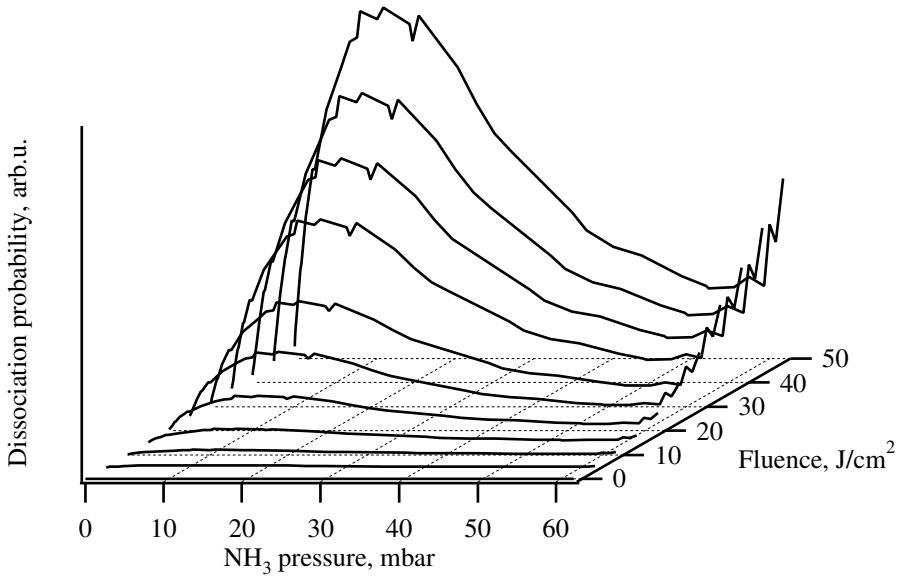

Figure 5.12: Dissociation probability as a function of CO_2 laser fluence and sample pressure. Overtone pre-excitation at 12624.3 cm^{-1}.

The most important result represented by the graphs in the Figure 5.11 and Figure 5.12 is that the dissociation yield does not show saturation behavior even at a fluence of ~ 50 J/cm^2, which is much higher than the 3-4 J/cm^2 maximum CO_2 laser fluence that can be used in industrial-scale isotope separation with collimated laser beams. This limit is imposed by the damage threshold of the IR materials suitable for use as reactor windows (BaF_2, KCl). Thus, even at this relatively high CO_2 laser fluence, the overall yield of the OP-IRMPD process is limited by the efficiency of the IRMPD step of the OP-IRMPD process. This leads us to the conclusion that the OP-IRMPD approach applied to ammonia for the nitrogen isotope separation would not be practical, at least if the third overtone of the NH stretch vibration is used for the pre-excitation step.

5.5 Conclusions

We have studied the IRMPD process of ammonia molecules pre-excited to different rovibrational levels in the spectral region of the third overtone of the symmetric NH stretch vibration (12450 - 12800 cm^{-1}). LIF detection of the NH_2 dissociation fragment has been employed to measure the dissociation yield of the process. The influence of sample pressure, dissociation laser fluence and time delay between pre-excitation and dissociation pulses on the multiphoton dissociation process has been investigated. The main results of the study are the following:

- Pre-excitation of the third overtone of the symmetric NH stretch vibration (ν_1) in ammonia drastically decreases the threshold fluence for dissociation. The fluence of 50 J/cm^2 applied in our experiments is at least 20 times lower than the typical fluences used in previous work for dissociation of ground state NH_3. This allows us to suppress completely (within the error bars of our measurements) dissociation of ground state molecules, while keeping a high dissociation yield of the pre-excited molecules, provided the sample pressure is below 50 mbar.

- The observed CO_2 laser fluence required for the dissociation of NH_3 molecules pre-excited to the $4\nu_1$ band is still too high for a practical application of the OP-IRMPD approach to laser isotope separation.

- Multiphoton dissociation of pre-excited ammonia molecules is strongly dependent on collisions. This is explained by the necessity of the rotational energy redistribution for the multiphoton excitation of the NH_3 molecule through the energy region of low density of vibrational and high density of rotational states.

- The character of multiphoton excitation of NH_3 pre-excited to different ro-vibrational levels substantially depends on the pre-excitation and dissociation frequencies. This is

explained in terms of a double resonance model assuming the occurrence of accidental resonances between the dissociation laser field and allowed ro-vibrational transitions from the pre-excited state.

- We have detected almost complete disappearance of one of the spectral lines in the action spectrum as compared to photoacoustic spectrum. This line did not appear with either increase of ammonia pressure or with the change of the dissociation laser frequency. The only explanation of this observation we see so far is that the wave function of the eigenstate corresponding to this absorption line has no (or very small) component corresponding to a $\nu_2 = 0$, required for the effective excitation by the CO_2 laser radiation.

Bibliography

[1] Commission on Atomic Weights and Isotopic Abundances report for the International Union of Pure and Applied Chemistry, *Pure and Applied Chemistry*, 1998, **70**, 217–235.

[2] R. Fiedler and G. Proksch, *Analytica Chimica Acta*, 1975, **78**, 1–62.

[3] P. Krumbiegel, T. Richter, B. Teichmann, C. Steinert, E. Rettner, C. Leicht, and D. Muller, *Isotopes Environ. Health Stud.*, 1997, **33**, 177–187.

[4] R. V. Ambartsumyan, V. S. Letokhov, G. N. Makarov, A. G. Platova, A. A. Puretski, and O. A. Tumanov, *Sov. Phys. JETP*, 1973, **37**, 392–398.

[5] V. S. Letokhov, E. A. Ryabov, and O. A. Tumanov, *Sov. Phys. JETP*, 1973, **36**, 1069–1073.

[6] J. D. Campbell, G. Hancock, J. B. Halpern, and K. H. Welge, *Opt. Commun.*, 1976, **17**, 38–42.

[7] J. D. Campbell, G. Hancock, J. B. Halpern, and K. H. Welge, *Chem. Phys. Lett.*, 1976, **44**, 404–410.

[8] A. Hartford Jr., *Chem. Phys. Lett*, 1978, **57**, 352–356.

[9] P. Avouris, M. M. T. Loy, and I. Y. Chan, *Chem. Phys. Lett.*, 1979, **63**, 624–629.

[10] I. Hanazaki, K. Kasatani, and K. Kuwata, *Chem. Phys. Lett.*, 1980, **75**, 123–127.

[11] G. Herzberg, *Infrared and Raman spectra of polyatomic molecules*, Krieger, Malabar, Florida, 1991.

[12] V. Špirko, *J. Mol. Spectr.*, 1983, **101**, 30–47.

[13] C. Léonard, N. C. Handy, S. Carter, and J. M. Bowman, *Spectochim. Acta A*, 2002, **58**, 825–838.

[14] C. Léonard, S. Carter, and N. C. Handy, *Chem. Phys. Lett.*, 2003, **370**, 360–365.

[15] T. Rajamäki, A. Miani, and L. Halonen, *J. Chem. Phys.*, 2003, **118**, 10929–10938.

[16] H. Lin, W. Theil, S. N. Yurchenko, M. Carvajal, and P. Jensen, *J. Chem. Phys.*, 2002, **117**, 11265–11276.

[17] W. Klopper, C. C. M. Samson, G. Tarczay, and A. G. Császár, *J. Comput. Chem.*, 2001, **22**, 1306–1314.

[18] H. Sasada, *J. Mol. Spect.*, 1980, **83**, 15–20.

[19] Š. Urban, V. Špirko, D. Papoušek, J. Kauppinen, S. P. Belov, L. I. Gershstein, and A. F. Krupnov, *J. Mol. Spectr.*, 1981, **88**, 274–292.

[20] Š. Urban, V. Špirko, D. Papoušek, R. S. McDowell, N. G. Nereson, S. P. Belov, L. I. Gershstein, A. V. Maslovskij, A. F. Krupnov, J. Curtis, and K. N. Rao, *J. Mol. Spectr.*, 1980, **79**, 455–495.

[21] I. Kleiner, G. Tarrago, and L. R. Brown, *J. Mol. Spectr.*, 1995, **173**, 120–145.

[22] S. L. Coy and K. K. Lehmann, *J. Chem. Phys.*, 1986, **84**, 5239–5249.

[23] K. K. Lehmann and S. L. Coy, *J. Chem. Soc., Faraday Trans. 2*, 1988, **84**, 1389–1406.

[24] S. L. Coy and K. K. Lehmann, *Spectrochimica Acta*, 1989, **45A**, 47–56.

[25] Physics Instrumentation Center, Troitsk, Russia, http://www.lasersys.ru.

Chapter 6

Conclusions

With a view towards developing a method for highly selective molecular laser isotope separation (MLIS) we have studied the possibilities of using the overtone pre-excitation - infrared multiphoton dissociation approach to laser separation of isotopes of carbon (Chapter 3), silicon (Chapter 4) and nitrogen (Chapter 5) using the CF_3H, $SiHCl_3$ and NH_3 molecules respectively. The separate detailed summaries of studies of each molecule are given in the conclusions of the corresponding chapters: sections 3.7 for CF_3H, 4.4 for $SiHCl_3$ and 5.5 for NH_3. Below we briefly summarize the key results of our studies and outline the perspectives of practical applications and subsequent development of the OP-IRMPD based laser isotope separation technique.

6.1 Separation of carbon isotopes

The most important result obtained in this work is the qualitative understanding of the dynamics of the OP-IRMPD process under collisional conditions and based on it the substantial improvement of the OP-IRMPD approach to carbon-13 isotope separation. The new approach with the pre-excitation of the first or the second overtone of the CH stretch vibration in $^{13}CF_3H$ molecule allows us to achieve levels of isotopic selectivity that are almost two orders of magnitude higher than in a typical process, based on IRMPD of ground state molecules. A particular arrangement (overlap of short pre-excitation and dissociation pulses) allows performing the OP-IRMPD process at high ($\approx$ 100 mbar) working pressures and brings the dissociation yield to practically relevant values. Moreover, the CO_2 laser fluence required for efficient dissociation of pre-excited molecules is considerably lower than that required for IRMPD of ground state molecules and below the typical optics damage threshold. This makes it possible to use collimated instead of focused laser beams and to provide near homogenous irradiation of a large working volume. The main drawback of using the overtone pre-excitation is the necessity for the second source of laser radiation operating in the spectral region of 1.68 μm in the case of

pre-excitation of the first and 1.14 μm in the case of second overtone. The lack of commercially available high repetition rate laser systems for these wavelengths is one of the main factors limiting the possibility of a precise estimation the production cost and of an immediate implementation of the new approach. This is not a fundamental limitation, however. The continuous improvement of power, stability and efficiency as well as the expansion of the operating spectral range of laser sources available on the market may make the OP-IRMPD approach economically feasible in the near future. Moreover, the OP-IRMPD approach has a principal advantage over the IRMPD and conventional non-laser methods of carbon-13 isotope separation. Namely, the minimum reachable value of the energy consumption by a single separation act (which is determined in the case of laser methods by the total energy of photons required for production of one atom of the desired isotope) is the lowest in the case of OP-IRMPD approach. This opens brilliant perspectives for the newly developed approach, since energy is becoming more and more expensive, making the energy-save technologies of top priority. The subsequent step in the development of the OP-IRMPD based method should include a laboratory-scale production of highly enriched carbon-13 to test our ideas on practical implementation of the OP-IRMPD based carbon-13 isotope separation process as well as the development of a suitable laser sources.

6.2 Separation of silicon and nitrogen isotopes

The experimental study of OP-IRMPD of $SiHCl_3$ molecule has shown a limited applicability of this approach on this molecule for highly selective silicon isotope separation due to a low discrimination in the dissociation of pre-excited *vs.* ground state molecules under the conditions of moderate dissociation yield. Consequently, this low discrimination practically limits the maximum isotopic selectivity achievable by OP-IRMPD method on $SiCl_3H$ to 50-100.

Overtone pre-excitation of ammonia molecule makes its multiphoton dissociation considerably easier, and allows a high level of discrimination in dissociation of pre-excited *vs.* ground state molecules. However, high fluences of the dissociation laser required for effective multiphoton excitation of NH_3 makes the OP-IRMPD approach on this molecule impractical for isotope separation of nitrogen.

We can conclude that the result of the study of possibilities of practical application the OP-IRMPD approach to highly selective laser separation of silicon and nitrogen isotopes using $SiHCl_3$ and NH_3 molecules respectively is negative. This does not mean, however, that the OP-IRMPD technique is not applicable for separation of isotopes of these elements. We believe, that a proper selection of the parent molecule and characteristics of laser radiation based on the understanding of physical basis of the process gained in this and other works fulfilled in our

laboratory [1–6] will allow us to develop efficient OP-IRMPD schemes for separation of isotopes of elements different from carbon.

Bibliography

[1] O. V. Boyarkin, M. Kowalzcyk, and T. R. Rizzo, *J. Chem. Phys.*, 2003, **118**, 93–103.

[2] J. Makowe, O. V. Boyarkin, and T. R. Rizzo, *J. Phys. Chem. A*, 2002, **106**, 5221–5229.

[3] J. Makowe, O. V. Boyarkin, and T. R. Rizzo, *J. Phys. Chem. A*, 2000, **104**, 11505–11511.

[4] J. Makowe *Isotopically Selective Infrared Multiphoton Dissociation of Vibrationally Pre-excited Silane* PhD thesis, Ecole Polytechnique Fédérale de Lausanne, Switzerland, 2000.

[5] M. Kowalzcyk *Highly Selective Molecular Laser Isotope Separation of Carbon-13* PhD thesis, Ecole Polytechnique Fédérale de Lausanne, Switzerland, 2000.

[6] R. Bossart PhD thesis, Ecole Polytechnique Fédérale de Lausanne, Switzerland, to be published.

Appendix A

Solution of dynamic equations for formation of C_2F_4

In assumption of equal recombination rates R for CF_2 fragments with different isotopic composition one can write for concentrations of $^{12}CF_2$ and $^{13}CF_2$:

$$\begin{cases} \frac{d[^{12}CF_2]}{dt} = -R[^{12}CF_2]\left([^{12}CF_2] + [^{13}CF_2]\right) \\ \frac{d[^{13}CF_2]}{dt} = -R[^{13}CF_2]\left([^{12}CF_2] + [^{13}CF_2]\right) \end{cases} \tag{A.1}$$

and for concentrations of produced C_2F_4 with different possible isotopic compositions:

$$\begin{cases} \frac{d[^{12,12}C_2F_4]}{dt} = \frac{R}{2}[^{12}CF_2]^2 \\ \frac{d[^{12,13}C_2F_4]}{dt} = 2\frac{R}{2}[^{12}CF_2][^{13}CF_2] \\ \frac{d[^{13,13}C_2F_4]}{dt} = \frac{R}{2}[^{13}CF_2]^2 \end{cases} \tag{A.2}$$

The solution of Equations (A.1) is:

$$\begin{aligned} [^{12}CF_2] &= \frac{[^{12}CF_2]_0}{1 + ([^{12}CF_2]_0 + [^{13}CF_2]_0)Rt}, \\ [^{13}CF_2] &= \frac{[^{13}CF_2]_0}{1 + ([^{12}CF_2]_0 + [^{13}CF_2]_0)Rt}, \end{aligned} \tag{A.3}$$

where $[^{12}CF_2]_0$ and $[^{13}CF_2]_0$ are the initial concentrations of $^{12}CF_2$ and $^{13}CF_2$ respectively.

Using the following notation:

$$\frac{1}{1 + ([^{12}CF_2]_0 + [^{13}CF_2]_0)Rt} \equiv f(t), \tag{A.4}$$

we can re-write (A.3) as:

$$\begin{aligned} [^{12}CF_2] &= [^{12}CF_2]_0 f(t), \\ [^{13}CF_2] &= [^{13}CF_2]_0 f(t). \end{aligned} \tag{A.5}$$

Applying the result (A.5) to Equations (A.2) and integrating over reaction time T we get for final concentrations of $^{12,12}C_2F_4$, $^{12,13}C_2F_4$ and $^{13,13}C_2F_4$:

$$
\begin{aligned}
[^{12,12}\mathrm{C_2F_4}] &= \frac{R}{2}[^{12}\mathrm{CF_2}]_0^2 \int_{t=0}^{T} f^2(t)dt \propto [^{12}\mathrm{CF_2}]_0^2, \\
[^{12,13}\mathrm{C_2F_4}] &= 2\frac{R}{2}[^{12}\mathrm{CF_2}]_0[^{13}\mathrm{CF_2}]_0 \int_{t=0}^{T} f^2(t)dt \propto 2[^{12}\mathrm{CF_2}]_0[^{13}\mathrm{CF_2}]_0, \\
[^{13,13}\mathrm{C_2F_4}] &= \frac{R}{2}[^{13}\mathrm{CF_2}]_0^2 \int_{t=0}^{T} f^2(t)dt \propto [^{13}\mathrm{CF_2}]_0^2.
\end{aligned}
\tag{A.6}
$$

Appendix B

Collisional quenching of LIF

For the proper interpretation of results of LIF based experiments the effect of collisional quenching has to be accurately taken into account. This is especially important in the case where the LIF signals for different pressures have to be compared one to another, for example, when the dissociation yield is measured as a function of sample pressure by means of LIF detection of a dissociation product. Below we discuss the influence of quenching in the particular cases of our experiments and the possibilities of data interpretation using the available information on the quenching constants. The results of the experimental estimation of NH_2^* on NH_3 collisional LIF quenching constant for typical NH_3 pressures of several tens of mbar used in our experiments are also discussed and compared with the available in literature values measured under substantially different NH_3 pressures.

B.1 General formula

The rate of the de-population of the upper level of the fluorescent transition is given by the Stern-Volmer equation:

$$R = \frac{1}{\tau_0} + k_q n, \tag{B.1}$$

where τ_0 is the zero pressure lifetime of the excited state (radiative lifetime), k_q is the collisional quenching constant, and n the concentration of buffer gas molecules.

As in the most of our experiments the temperature of the sample is constant (room temperature), one can re-write (B.1) using pressure instead of concentration for convenience of subsequent calculations:

$$R = \frac{1}{\tau_0} + k'_q p, \tag{B.2}$$

where p is the quencher pressure, and k'_q is the quenching constant in units of $[\mathrm{mbar}^{-1}\mathrm{s}^{-1}]$. Under the *normal conditions* k'_q is connected with k_q by one of the following expressions (depending

on the units of k_q):

$$\begin{aligned} k'_q[\mathrm{mbar}^{-1}\mathrm{s}^{-1}] &= \frac{k_q[\mathrm{cm}^3\mathrm{molecule}^{-1}\mathrm{s}^{-1}]}{3.771 \times 10^{-17}}, \\ k'_q[\mathrm{mbar}^{-1}\mathrm{s}^{-1}] &= \frac{k_q[\mathrm{cm}^3\mathrm{mol}^{-1}\mathrm{s}^{-1}]}{2.271 \times 10^{7}}. \end{aligned} \tag{B.3}$$

In order to be able to eliminate the influence of LIF quenching on the experimental result we have to determine the quenching correction factor, ε_q, that is the ratio of the measured LIF signal, S_{meas} to the signal that would be measured in the absence of quenching, S:

$$\varepsilon_q = \frac{S_{meas}}{S}. \tag{B.4}$$

In our experiments we do not monitor the LIF signal continuously, but rather integrate it within a certain time interval Δt after the excitation of the upper fluorescent level by the probe laser pulse. Taking this into account we can get the following expression for S_{meas} and S:

$$\begin{aligned} S_{meas} &= \eta \frac{1}{R} \left(1 - e^{-R\Delta t}\right), \\ S &= \eta \tau_0 \left(1 - e^{-\frac{\Delta t}{\tau_0}}\right), \end{aligned} \tag{B.5}$$

where η is a constant describing the detection system.

Combining Equations B.4 and B.5 we get:

$$\varepsilon_q = \frac{1}{R\tau_0} \frac{1 - e^{-R\Delta t}}{1 - e^{-\frac{\Delta t}{\tau_0}}}. \tag{B.6}$$

Now we can apply the quenching correction factor ε_q to the measured LIF signal S_{meas} and get the value S which is independent on the effect of the collisional quenching:

$$S = \frac{S_{meas}}{\varepsilon_q}. \tag{B.7}$$

In the following sections the correction factor ε_q is estimated for the cases of LIF detection of the CF_2 fragments in the bath of the CF_3H molecules and of the NH_2 fragments in the bath of NH_3.

B.2 Quenching of CF_2^* on CF_3H

To our knowledge, the constant of CF_2 fluorescence quenching on CF_3H molecules has not been measured. However, in order to estimate the effect of quenching on our results one can extrapolate the available data for other quenchers. The data on quenching of CF_2 fluorescence by CF_2Br_2, C_2F_4, CF_2Cl_2, CF_2HCl, CF_4 [1] and by C_3F_6 [2] are summarized in the Table B.1. The values of radiative lifetime τ_0 obtained in [1] and [2] were 55 ns and (62±4) ns respectively.

Quencher	k_q, $cm^3mol^{-1}s^{-1}$	k'_q, $mbar^{-1}s^{-1}$
CF_2Br_2	$(2.4 \pm 0.6) \times 10^{14}$	1.1×10^7
C_3F_6	$(7.1 \pm 0.7) \times 10^{13}$	3.1×10^6
C_2F_4	$(4.7 \pm 0.3) \times 10^{13}$	2.1×10^6
CF_2Cl_2	$(2.0 \pm 0.2) \times 10^{13}$	8.8×10^5
CF_2HCl	$(1.5 \pm 0.2) \times 10^{13}$	6.6×10^5
CF_4	$(2.0 \pm 0.9) \times 10^{12}$	8.8×10^4

Table B.1: Values of quenching rate constants for fluorescence of CF_2 fragment excited to $\tilde{A}^1B_1$ state in presence of different quenchers [1, 2]. The corresponding values of k'_q in units of [$mbar^{-1}s^{-1}$] are also given in the third column.

The quenching constant for the CF_3H quencher molecules is, most likely, close to that of CF_2HCl, as the structures of these two molecules are rather similar. Figure B.1 represents the quenching correction factor ε_q as a function of buffer gas pressure calculated with $k'_q = 6.6 \times 10^5$ $mbar^{-1}s^{-1}$ (corresponds to CF_2HCl) and with twice higher and twice lower values of k'_q. τ_0 is 62 ns and Δt is 270 ns.

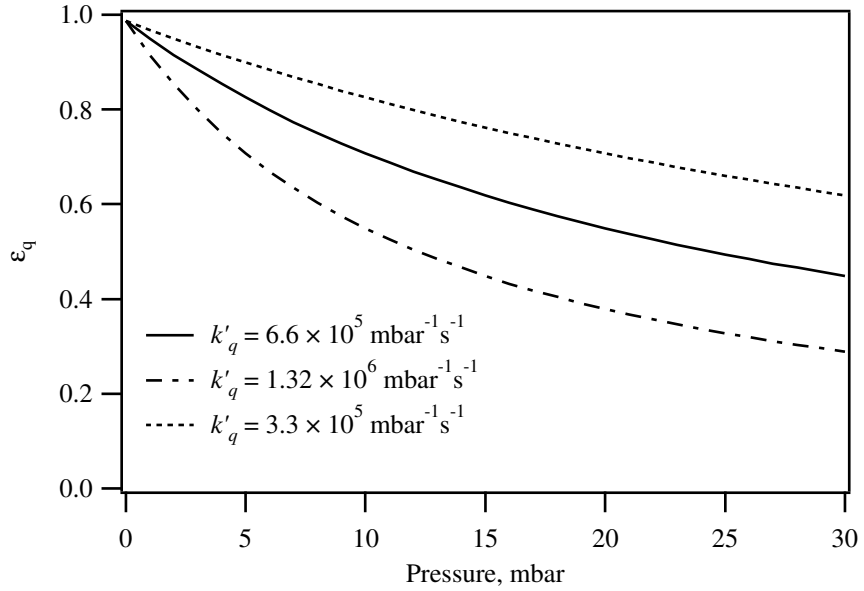

Figure B.1: CF_2 quenching correction coefficient ε_q as a function of pressure for k'_q value corresponding to CF_2HCl quencher molecule and for values $2k'_q$ and $k'_q/2$. $\Delta t = 270$ ns.

As it can be seen from the Figure B.1, quenching becomes considerable already at pressures above 5-10 mbar. We must, therefore, consider the results of LIF experiments with varying sample pressure only as an estimating data which has to be verified using a detection method which is not influenced by the collisional effects (for example, absolute measurements of product

concentration using the masspectrometric detection technique)[1]

B.3 Quenching of $SiCl_2^*$ on $SiHCl_3$

The constant of $SiCl_2$ fluorescence quenching has been measured for SiH_2Cl_2 quencher in the work [4]. The radiative lifetime τ_0 of the $^1B_1$ electronic state of $SiCl_2$ has been measured in the works [4] and [5]. We will use these values for qualitative estimating the order of magnitude of the influence of collisional fluorescence quenching on the results of our study of OP-IRMPD of $SiHCl_3$ by LIF detection of $SiCl_2$. Figure B.2 shows the quenching correction factor as a function of sample pressure calculated using the values of quenching constant and $SiCl_2$ radiative lifetime from the references [4] and [5].

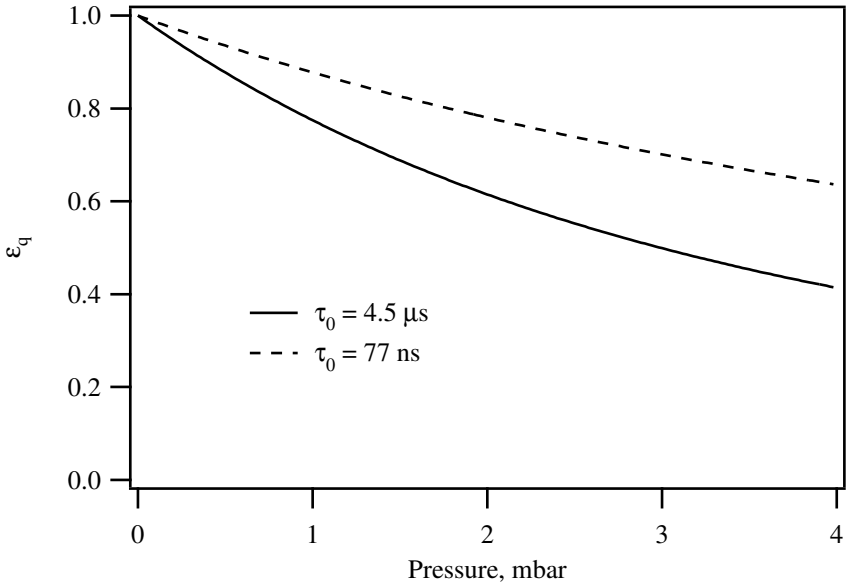

Figure B.2: $SiCl_2$ quenching correction coefficient ε_q as a function of pressure for $k'_q = 2.6 \times 10^6 \text{mbar}^{-1}\text{s}^{-1}$ (corresponds to SiH_2Cl_2 quencher molecule [4]) and for τ_0 values from references [4] (4.5 μs) and [5] (77 ns). $\Delta t = 270$ ns.

As it can be seen from the Figure B.2, the influence of quenching on the experimental results is considerable even at relatively low pressures. We cannot use the ϵ_q values represented by Figure B.2 for correcting our experimental data because 1) these values correspond to SiH_2Cl_2 rather than $SiHCl_3$ quencher, and 2) the variation of measured values of radiative lifetime in different works is very high (and, hence, its low trustworthiness). The results of calculations

[1] Recently Richard Bossart has measured the quenching constant for the CF_3H quencher using the CF_3H OP-IRMPD for production of the CF_2 radicals [3]. The obtained value for k'_q is $(1.1 \pm 0.1 \times 10^5)$ $\text{mbar}^{-1}\text{s}^{-1}$ and $\tau_0 = 63$ ns. Using these values we estimated the CF_3H pressure above that the LIF quenching effect is considerable to be in order of 20-25 mbar

represented in Figure B.2 should be considered only as an indication that the measured LIF signals in our experiments provide only a lower limit for $SiHCl_3$ dissociation yield.

B.4 Quenching of NH_2^* on NH_3

The NH_2 collisional LIF quenching in the case of NH_3 as a quencher has been studied in several works [6–11]. The results obtained in different experiments under different conditions considerably differ from each other. Although the process of collisional energy redistribution within the NH_2 radical and between the NH_2 radical and a quencher is not yet completely understood, one can speak about the strong dependence of the quenching constant and the radiative lifetime on the initial and final states of the LIF. Thus the quenching constant and the radiative lifetime of the excited level have to be measured separately for each particular experimental configuration.

Halpern *et al.* [7] measured the radiative lifetimes and quenching constants of the NH_2 radical excited to the different rotational levels within the $\Sigma(0,9,0)$ ro-vibronic state of $NH_2(^2A_1)$. The excitation to the same state has been applied in our ammonia OP-IRMPD experiments. The difference between the Halpern's and our experimental conditions are the following:

1. Method of producing the NH_2: UV flash photolysis of NH_3 in Halpern *et al.* and OP-IRMPD of NH_3 in our experiments;

2. Bottom level of the LIF transition: Halpern *et al.* registered the dispersed fluorescent signal in the spectral range 602 ± 5 nm, whereas we used the set of BG-40 and RG-610 filters transparent in the range of 610-630 nm;

3. Typical NH_3 pressures: 1-10 mTorr in [7] and up to 70 mbar in our experiments.

The following values of radiative lifetime τ_0 and quenching constant has been obtained in [7] for the case of excitation of 3_{03}, 4_{04}, 5_{05} $\Sigma(0,9,0)$ levels of $NH_2(^2A_1)$ (NH_2 LIF excitation at 597.72 nm):

$\tau_0 = (10.0 \pm 1.7)$ μs,

$k_q = (1.0 \pm 0.1) \times 10^{-9}$ cm^{3}molecule^{-1}s^{-1}.

Applying (B.3) to k_q we get the following value for k'_q:

$k'_q = 2.65 \times 10^7$ mbar^{-1}s^{-1}.

In order to check the validity of Halpern *et al.* data for our experimental conditions we have measured the decay rates of the LIF signal after the excitation of the NH_2 $^2A_1$ electronic state by a short (3-4 ns) laser pulse at different pressures of ammonia. The corresponding decay curves are represented in the Figure B.3.

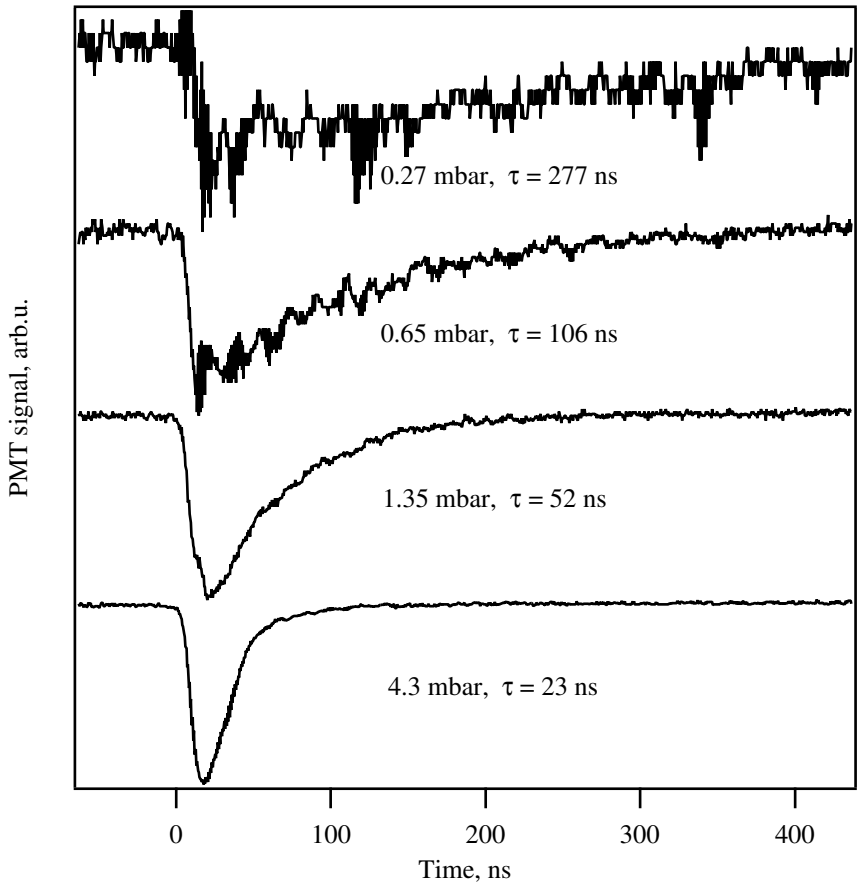

Figure B.3: Decay of the LIF signal at 610-630 nm after the excitation of NH_2 at 597.72 nm at different ammonia pressures. Signals are scaled in order to give better representation of the decay dynamics. Corresponding decay times τ are also shown.

Figure B.4 represents the fluorescence decay rates corresponding to the curves of the Figure B.3 as a function of ammonia pressure (Stern-Volmer plot). Linear fit of this data gives the following value of the quenching constant:

$k'_q = (9.7 \pm 0.9) \times 10^6$ mbar^{-1}s^{-1},

that is more than twice smaller than the value obtained by Halpern *et al.* [7]. We do not determine the radiative lifetime of the upper fluorescent state from the curve represented in the Figure B.4 as the corresponding error bar is too big. However, using the fact that the τ_0 value in all the available data is not shorter than 10 μs, that is still much longer than the typical total LIF decay time in our experiments (τ <150 ns) one can neglect the first term in the Stern-Volmer equation (B.2) and use for analysis of NH_2 LIF results the following simplified expression:

$$R = k'_q p. \tag{B.8}$$

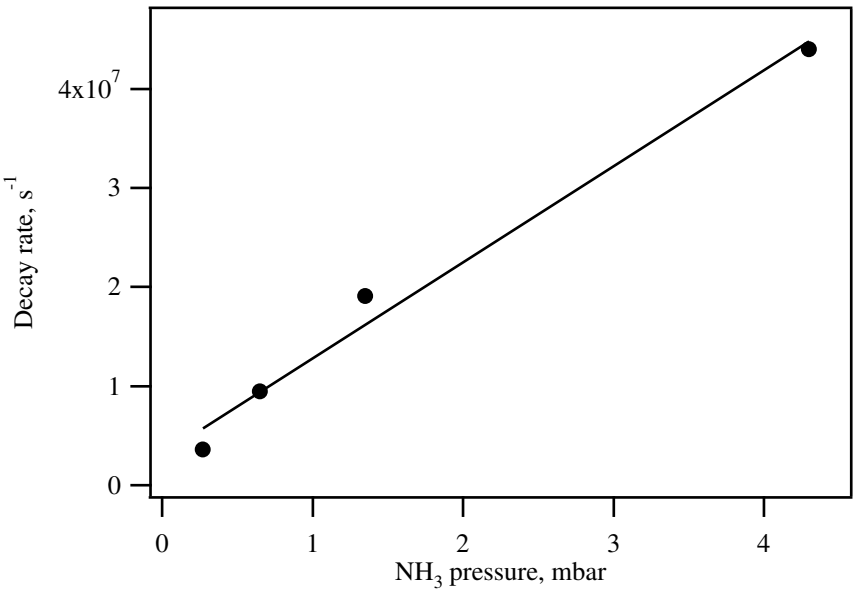

Figure B.4: Fluorescence decay rate as a finction of NH_3 pressure (Stern-Volmer plot).

We can also assume that $e^{-\frac{\Delta t}{\tau_0}}$ in the Equation (B.6) is approximately zero. In this case the expression for the quenching correction factor ε_q is the following:

$$\varepsilon_q \approx \frac{1}{k'_q p \tau_0}\left(1 - e^{-k'_q p \Delta t}\right) \propto \frac{1}{p}\left(1 - e^{-k'_q p \Delta t}\right). \tag{B.9}$$

As in the case of the ammonia OP-IRMPD experiments we are interesting in the relative dissociation yield of the process (yield normalized on the concentration of the irradiated molecules), Y_{rel}, we have to correct the measured LIF signal, S_{meas} also on the sample pressure:

$$Y_{rel} \propto \frac{S}{p} \propto \frac{S_{meas}}{\varepsilon_q p}. \tag{B.10}$$

The correction factor, $\varepsilon_q p$ as a function of the ammonia pressure is shown in the Figure B.5. As it can be seen from the figure, the correction factor is considerable only at ammonia pressures below 1 mbar. So, only at low pressures the correction of the LIF signal is necessary whereas at pressures above 1 mbar the LIF signal is proportional to the relative NH_2 dissociation yield and no additional corrections are required.

Finally we have to discuss the possible reasons for the considerable difference in the values of the quenching constant k'_q obtained by Halpern *et al.* [7] and in our experiments. The differences in the experimental conditions have been described earlier in the text. The first difference (method of NH_3 dissociation) should not influence the result because:

1. in both cases most of produced NH_2 created in the ground electronic state $NH_2(^2B_1)$ [7, 12], and

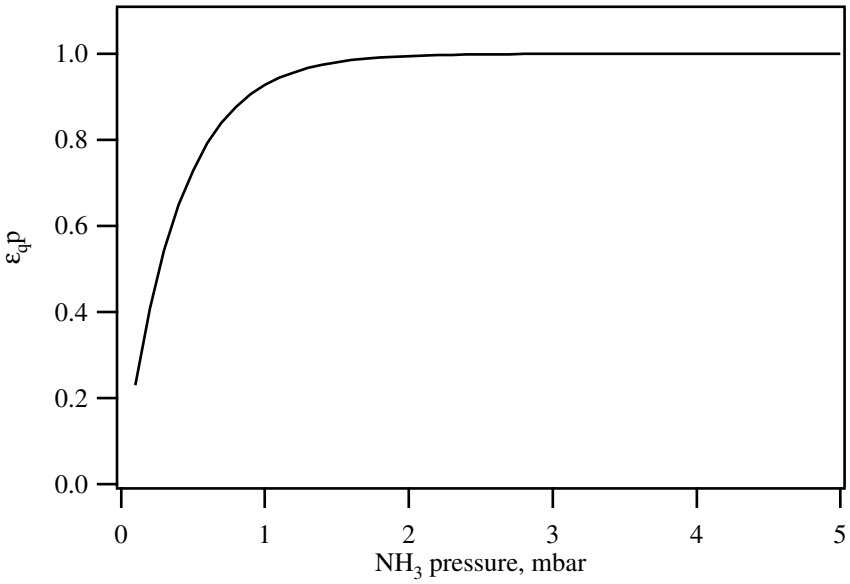

Figure B.5: LIF correction factor for calculation the relative NH_2 dissociation yield. $k'_q = (9.7 \pm 0.9) \times 10^6$ $\text{mbar}^{-1}\text{s}^{-1}$, $\Delta t = 270$ ns.

2. in both experiments LIF excitation laser is tuned in resonance with the same ro-vibronic transition which results in the excitation of the same states.

The difference in the spectral range of the dispersed fluorescence signal registered in two experiments can considerably affect the result. A strong dependence of the NH_2 LIF signal dynamics on the both initial and final state of the registered transition has been observed in the works [8,10]. We consider the difference in the bottom levels of the registered LIF transition as the main factor responsible for the different values of k'_q obtained in [7] and in our work. However, we cannot exclude the possibility of an influence of the ammonia pressure on the deactivation constant[2]. This question has to be discussed in more details.

The NH_3 pressures used in the work [7] were in the range of 1 to 10 mTorr, which is much lower than typical pressures applied in NH_3 IRMPD experiments (up to several hundreds Torr). While the radiative lifetime τ_0 does not depend on collisional processes, the conserving of the collisional quenching constant k'_q for such different conditions is questionable. Avouris *et al.* [13] based on the observation that the collisional behavior of the LIF signal does not depend on the length of the probe laser pulse have concluded that the corrections based on the results of Halpern *et al.* [7] are inappropriate for ammonia IRMPD experiments. He suggested that the saturation of electronic quenching observed earlier in over molecules [14, 15] takes place in the NH_2 LIF quenching at higher (up to 20 Torr in [13]) ammonia pressures. Our

[2]Although in this consideration the k'_q value vary in function of the ammonia pressure, we are using here and later on the generally accepted term *"quenching constant"*.

results described above shows that the assumption about the complete quenching saturation at pressures of several mbar is not correct (see, for example, Fig B.3). Our results do not exclude, however, the possibility of a change of the quenching constant with NH_3 pressure. One more fact which can indirectly support this assumption is the decrease of the NH_2+NO reaction rate with ammonia pressure observed in several works [16–19]. The mechanism of this decrease is not yet completely clear and we can assume that the same or similar mechanism can be responsible for the decrease of the NH_2 LIF quenching rate with NH_3 pressure. This assumption, however, was never discussed in publications concerning the NH_2 collisional LIF quenching and hence this question requires a special comprehensive investigation. OP-IRMPD of ammonia could be used for the production of NH_2 radicals required in the corresponding experiments.

From the point of view of the interpretation of our experimental results, the variation of the quenching constant with pressure does not affect considerably the correction factor obtained in the assumption of constant k'_q (for the estimation of possible variation of the quenching constant within the pressure range used in our experiments we used the Halpern's value of k'_q [7] for the NH_3 pressure of several mTorr and our values for pressure of several mbar and extrapolated the k'_q(p) function on the pressure range of our experiments).

Bibliography

[1] H. Hack and W. Langel, *J. Photochem.*, 1983, **21**, 105–110.

[2] L. Rubio, M. Santos, and J. A. Torresano, *J. Photochem. Photobiol.*, 2001, **146**, 1–8.

[3] R. Bossart PhD thesis, Ecole Polytechnique Fédérale de Lausanne, Switzerland, to be published.

[4] R. C. Sausa and A. M. Ronn, *Chem. Phys.*, 1985, **96**, 183–189.

[5] M. Suzuki, N. Washida, and G. Inoue, *Chem. Phys. Lett.*, 1986, **131**, 24–30.

[6] M. Lenzi, J. R. McNesby, A. Mele, and C. N. Xuan, *J. Chem. Phys.*, 1972, **57**, 319–323.

[7] J. B. Halpern, G. Hancock, M. Lenzi, and K. H. Welge, *J. Chem. Phys.*, 1975, **63**, 4808–4816.

[8] V. M. Donnelly, A. P. Baronavski, and J. R. McDonald, *Chem. Phys.*, 1979, **43**, 283–293.

[9] R. Wilhelm and J. Lindner, *J. Chem. Phys.*, 2001, **114**, 7379–7387.

[10] C. Petrongolo, H. Fan, I. Ionescu, D. Kuffel, and S. A. Reid, *J. Chem. Phys.*, 2003, **119**, 2614–2617.

[11] J. Lindner and R. Wilhelm, *J. Chem. Phys.*, 2002, **117**, 4878–4888.

[12] J. D. Campbell, G. Hancock, J. B. Halpern, and K. H. Welge, *Opt. Commun.*, 1976, **17**, 38–42.

[13] P. Avouris, M. M. T. Loy, and I. Y. Chan, *Chem. Phys. Lett.*, 1979, **63**, 624–629.

[14] S. J. Strickler and D. B. Howell, *J. Chem. Phys.*, 1968, **49**, 1947–1951.

[15] P. Avouris, W. M. Gelbart, and M. A. El-Sayed, *Chem. Rev.*, 1977, **77**, 793–833.

[16] K. Yamasaki, A. Watanabe, A. Tanaka, M. Sato, and I. Tokue, *J. Phys. Chem. A*, 2002, **106**, 6563–6569.

[17] M. Wolf, D. L. Yang, and J. L. Durant, *J. Phys. Chem A*, 1997, **101**, 6243–6251.

[18] M. Wolf, D. L. Yang, and J. L. Durant, *J. Photochem. Photobiol. A*, 1994, **80**, 85–93.

[19] V. P. Bulatov, A. A. Ioffe, V. A. Lozovsky, and O. M. Sarkisov, *Chem. Phys. Lett.*, 1989, **161**, 141–146.

Appendix C

Control of the CO_2 laser pulse duration

A typical pulse of commercially available TEA CO_2 lasers consists of the initial intensive peak (100-300 ns) and a long (2-6 μs) tail containing up to 80% of the total pulse energy. The tail of the pulse does not contribute to the isotope separation process, but produces undesired thermal stresses in the optical elements of the reaction cell. Simple methods of CO_2 laser pulse shaping (adjusting the laser mixture composition, discharge current and resonator coupling) may result in some redistribution of the pulse energy from the tail to the initial peak of the pulse, but do not solve the problem completely. Therefore, we aimed to find a way to block the tail of a pulse of a commercial TEA CO_2 laser (Lumonics-840). The requirements for the resulting pulses are the following:

1. Complete blocking of the pulse tail;
2. High level of pulse-to-pulse reproducibility;
3. Possibility of adjusting the duration of the pulse.

Two different approaches to CO_2 laser "tail cutting" have been studied: "laser induced mirror" and "plasma shutter".

C.1 Laser induced mirror

The laser induced mirror approach [1] is based on the creation of free charge carriers in semiconductor by absorbing the light of a near IR switching laser resulting in the increasing the reflectivity of the irradiated material. A schematic diagram of an optical layout we employed for evaluating the capabilities of laser induced mirror technique to control the CO_2 laser pulse

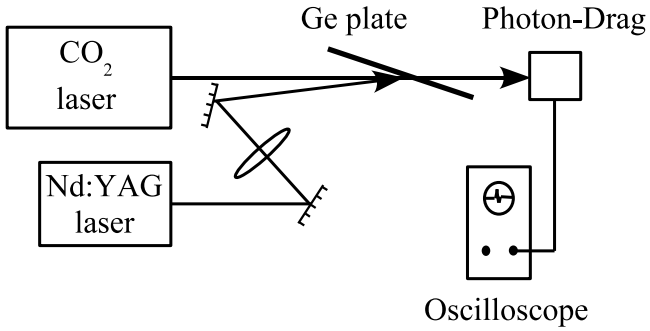

Figure C.1: Schematics of a set-up used the laser induced mirror effect for CO_2 laser pulse duration control.

duration is shown in Figure C.1. The CO_2 laser beam passes through a Brewster angle Ge plate. This Ge plate can be irradiated by 1.064 μm radiation of a pulsed Nd:YAG laser (Lumonics YM-600) synchronized with the CO_2 laser. In the absence of 1.064 μm irradiation, the CO_2 laser beam passes through the plate without any considerable change in intensity or pulse shape (Figure C.2, left side). If the switching laser pulse irradiates the Ge plate during the CO_2 laser

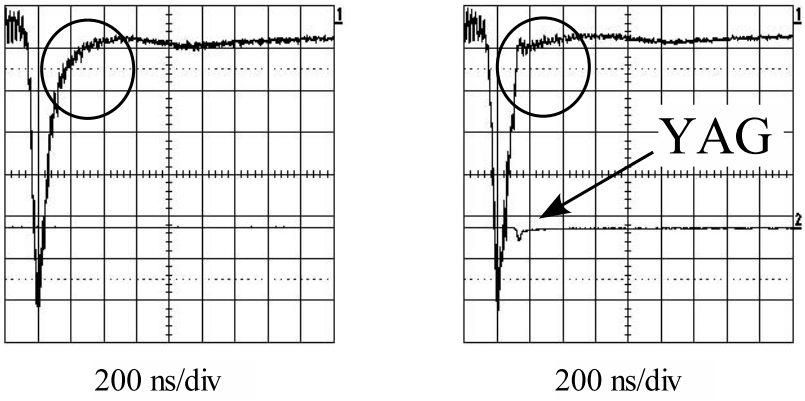

Figure C.2: CO_2 laser pulse "tail cut" with laser induced mirror.

pulse, a fraction of the CO_2 laser radiation is reflected due to the induced mirror (Figure C.2, right side). The induced reflectivity can reach 80% during the switching laser pulse. However, the effect of laser induced mirror rapidly decreases after the end of the Nd:YAG laser pulse and completely disappears in about 100 ns. We also tested the possibility of using silicon instead of germanium as a material for the switching element. In this case the effect of the induced mirror is longer, providing almost complete blocking of the CO_2 laser tail. However, silicon absorbs a considerable fraction of the CO_2 laser pulse energy (about 50% in the case of 3 mm thick Si plate used in our experiments). Such a high absorption, first, limits the CO_2 laser fluence which

can be used in the experiments, and, second, causes warming of the switching element which results in uncontrolled changing its optical properties, and, potentially, mechanical damage. So, the laser induced mirror technique cannot be used for the effective cutting of the about 6 μs long CO_2 laser pulse tail (at least in our configuration: several ns long switching laser pulse, germanium or silicon as a material for the switching element). Therefore we decided to use the plasma shutter technique for this purpose.

C.2 Plasma shutter

The idea of plasma shutter [2–5] is based on avalanche gas ionization under the action of CO_2 laser radiation resulting in the formation of self-maintaining plasma effectively absorbing laser photons. We can distinguish between *active* and *passive* plasma shutters. In the *active* plasma shutter, plasma formation is initiated by an electric discharge whereas in the *passive* one plasma is initially formed by an optical breakdown in the gas caused by the focused radiation of the laser pulse which has to be cut. A schematics demonstrating the principle of *active* and *passive* plasma shutters are shown in the Figure C.3. The CO_2 laser beam is focused into a gas filled

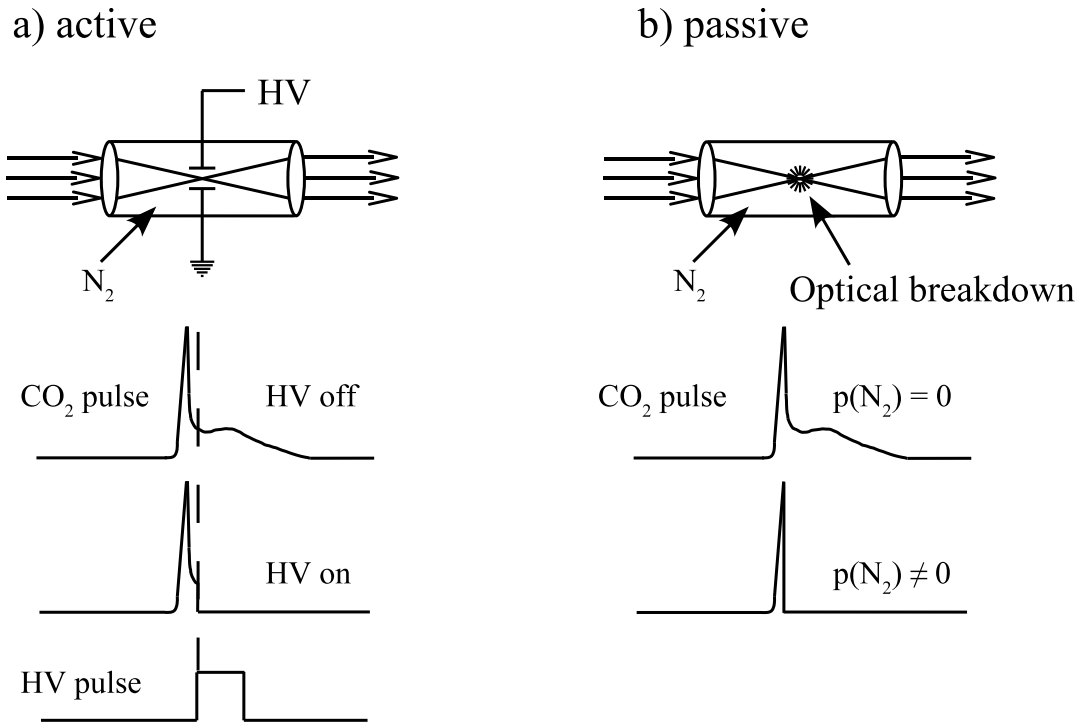

Figure C.3: Principle of *active* and *passive* plasma shutters.

cell (usually nitrogen, argon or helium is used depending on the required for a particular case combination of pressure and optical breakdown intensity). In the case of an *active* plasma

shutter (C.3 *a*) the CO_2 laser intensity is just below the breakdown value. Thus, the CO_2 laser pulse passes through the cell without modification. However, if a HV pulse is applied to the electrodes located in the two opposite sides of the focal point, an electrical discharge occurs between them. Ions, created in the discharge, efficiently absorb the CO_2 laser photons that results in an increase of the ions temperature, and, consequently, a fast avalanche ionization of the gas in the focal volume. The part of the laser pulse located in time after the initial ionization process is absorbed and partially scattered by plasma. Thus, by changing the HV pulse position one can control the CO_2 laser pulse duration.

In the *passive* plasma shutter configuration (Figure C.3 *b*), the length of the pulse cannot be controlled within such a wide range as in *active* plasma shutter. Optical breakdown occurs when the intensity of the CO_2 laser radiation reaches a certain threshold value, determined by the used gas and the pressure. Thus, breakdown can occur only during the initial rise of the laser intensity (positive slop of the first spike of CO_2 laser pulse). In the limits of the rise-up time the breakdown moment can be controlled by changing the gas pressure (higher pressure results in a lower breakdown threshold and longer plasma decay). As long as the intensity of the CO_2 laser radiation is sufficient to compensate the plasma decay (this intensity is much lower than the breakdown threshold), a self-maintaining plasma recreation process will take place resulting in blocking the laser radiation. When the laser intensity drops to a very small value (in the end of the pulse tail), plasma creation slows down and then stops. Once the plasma creation is stopped, the remaining lifetime of plasma will depend on the gas used and on the gas pressure. At a higher pressure the plasma ions fly out from the focal point slower and, hence, the longer plasma lifetime. We prefer therefore to use possibly high gas pressures to have a longer plasma lifetime. In order to increase the working pressure keeping the breakdown moment constant one can increase the size of the laser beam waist, for example by using longer focal length lenses.

A photo of the plasma shutter cell we have built is shown in the Figure C.4. This plasma shutter can be used both in the active and in the passive configuration. It represents a hermetic brass cell with a length adjustable in the range of 10-20 cm. 2.8 cm diameter ZnSe lenses with F=6.35 or 8.9 cm are used as cell windows. To trigger the HV pulse in the active configuration the CO_2 laser beam was split by a BaF_2 plate and a fraction (10-15%) of the beam was directed in the second cell (trigger cell) where it was focused into an electrode surface. A spark created by the initial part of the pulse caused a discharge between the electrodes shortening an electrical chain initiating the electrical discharge in the shutter cell. The delay between the initial spark and the discharge in the plasma shutter was controlled by the length of a cable connecting the HV power supply and the electrode of the shutter. In the passive configuration the second cell was not used.

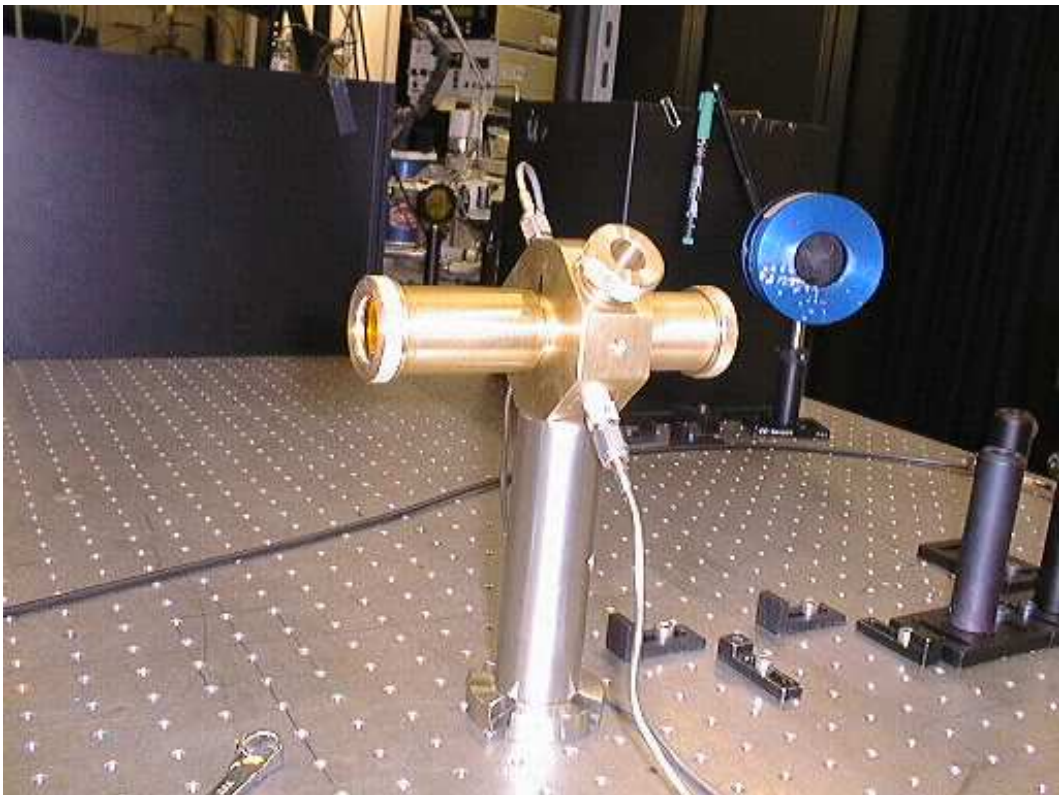

Figure C.4: Plasma shutter.

We found that the stability of the plasma shutter working in the active configuration was quite low. Although the moment of the shutter closing did not change considerably from pulse to pulse, we observed "skipped pulses", *i.e.* some CO_2 laser pulses passed through the plasma shutter without cutting. The frequency appearance of skipped pulses increased during about the first 30 minutes (at 10 Hz repetition rate) and finally all pulses passed the shutter cell without modification. We found, that this behavior has been caused by degradation of an electrode in the trigger cell under the action of focused laser radiation. Stability of the cutting is of high importance for us, because even a single skipped CO_2 laser pulse can damage the reaction cell windows. Thus, we finally decided to use the passive plasma shutter configuration, sacrificing the flexibility in the selection of the moment of cutting.

Figure C.5 represents the shapes of CO_2 laser pulse in the output of the nitrogen filled plasma shutter operating in the passive configuration. The output of the empty plasma shutter corresponds to the initial CO_2 laser pulse shape. At N_2 pressure starting from 0.5 bar we observe occasional breakdowns corresponding, likely, to the most powerful laser pulses. At pressure of about 0.8 - 1.0 bar the process stabilizes (all pulses produce breakdowns). This pressure corresponds to maximal achievable pulse duration of 100 ns (FWHM). Subsequent increase of nitrogen pressure results in shorter pulse durations. Almost complete blocking of

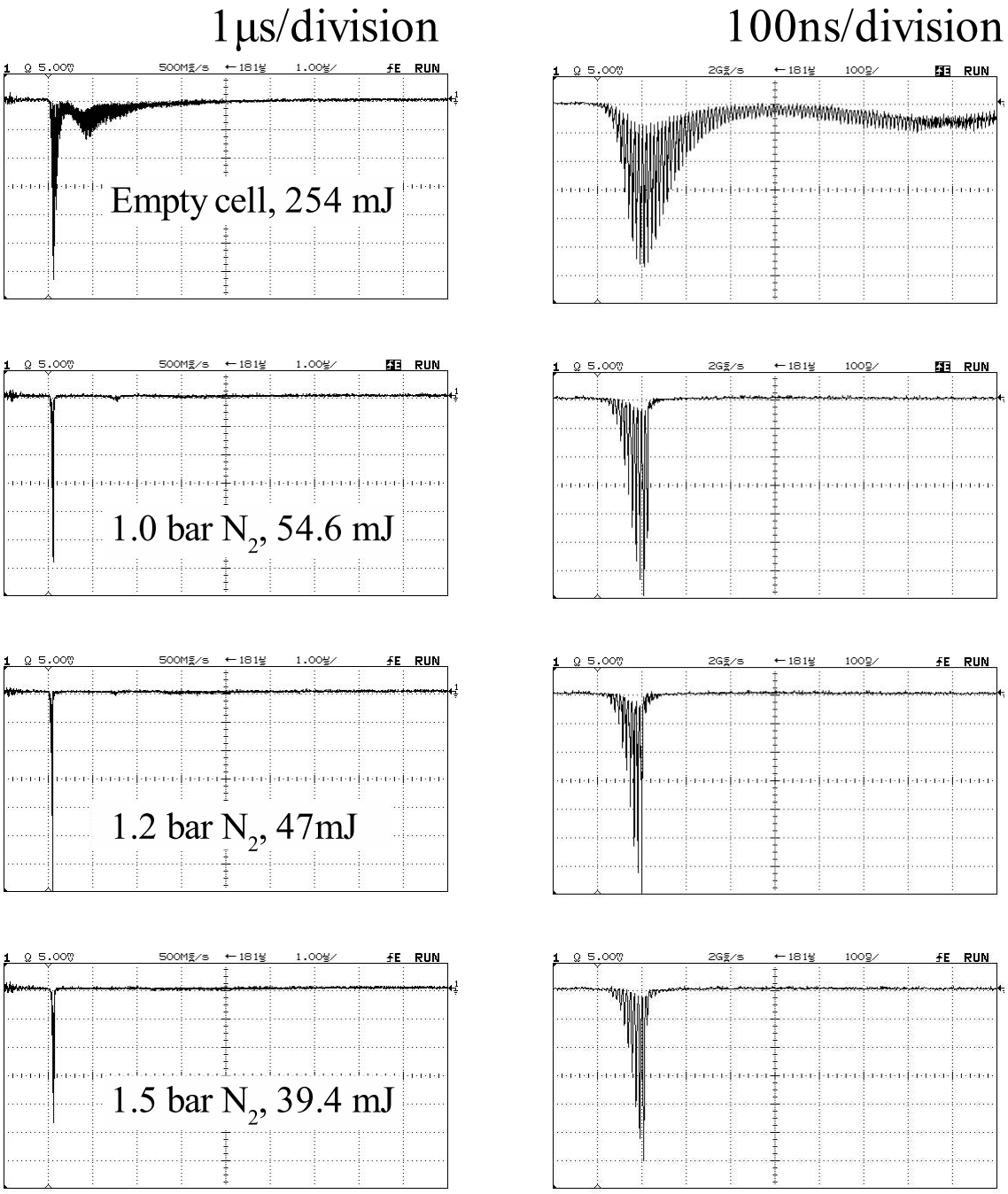

Figure C.5: CO_2 laser pulse "tail cut" with passive plasma shutter.

the pulse should be reachable at sufficiently high pressures. We did not increase the pressure above 2.0 bar, however, in order to avoid lenses damage. The 50 - 100 ns adjustment range together with high pulse-to-pulse stability (time stability and absence of skipped pulses) allowed us to perform experiments required for evaluation of short CO_2 laser pulse potentials for OP-IRMPD based approach to carbon-13 isotope separation.

Bibliography

[1] A. J. Alcock and P. B. Corcum, *Can. J. Phys.*, 1979, **57**, 1280–1289.

[2] E. Yablonovich, *Phys. Rev. A*, 1974, **10**, 1888–1895.

[3] V. Parthasarathy, S. Nad, K. A. Rao, and S. K. Sarkar, *J. Photochem. Photobiol. A*, 1998, **115**, 1–6.

[4] T. Gasmi, H. A. Zeaiter, G. Ropero, and A. G. Ureña, *Appl. Phys. B*, 2000, **71**, 169–175.

[5] A. K. Nayak, V. Parthasarathy, and S. K. Sarkar, *IR Phys. Technol.*, 2001, **42**, 535–540.

Appendix D

Influence of CF_2 sticking to the reaction cell walls

The collection of the dissociation products is an important stage of an OP-IRMPD based isotope separation process. CF_2 fragments produced by OP-IRMPD of CF_3H are chemically stabilized in a dimerization reaction

$$CF_2 + CF_2 + M \longrightarrow C_2F_4 + M.$$

However, dimerization is not the only possible reaction of CF_2 fragments. The influence of different reactions has been analyzed in work [1] where it has been shown that only CF_2 sticking to the reaction cell walls is competitive with the dimerization process. Here we analyze the influence of sticking to the walls and estimate under which process configurations such an influence can be negligible.

D.1 General formula

The overtone pre-excitation is described by the following equation[1]:

$$\begin{aligned} [CF_3H^*] &= x'_{op}[CF_3H]_0, \\ x'_{op} &= \frac{1}{2}(1 - e^{-2\sigma_{op}F_{op}}), \end{aligned} \tag{D.1}$$

where $[CF_3H]_0$ is the initial concentration of CF_3H, x'_{op} the pre-excitation probability, $[CF_3H^*]$ the concentration of pre-excited molecules, σ_{op} and F_{op} are absorption cross-section and pre-excitation laser fluence correspondingly.

[1] The molecular concentrations in the subsequent equations are the concentrations of carbon-13 containing molecules. On the other hand, pressure p is the total sample pressure, including ^{13}C and ^{12}C species.

The IRMPD step under collisional conditions can be described by the two-step relaxation - one step dissociation model [2]. According to this model the initial concentration of the dissociation fragments (CF_2) right after the CO_2 laser pulse is:

$$\begin{aligned} &[\mathrm{CF_2}]_0 = x'_{irmpd}[\mathrm{CF_3H^*}], \\ &x'_{irmpd} = (1 + k'p)e^{-k'p}, \end{aligned} \tag{D.2}$$

where x'_{irmpd} is the dissociation probability for a pre-excited molecule, p the CF_3H pressure and k' a constant (for fixed time delay between pre-excitation and dissociation laser pulses).

Dimerization and sticking to the walls are described by the following dynamics equation (See [3]):

$$\frac{d[\mathrm{CF_2}]}{dt} = -2k_{dim}[\mathrm{CF_2}]^2 - R_{wall}[\mathrm{CF_2}], \tag{D.3}$$

where k_{dim} is the dimerization constant and R_{wall} the adsorption rate. R_{wall} depends on adsorption probability, geometry of the reaction cell and CF_2 distribution in the volume.

The solution of (D.3) is

$$\begin{aligned} &[\mathrm{CF_2}] = \frac{D}{(1 + DX')e^{R_{wall}t} - DX'}, \\ &X' = \frac{2k_{dim}}{R_{wall}}, \\ &D = [\mathrm{CF_2}]_0 = x'_{op}x'_{irmpd}[\mathrm{CF_3H}]_0. \end{aligned} \tag{D.4}$$

Using this solution, we can find the probabilities of dimerization (x'_{dim}) and sticking to the walls (x'_{wall}) for CF_2 fragments:

$$\begin{aligned} &x'_{dim} = [CF_2]_0^{-1} \int_0^\infty 2k_{dim}[CF_2]^2 dt = 1 - \frac{ln(1 + DX')}{DX'}, \\ &x'_{wall} = 1 - x'_{dim} = \frac{ln(1 + DX')}{DX'}. \end{aligned} \tag{D.5}$$

And finally, we can write an expression for C_2F_4 productivity:

$$[\mathrm{C_2F_4}] = \frac{1}{2}x'_{op}x'_{irmpd}x'_{dim}[\mathrm{CF_3H}]_0. \tag{D.6}$$

D.2 Mass-spectrometer signal as a function of sample pressure

The mass-spectrometer signal is proportional to the relative concentration $\frac{[\mathrm{C_2F_4}]}{[\mathrm{CF_3H}]}$ of the produced C_2F_4 molecules. Taking also into account that the pre-excitation probability does not depend on sample pressure and assuming that $^{13}CF_3H$ consumption during the experiment is negligible one can write for the signal S:

$$S \propto x'_{irmpd}x'_{dim}. \tag{D.7}$$

For the concentration of pre-excited $^{13}CF_3H$ we can write:

$$[CF_3H] = x'_{op}[CF_3H]_0 = C'p, \tag{D.8}$$

where C' is a constant.

Then, for an initial $^{13}CF_2$ concentration D we get:

$$D = x'_{op}x'_{irmpd}[CF_3H]_0 = C'p(1 + k'p)e^{-k'p}. \tag{D.9}$$

And, for the mass-spectrometer signal:

$$S = C(1 + k'p)e^{-k'p}\left(1 - \frac{ln\left(1 + p(1 + k'p)e^{-k'p}X''\right)}{p(1 + k'p)e^{-k'p}X''}\right), \tag{D.10}$$

$$X'' = X'C'.$$

Now we can use the function (D.10) for fitting the experimental data using C, k' and X'' as fit parameters. Figure D.1 represents a result of such a fitting for a low-yield experiment (overtone pre-excitation at 3_1 band, big passive volume of the reactor cell ($V_{active}/V_{total} \approx 10^2$).

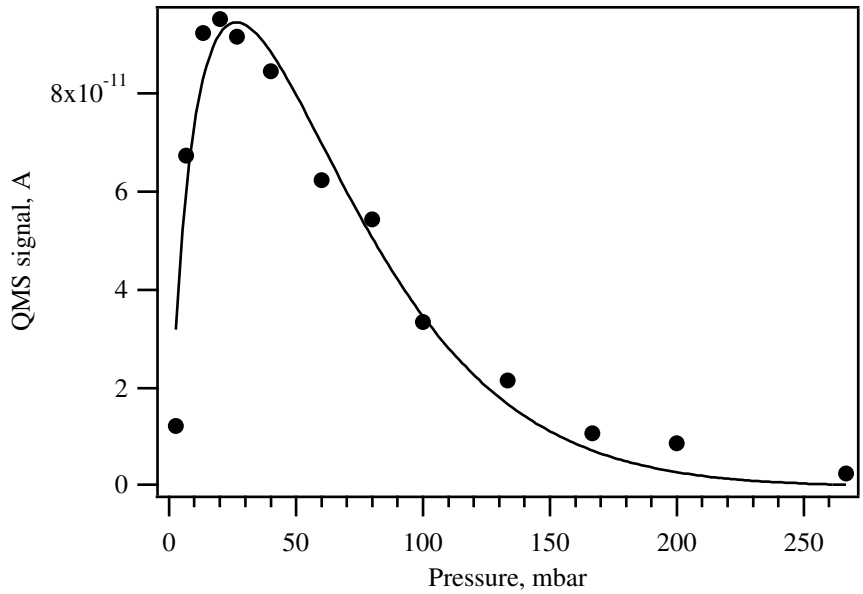

Figure D.1: Fit of the experimental curve. Fitting coefficients (± one standard deviation) are: $C = (1.9 \pm 0.4) \cdot 10^{-10}$, $k' = (0.025 \pm 0.002)mbar^{-1}$, $X'' = 0.16 \pm 0.07$.

Using the equations (D.2), (D.5) and (D.9) and fitting coefficients from the Figure D.1 we can calculate the fractions of pre-excited molecules which has been:

1. dissociated (x'_{irmpd}),
2. dissociated and converted into C_2F_4 *via* dimerization ($x'_{irmpd}x'_{dim}$), and

3. dissociated and stuck to the reactor walls ($x'_{irmpd}x'_{wall}$).

The corresponding curves are shown in Figure D.2.

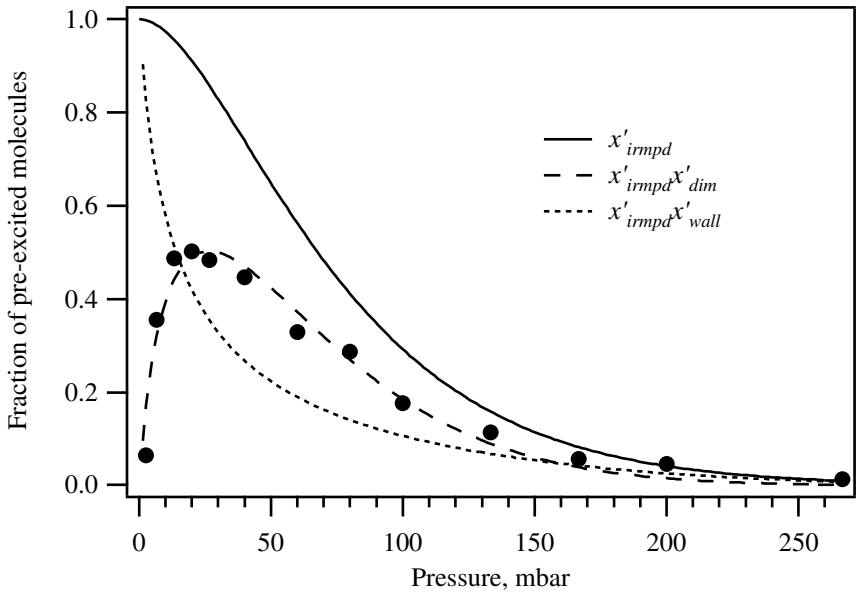

Figure D.2: Probabilities of different reaction channels for pre-excited CF_3H and normalized experimental data points as a function of sample pressure.

The data points normalized using the C fitting coefficient are also shown in Figure D.2. To verify the represented calculations we have calibrated the mass-spectrometer using a CF_3H+C_2F_4 mixture of known composition. This calibration allowed us to measure the absolute concentration of C_2F_4, and, for known pressure and cell volume, the absolute amount of C_2F_4 in the cell. Using the known absorption cross-section and pre-excitation laser fluence we calculated the amount of pre-excited molecules in the volume irradiated by the pre-excitation and dissociation lasers. A comparison of the amount of pre-excited molecules with the amount of produced C_2F_4 allows us to estimate the $x'_{irmpd}x'_{dim}$ value, which is in agreement with the calculation results.

Figure D.2 shows that in the configuration of our experiment CF_2 sticking to the reaction cell walls plays a significant role in the isotope separation process. For example, at sample pressure of 70 mbar almost 35% of dissociation fragments are lost due to the sticking. However, probability of sticking to the walls depends on the initial concentration of CF_2 fragments D (see Equation (D.5)). An increase of D will lead to increase of dimerization probability x'_{dim}. Figure D.3 shows the $x'_{irmpd}x'_{dim}$ value for the D value which is ten times higher than the corresponding value in the experiment represented by Figure D.1. Such or even higher increase of D can be reached by using the pre-excitation at first instead of second overtone of CH stretch vibration, by increase the fluence of pre-excitation laser and by increase the ratio of active to

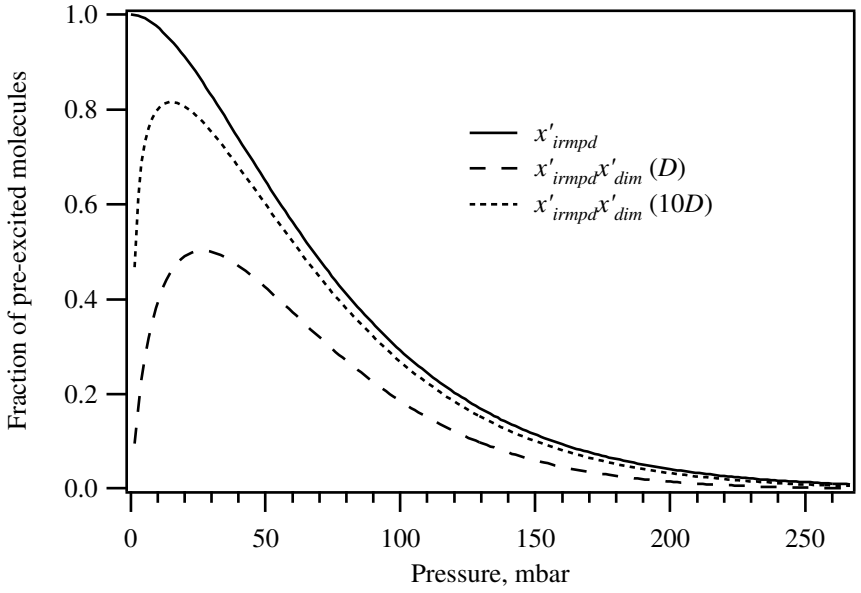

Figure D.3: $x'_{irmpd}x'_{dim}$ for D value of Figure D.1 and for ten times higher D.

passive volumes of the cell. For the curve represented in the Figure D.3 only 7.5% of CF_2 are lost on reactor walls at 70 mbar. Thus, we can conclude about negligibility of sticking to the walls in a properly designed industrial-scale setup.

In our research set-up which is not optimized for maximal process yield and required selectivity the CF_2 loses on the reaction cell walls can reach several tens percents. We can, however, avoid an influence of this process on the dissociation yield measurements results measuring the depletion of $^{13}CF_3H$ instead of C_2F_4 concentration (see Chapter 3).

In the conclusion we have to point out two important approximations which have been made in the description of the process dynamics represented in this appendix. First, k_{dim} is assumed to be constant. F. Battin-Leclerc *et al.* have shown, however, that the high pressure limit of the bimolecular CF_2 recombination is not reached at pressures used in our work [4]. Hence k_{dim} increases with an increase of pressure. Second, the probability for the CF_2 fragments to reach the reaction cell walls depends on diffusion speed and, hence, decreases with an increase of sample pressure. This has not been taken into account in the Equation (D.3). We assume that these approximations are responsible for the small discrepancy between the experimental data and the fitting curve obtained using the Equation (D.10) (see Figure D.1).

Bibliography

[1] M. Kowalzcyk *Highly Selective Molecular Laser Isotope Separation of Carbon-13* PhD thesis, Ecole Polytechnique Fédérale de Lausanne, Switzerland, 2000.

[2] O. V. Boyarkin, M. Kowalzcyk, and T. R. Rizzo, *J. Chem. Phys.*, 2003, **118**, 93–103.

[3] M. M. Ivanenko, H. Handreck, J. Göthel, W. Fuß, K.-L. Kompa, and P. Heiring, *Appl. Phys. B*, 1997, **65**, 577–582.

[4] F. Battin-Leclerc, A. P. Smith, G. D. Hayman, and T. P. Murrells, *J. Chem. Soc., Faraday Trans.*, 1996, **92**, 3305–3313.

Appendix E

Gaussian beams

E.1 Characteristics of Gaussian beams

Very often the intensity and fluence distribution in the laser beam is Gaussian [1] and described by the following equation:

$$\boxed{G(r) = e^{-2\frac{r^2}{\omega^2}}} \qquad \text{or} \qquad G(x,y) = e^{-2\frac{x^2+y^2}{\omega^2}}, \tag{E.1}$$

where r is the distance from the beam center, x and y the Cartesian coordinates, and ω the $1/e^2$ radius of the spot (at the distance ω from the point of maximum intensity, intensity drops by a factor of e^2)

Figure E.1 shows the profile of Gaussian beam.

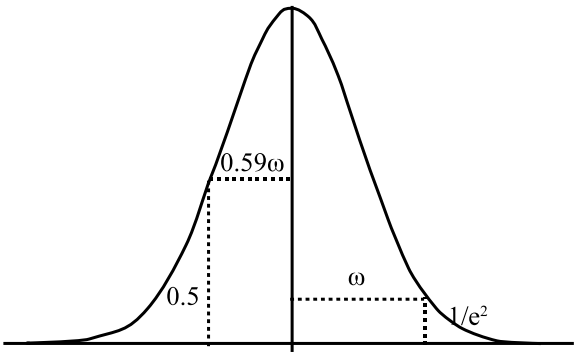

Figure E.1: The Gaussian.

One of the commonly used ways to specify the size of a Gaussian beam apart from using the $1/e^2$ radius w is to use its Full Width at Half Maximum (FWHM) a diameter of the beam where its intensity drops by a factor of 2 compared to the value in the center. One can establish a simple connection between ω and FWHM, for this we will first determine the *Half* Width at

Half Maximum H:

$$\begin{aligned} &\frac{\text{FWHM}}{2} \equiv H, \\ &e^{-2\frac{H^2}{w^2}} = 0.5 \quad \Rightarrow \quad H \approx 0.59\omega. \end{aligned} \tag{E.2}$$

Fractions of total laser pulse energy within FWHM can be determined as:

$$\boxed{\frac{E_{fwhm}}{E} = \left(\int_0^H 2\pi r G(r) dr\right) / \left(\int_0^\infty 2\pi r G(r) dr\right) = 0.5} \tag{E.3}$$

where E is the total laser pulse energy and E_{fwhm} is the energy within FWHM.

Consequently, the average laser fluence within FWHM (Φ_{fwhm}) is:

$$\Phi_{fwhm} = \frac{0.5E}{\pi H^2} \approx \frac{0.5E}{\pi(0.59\omega)^2} \approx \frac{1.44E}{\pi\omega^2}. \tag{E.4}$$

Another generally accepted way of specification of the energy fluence of a Gaussian laser beam is the peak fluence Φ_0:

$$\Phi(r) = \Phi_0 G(r) \qquad \Rightarrow \qquad \Phi_0 = \frac{\Phi(r)}{G(r)},$$

where $\Phi(r)$ is the fluence distribution in the beam having a Gaussian profile.

If the laser pulse energy E and the beam size is known, one can calculate Φ_0 as:

$$\begin{cases} E = \int_0^\infty 2\pi r \Phi(r) dr = \Phi_0 \int_0^\infty 2\pi r G(r) dr \\ \int_0^\infty 2\pi r G(r) dr = \frac{\pi\omega^2}{2} \end{cases} \qquad \Rightarrow \qquad \Phi_0 = \frac{2E}{\pi\omega^2}. \tag{E.5}$$

Comparing Equations (E.4) and (E.5) we can establish the direct connection between Φ_{fwhm} and Φ_0:

$$\boxed{\Phi_{fwhm} \approx 0.72\Phi_0} \tag{E.6}$$

The average fluence within FWHM differs less than 30% from the peak fluence, whereas (as it can be seen from the Figure E.1 and confirmed by simple calculations that are not shown here) the average fluence within bigger limits decreases steeply with increase of averaging area. As the IRMPD probability steeply decrease with decrease of fluence (see for example [2]), in this work we use Φ_{fwhm} to specify laser fluence and assume that 50% of total pulse energy concentrated within FWHM is active in the IRMPD process.

E.2 Measurement of beam profile

Two methods of beam profile measurement were used in our work. In the first of these methods a thin slit scanned through the beam is used (Figure E.2).

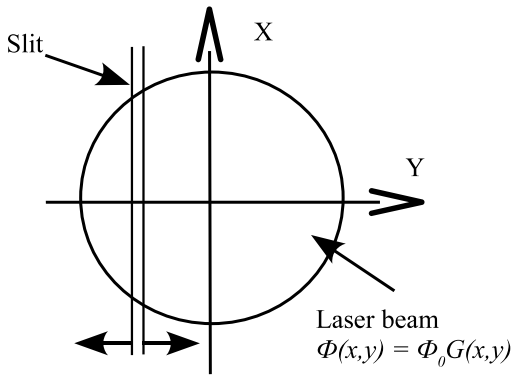

Figure E.2: "Slit" method of beam profile measurement.

If the slit width is much smaller than the beam diameter and beam profile is Gaussian, the measured intensity distribution is:

$$G'(x) = \int_{-\infty}^{\infty} e^{-2\frac{x^2+y^2}{\omega^2}} dy = e^{-2\frac{x^2}{\omega^2}} \int_{-\infty}^{\infty} e^{-2\frac{y^2}{\omega^2}} dy = const \cdot e^{-2\frac{x^2}{\omega^2}}, \tag{E.7}$$

Thus, measured distribution corresponds to within a constant to the intensity distribution in a longitudinal section of the beam and

$$\omega = \omega', \tag{E.8}$$

where ω' is the $1/e^2$ radius of the measured intensity distribution.

The second method of beam profile measurement consist of measurement of the fraction of pulse energy passed through an iris of known diameter d (Figure E.3) with consequent reduction of the Gaussian profile.

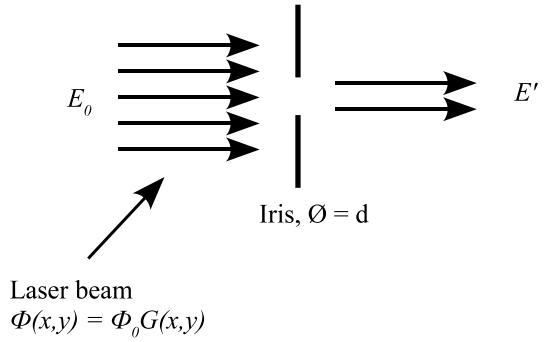

Figure E.3: "Iris" method of beam profile measurement.

The size of the beam can be determined as:

$$\frac{E'}{E_0} = \left(\int_0^{d/2} 2\pi r G(r) dr \right) / \left(\int_0^{\infty} 2\pi r G(r) dr \right) \quad \Rightarrow \quad \boxed{\omega = \frac{d}{\sqrt{-2Log(1 - \frac{E'}{E_0}))}}} \tag{E.9}$$

where E_0 and E' are the laser pulse energies measured before and after the iris.

Both "slit" and "iris" methods will produce an accurate result only if the profile of laser beam is close to Gaussian.

E.3 Focusing of Gaussian beams

In the general case a divergent Gaussian beam with $1/e^2$ radius ω_1 can be focused to the spot size ω_f which is determined as follows::

$$\omega_f = f\left(\left(\frac{\lambda}{\pi\omega_1}\right)^2 + \frac{\omega_1^2}{R^2}\right)^{1/2}, \tag{E.10}$$

where f is the focal length and R the radius of curvature of the phase front before the lens.

In the case of collimated Gaussian beam ($R = \infty$) Equation (E.10) transforms to:

$$\omega_f = \frac{f\lambda}{\pi\omega_1}. \tag{E.11}$$

E.4 M^2

The propagation of a "real" near-Gaussian beam can be described by the equations describing the propagation of Gaussian beam where λ is replaced by $M^2\lambda$, where M^2 is a characteristic of the laser source. For example, for the focal spot size we have:

$$\omega_f = \frac{M^2 f\lambda}{\pi\omega_1}. \tag{E.12}$$

Bibliography

[1] A. E. Siegman, *Lasers*, Sausalito, California University Science Books, 1986.

[2] V. S. Letokhov, *Nonlinear Laser Chemistry*, Springer-Verlag, Berlin, Heidelberg, New York, 1983.

Acknowledgments

During the last four years I have encountered many kind people who took part in the outcome of my thesis to whom I would like to express my personal thanks:

Professor Thomas R. Rizzo, who accepted me in his group allowing me to participate in the challenge of modern laser spectroscopy for the insightful discussions during the progression of this work, as well as for critical reading and help in the correction of this manuscript.

Professor Pierre Vogel, Professor Majed Chergui, Professor Alexander A. Makarov, Dr. Georg L. Seyfang, for serving on the thesis examination committee,

Dr. Oleg Boiarkine for the guidance and encouragement that he gave me throughout my work and writing this thesis,

Richard Bossart, with whom I shared the lab during almost three years for his help in experiments, for very helpful discussions of theoretical aspects of laser isotope separation and for critical reading of the draft of this thesis,

Marianne Dang, Professor Tino Gäumann, Dr. Rainer Beck, Dr. Andrea Callegari, Dr. Marcel Drabbels, Dr. Aziz Kasimov, Dr. Dimitrios Papageorgopoulos, Amanz Ruf, Cédric Bovet, Andreas Braun, Christelle Cardon, Rachele Chianese, Thanh Tung Dang, Anthi Kamariotis, Jordan Katz, Monika Kowalczyk, Evgeniy Loginov, Joachim Makowe, Pavel Maksyutenko, Plinio Maroni, Sébastien Mercier, Antoine Milon, Julia Rebstein, David Rueda, Marco Sacchi, Mathieu Schmid, Patrice Theulé, former or current colleagues of the LCPM, for their helpfulness and pleasant work atmosphere,

the mechanical and electrical workshops, for the technical assistance and for producing wonderful laboratory equipment.

I wish to thank people without whom this work would never be possible: my parents *Nikolaj* and *Larisa Polianski*, my friends, my teachers from St. Petersburg State University *Dr. Valery Borisov, Dr. Alexander Pastor,* and *Professor Valery Nemets.*

Particularly, I wish to express my special gratitude to my dear wife *Galina* for her invaluable support and for being with me during bright and dark periods of my life.

Curriculum Vitae

Born

April 22, 1976 in Krasnogorodsk (Pskov region), Russia.

Education

- *1997-2000* Master degree in physics. Saint-Petersburg State University (Russia).
- *1993-1997* Bachelor degree in physics. Saint-Petersburg State University.

Experience

- *2000-2004* Ph.D. research project "Overtone pre-excitation – infrared multiple photon dissociation under collisional conditions: New potential for laser isotope separation", Laboratory of molecular physical chemistry (LCPM), EPFL, Lausanne.
- *1999-2000* master diploma project "LIF analysis of mixtures of complex organic compounds" – 6 months, department of physics of Saint-Petersburg State University.
- *1997* diploma project "Development of the LIDAR system for atmospheric ozone probing" – 2 months, department of physics of Saint-Petersburg State University.

Publications

- M. Polianski, O. V. Boyarkin, T. R. Rizzo. "Collisionally assisted approach for highly selective carbon-13 laser isotope separation", submitted to J. Chem. Phys.
- M. Polianski, O. V. Boyarkin, T. R. Rizzo, V. M. Apatin, V. B. Laptev, E. A. Ryabov. "Infrared Laser Chemistry of Trichlorosilane in View of Silicon Isotope Separation", J. Phys. Chem. A **2003**, 107, 8578
- V. B. Borisov, V. M. Nemets, M. N. Polyanskii, A. A. Solov'ev. "Possibility of application of the multidimensional statistical analysis of spectra in the LIF study of complex mixtures of organic compounds", Analitica i kontrol **2000**, 4, 151 (in Russian)
- V. B. Borisov, V. M. Nemets, A. A. Pastor, M. N. Polyanskii, A. A. Solov'ev. "Laser fluorescence technique for analysis petroleum products and detection of organic compounds in water", Pribory i Sistemy Upravleniya **1999**, 6, 43 (in Russian)

Presentations

- "Collisionally-enhanced, highly selective laser isotope separation of carbon-13" with O. V. Boyarkin, R. Bossart and T. R. Rizzo, The XIV symposium on atomic, cluster and surface physics; La Thuile, Italy, **2004** (poster)
- "Overtone pre-excitation - infrared multiphoton dissociation approach for highly selective laser isotope separation" with O. V. Boyarkin, R. Bossart and T. R. Rizzo, Swiss Chemical Society - Fall Meeting; Lausanne, Switzerland, **2003** (poster)
- "Overtone pre-excitation - infrared multiphoton dissociation approach for highly selective laser isotope separation" with O. V. Boyarkin, R. Bossart and T. R. Rizzo, 39th Symposium on Theoretical Chemistry "Molecular Spectroscopy and Dynamics"; Gwatt Lake Thun, Switzerland, **2003** (poster)
- "Control of the CO_2 laser pulse duration for application in laser isotope separation" with O. V. Boyarkin and T. R. Rizzo, Conference on Laser Optics for Young Scientists; St. Petersburg, Russia, **2003** (poster) – awarded by the "Best Paper Award"
- "Overtone pre-excitation - infrared multiphoton dissociation technique for carbon isotope separation" with O. V. Boyarkin and M. Kowalczyk, International Quantum Electronics Conference / Conference on Lasers, Applications and Technologies; Moscow, Russia, **2002** (poster)

Additional Qualifications

Languages

- *Russian:* native;
- *English:* advanced level (working language since 2000);
- *French:* good understanding and basic speaking.

Computer Skills

- *Operating systems:* Windows, Linux;
- *Programming:* C/C++, Win32 API, GTK+;
- *Data acquisition and analysis:* IgorPro, Origin, Mathematica, LabView;
- *Office and text tools:* LaTeX, OpenOffice.org, MS office, etc;
- *Designing:* QCad, basics of AutoCad and SolidWorks.

List of Figures

List of Tables